THE UNIVERSITY OF MICHIGAN
COLLEGE OF ENGINEERING
Department of Nuclear Engineering

Technical Report

CONFORMATION AND DYNAMICS OF POLYMER CHAINS

Gerard Jannink

ORA Project 07404

supported by:

NATIONAL SCIENCE FOUNDATION
GRANT NO. GK-476
WASHINGTON, D.C.

administered through:

OFFICE OF RESEARCH ADMINISTRATION ANN ARBOR

November 1966

This report was also a dissertation submitted in partial fulfillment of the requirements for the degree of Doctor of Philosophy in The University of Michigan, 1966.

TABLE OF CONTENTS

LIST OF TABLES

LIST OF FIGURES

LIST OF FIGURES (Continued)

LIST OF FIGURES (Concluded)

ABSTRACT

We consider the relation between conformation, normal frequency distribution, and force field of a backbone chain. In particular, it is asked whether a conformation can be identified from the analysis of the frequency distribution and whether information about the force field can be gained by examining the frequency distribution at different conformations.

To determine the frequency distribution, we use the symmetry of the dynamical matrix and the property of Sturm sequences. We discuss the performances of the Givens' transformation and the negative eigenvalue theorem of Dean and Bacon.

In Chapter III we consider chains with one degree of freedom per repeat unit. A fold at a unit j in the extended chain tends to uncouple the vibrational motion on both sides of j. Conversely, the local unfolding of a folded chain enhances the coupling and produces out-of-band modes. From the ordering of the out-of-band modes, statistical aftereffects can be detected. The out-of-band modes are determined by the Green's function method. Such a model could be used to follow the helix-coil transition.

In Chapter IV we consider chains with two degrees of freedom per repeat unit. In addition to the uncoupling effect, the fold also couples the motions of the two species. When the force constants are of the same order of magnitude, the uncoupling effect is dominant. Otherwise, the coupling effect is dominant.

In Chapter V we calculate the dynamical matrix elements of the Kirkwood-Pitzer model of a folded polyethylene backbone chain. The numerical calculations with the Givens-Sturm procedure indicate a one to one correspondence between modes (~ 670 cm^{-1}) in the stretch-bend gap and folds, for low concentrations of folds. The distribution of the modes in the forbidden gap also reflects the fold distribution along the chain.

We compare thermodynamical functions for several concentrations and correlations of folds in Chapter VI. These functions have a vibrational and a potential component. The latter is derived from the one-dimensional Ising model, which also yields the average ratio of T to G configurations and the pair correlation as a function of the temperature dependent configuration energy J and the temperature independent correlation energy U. Volume exclusion and three-dimensional nonbonded interactions are, however, expected to modify the result.

We conclude that conformations have two characteristic parameters reflected in the frequency distribution, namely the range of allowed dihedral angular values and the ordering of configurations along the chain. The frequency distribution for a given conformation depends, however, on the force constants ratio when the number of degrees of freedom is greater than one. Hence, the interpretation of frequency distributions is to be made in terms of both conformations and force field. We suggest that chains generated by a Markov process and by a random walk with no self-intersection could be separated by their frequency distribution.

CHAPTER I

INTRODUCTION

A polyethylene chain is composed of several thousand CH_2 repeat units linked by carbon to carbon bonds. The combinations allowed by the tetrahedral carbon bonds configuration are not energetically equivalent and the structure in which the carbon to carbon bonds are coplanar is favored. Accordingly the backbone of the isolated chain is represented as a planar zigzag. Chains in a sample do not conform to this state. In fact planar sections of a chain are found, however the chains also exhibit folds along the C-C bonds.

Experimental evidence indicates in which way folds are distributed along a chain. X-ray diffraction patterns show a combination[1] of ordered and disordered structures. This interpretation is particularly convincing when the patterns are examined from fusion to room temperature.[2] The widths of nuclear magnetic resonance absorption lines decrease[3] rapidly for temperatures above the glass transition temperature. This narrowing is interpreted as the onset of internal rotations about C-C bonds, and since the rotations are assumed forbidden in the crystal structure, there must be other regions in which they take place. Density measurements also indicate that the liquid state solidifies only partially into the more dense crystal structure. Other experiments illustrate the same point, that ordered and disordered regions coexist or that folds tend to concentrate in so-called amorphous regions.

In this perspective a quantitative description of chain structure is given by the crystal volume percentage. Data from the above experiments are used to evaluate this quantity. Their interpretation creates difficulties which are of interest to consider. The intensity curve of the diffracted X-rays shows two peaks of different shape which are assigned to crystal and amorphous volumes, respectively. It is argued[4] that the area under the amorphous peak provides a good measurement of amorphous volume; this area is evaluated with respect to a curve extrapolated from the liquid state. However this peak also contains a contribution from the diffuse thermal scattering by crystal regions. The difficulty in density measurement is of the same nature. One also takes the liquid state as a "standard density" for amorphous regions. But molecules in an amorphous region are joined to neighboring crystalline regions, which exert constraints and produce local variations from the standard density. The assumption in the nuclear magnetic resonance technique is not valid.[3] Internal rotations do take place in crystalline regions and their contribution has to be separated from the observed value.

The difficulty in interpreting these experimental results is attributed in part to the lack of resolution of methods of observation and to the inherent ambiguity in wave interaction, as reflected in the phase problem. An important part is however due to the simplifying assumptions on the structure of the chains. There is in fact a multiplicity of structures confirmed by experiment. In the theory of fringed micelles, planar

sections of several chains are seen to form crystallites with an orthorhombic lattice. The chains separate at each crystal boundary, traversing successive regions of random and aligned arrangements. Keller and O'Connor have observed with an optical microscope thin lozenged shaped platelets disposed in layers. A surprise came in 1958 with the interpretation[5] of their experiment. It was first established by low angle X-ray scattering, that the platelets have a thickness of 100 A°. Next, electron diffraction patterns revealed that the c axis of the chains runs perpendicular to these platelets. The conclusion from these results was that the chain folds back and forth between the 2 lozenges' faces. In this theory, the amorphous contribution[1] comes from lattice defects such as a chain escaping and reentering the same crystallite.

The difference in these two structures was later traced back to the polymerization process. The first is more likely to occur in a sample produced by cooling melted polyethylene. The second occurs in samples grown from dilute solutions. For certain authors[6,7] the two concepts of fringed micelles and folded chains are not "exclusive of each other." The degree to which these structures interpenetrate is however unclear.

At this stage, we give a more detailed quantitative description of chain structure by the following characteristics[8]:

-average sequence length of chains in the crystalline regions,

-average sequence length in amorphous regions,

-expected number of crystalline sequences per chain,

-expected number of amorphous sequences per chain.

We now mention briefly, for later reference, some factors involved in the determination of these characteristics. In the molecular field theory, they are determined by weak forces of long range. However, the same characteristics can also be derived from stronger forces of shorter range. Their effect is expressed in form of a transfer matrix,[8] whose elements are fitted to reproduce the observed characteristics.

Several authors obtain the size of crystallites as a result of thermodynamical equilibrium. In one approach the free energy has two components.[9] The first is the harmonic vibration component and is a decreasing function of N, the number of atoms in the chain. The second is the molecular field component and it is an increasing function of N. The increase is caused by the thermal smearing of the periodic potential. The total free energy reaches a minimum at a given $\bar{N}$, from which the size of the crystallite is determined.

An important consideration in amorphous regions is the entropy per link.[10] This quantity is a measure of the number of permissible ways of adding a new link to a chain. Because of the volume exclusion principle, the entropy per link is a decreasing function of N. This effect is recognized to be important, but difficult to evaluate.

For other authors the size of crystallites does not correspond to a minimum of free energy. They claim[11] that the "anharmonic nature of the thermal motion of atoms must destroy the long range order at a quite characteristic distance."

The other issue raised by the interpretation of experimental data is the choice of an observable which would best reflect the structure of chains in a sample.

It was seen that the interpretation of the scattering curve for X-ray diffraction is ambiguous because the contributions of structure in disordered regions and of thermal activity in crystal lattice do not separate. An alternative approach is to consider the chain as a system of coupled oscillators and observe the normal frequencies, in the form, for example, of the frequency distribution. The spectrum is known to be very sensitive to dimension of the lattice, range of forces and, hopefully, structure. Methods to detect normal frequencies are infrared absorption, Raman scattering, and inelastic neutron scattering. It is interesting to note that the proton spin states provide a mechanism both for the incoherent neutron scattering[12] and the nuclear magnetic resonance techniques.

The effect of folds on the frequency distribution was formulated some time ago.[13] The problem is the interpretation of the spectrum for the noncrystalline structure. A program was established "to achieve complete interpretation of the spectrum, to study spectral difference which arise from presence of noncrystalline structure and identification of such structures."[13] The spectrum is sensitive to chain folds in two ways: the environment[13] and the intramolecular or direct forces. The environment can be thought of as a molecular field. Its dependence on structure is for instance given by the averaged squared polarization

vectors which produce a "smearing" of the potential. Or it can be thought of as the effect of weak intermolecular forces. There the overall chain structure is reflected by the intermolecular distances. As for the intramolecular or direct forces, they are locally modified by the change in relative orientation of C-C and C-H bonds. The binary interaction strength may be invariant under a fold. It was indeed verified[5] that a chain in the orthorhombic lattice can twist by an angle of 82° and fold without affecting valence or interatomic distances. The resultant of forces exerted on one atom will however change if they are differently oriented with respect to each other. Since in the vicinity of a fold the relative orientations of binary interactions do change, resultant forces are modified.

It is significant that the author in Ref. 13 mentions environment before direct effects. Important results have been related to environment such as limited growth of crystallites. On the other hand, direct effects modify the stronger bonds and cannot be overlooked as the concentration of folds increases. Their calculation is a prerequisite to the evaluation of the field in Ref. 12, since the averaged squared harmonic amplitude depends on structure. Also, the refinement of force constants is only meaningful if the noncrystalline bands are identified. A controversy has actually developed as to which effect is dominant: some authors argue for direct effects,[7] others show in recent calculations[22] the importance of environment, especially in the acoustic range of the harmonic spectrum. Controversies on the relative importance of force

range, force constant, and dimensionality are known elsewhere, as in the Ising problem.[14] The issue in the Ising problem is the singularity of the phase transition. The same singularity can be related either to a weak molecular field in a one-dimensional lattice or to a stronger nearest neighbor interaction in a two-dimensional lattice. Here local fold defects are opposed to three-dimensional lattice effects in the interpretation of the unidentified features of the harmonic spectrum.

The polyethylene spectrum can be divided into two parts, one associated, with internal modes of the CH^2 group, the other with the skeletal vibrations. A separation line can be drawn at 1150 cm^{-1}, although the CH^2 rocking mode overlaps into the skeletal band. We are concerned here with this lower part of the spectrum. This region of the spectrum has been investigated only recently using the far infrared and neutron scattering techniques. The interpretation of observed data is still controversial because of lack of resolution and because these modes are most sensitive to the effects of configurations. For instance Kirkwood[15] argued that "evidence that modes are not greatly affected by the configurations among which the molecule is distributed is provided by the sharpness of the Raman lines of the hydrocarbons. However this statement need not to be taken too seriously as far as lower frequencies are concerned, since there seems to be no reason why their pattern might not be considerably affected by configurations and by interaction with the torsional modes." This interaction is indeed a key issue. The torsional motion of the isolated planar skeleton is an independent, one

dimensional motion. Folds of the chain introduce local couplings with the stretch-bend motion. On the other hand these modes are uniformly mixed in the orthorhombic lattice model. They produce a splitting and a shift in the dispersion relations, and singularities in the frequency spectrum which will be interesting to compare with the local effects.

There is a great variety of polyethylene chain models, varying in complexity. Each model has its strength and each has its weaknesses.[16] The Stockmayer-Hecht[17] model is certainly the simplest and it has produced an astonishing amount of information. It consists of parallel linear chains disposed in a rectangular three-dimensional lattice. Each mass unit, which represents a CH^2 group, is dynamically related to its nearest neighbor on each axis and to the next nearest neighbors on the diagonals. A bending force along the C axis is introduced at each vertex. The Kirkwood-Pitzer[18] model treats the isolated backbone chain with next nearest neighbor interactions in the zigzag plane, and third order interactions in the out of plane motion. A common[19] feature of simple models is the grouping of the CH^2 atoms into one mass point. The high carbon to hydrogen mass ratio justifies this procedure. However contribution of some hydrogen motion is known to be important in the backbone spectrum.

In the choice of a model, the following factors come into account: the order of the dynamical matrix is proportional to the dimension of the lattice and the number of atoms; the disposition of the nonzero matrix elements in the matrix depends on the degree of interaction. A numerical calculation is limited both by the size and the bordering of

the matrix. When the chain is incorporated in a lattice, translational and other symmetries allow a decomposition into blocks of smaller order. When the structure of the chain is random, partial diagonalization is impractical. A compromise has then to be made between dimension of the model, range of interaction, and length of the chain. We shall first consider very simplified models (Chapter III). Our aim is however to derive information from the Kirkwood model (Chapter V).

These models deal with the isolated chain. A major problem is to take account of the environment. We shall introduce the latter in the form of correlations between configurations of neighboring vertices (Chapter III). These correlations can be determined by comparing observed and calculated frequency spectra and thermodynamical functions (Chapter VI). Frequency distributions of the extended chains are calculated from the dispersion relations and the uniform mode distribution in the reciprocal lattice. The calculation is performed analytically for the simple models in which case the result has the form of a histogram. The analytical derivation has the advantage of listing all the singularities and determining the type to which they belong. The type is the number of negative coefficients of the second order Taylor expansion of the dispersion relation at the singularity. The periodicity of the lattice requires that there be at least 1 maximum, 1 minimum, and 6 saddle points.[20] Genensky and Newell[21] derived however 18 singularities from the Stockmayer-Hecht model (Table I). The position of each one of them in the frequency scale is given as a function of the force constants.

TABLE I

COMPARISON OF SINGULAR FREQUENCIES FROM DIFFERENT MODELS
(cm^{-1})

Isolated Chain**	Stockmayer-Hecht Model*	Chain in Crystal; Grouped Methyl Unit (Ref. 19)**	Chain in Crystal (Ref. 22)**
	28		
			61
			77
		80	
		100	
	110-ϵ, 110		
	114-ϵ, 114		117
			139
190			188
		200	220
			240
	319		
	321		
	332		
	335		
520	500	500	500

Note: These singularities are calculated from the dispersion relations for phonon propagation. The singularities of the S-H model are all saddle point types with the exception of 114 cm^{-1} which is a maximum. The value of ϵ is $\gamma^2/4\kappa$, where γ is the force constant for the diagonal bond, and κ the bending force constant.

*The S-H results are normalized to the 500 cm^{-1} cut off (S-H is the abbreviation for Stockmayer-Hecht model).

**The values of the force constants are (millidynes/A°):
4.10; 0.2676; 0.035 for the isolated chain (stretch)
4.0; 0.25; 0.03, for Ref. 19 (bend)
4.622; for Ref. 22 (torsion motion)

In this way the typical features of the polyethylene chain could be distinguished from the three-dimensional cubic lattice. It was for instance found that the torsion "cut off peak" is the coalescence of two slope discontinuities which degenerate into a logarithmic singularity as the diagonal force constant tends to zero.

Experimentally detected peaks are listed in Table II. Results of Ref. 7 were discussed before the calculations of Ref. 22 were known.

TABLE II*

SOME OBSERVED SINGULAR FREQUENCIES AND FREQUENCY ACCUMULATIONS (cm^{-1})

Ref. 7	Attribution (Ref. 7)	Ref. 23	Infrared (Ref. 24)
60	fold		
130	fold	130	
		160	
340	fold		
			540
			560
			573
			600
			617
			622

*These data do not include the well known events such as 500 cm^{-1}.

It is seen from Ref. 22 that although intermolecular forces are weak, they nevertheless produce a displacement of the dispersion maximum, in a range beyond 60 cm^{-1}. The argument in favor of chain folds need not however be overlooked. In this respect it is interesting to consider

the spectrum beyond the glass transition, as reported in Ref. 7. The high frequency cutoff of the bend mode is washed out, whereas the "torsion" peak remains. The secondary peaks are shifted from 390 and 125 cm^{-1} to 250 and 90 cm^{-1}. The peak at 60 cm^{-1} disappears and the negligable continuum in the forbidden stretch-bend gap rises to the density level of the bending continuum. The authors emphasize the "different departure" of the 2 acoustic modes from normal behavior. They interpreted this feature by a change in boundary conditions between crystalline and amorphous regions brought about by the onset of internal rotations. This enhanced rotational activity would have to perturb the stretch-bend propagation more than the torsional motion. If there are no amorphous regions as proposed in Ref. 1, one can conclude that these rotations occur at the regularly spaced folds of the crystallites and the defects distributed along the planar section of the chain. The latter are considered in Ref. 3.

Planar and transverse contributions are superposed in the frequency distribution of Ref. 7 by random orientation of the crystallites. Stretching the polyethylene sample makes them aligned. The chains may also unfold. Scattering on such a sample[23] allows separate investigation of in and out of plane activity. The authors of Ref. 23 found however a "persistence" of the torsional mode in the longitudinal component, which indicates a coupling between these motions. Contrary to the previous explanation they suggested that this coupling is the result of intermolecular forces. One could also argue that the chains are not really

unfolded and that the residual folds provide the mixture of the modes.

Table II lists the observed "structures" of the acoustic modes unidentified with respect to the planar isolated chain.

Although their interpretation tends to be given in terms of intermolecular effects, it is reasonable to inquire into the direct effects of folds regularly spaced in crystals and randomly distributed in amorphous regions. The forces involved are an order of magnitude greater than intermolecular forces and evidence is given that the folding concentration is not negligible. The mechanism through which forces applied to a particular mass point are altered is the reorientation of their respective directions, which can considerably affect direction and magnitude of their resultant.

CHAPTER II

CALCULATION AND INTERPRETATION OF FREQUENCY DISTRIBUTIONS

Two approaches[25] have been recently formulated on the statistical inference of complex systems. In such problems only a limited amount of information is available. The information is however sufficient either to define the nature of a system or to specify the state in which it is. The two approaches are based on the "renouncement[25] of exact knowledge" of either nature or state of the system. The outcome of the analysis depends on the approach. Typically, a system of harmonic oscillators has a well defined nature. Its states are the occupation numbers, whose probability distribution only is known. The outcome is the determination of the overall thermodynamical behavior of the system. In the example of the heavy nucleus,[26] the states are on the contrary observed with great accuracy, yet the laws of interaction between elementary particles are unknown. There, statistical mechanics predicts laws on the nature of the system such as the repulsion of levels.[26]

What is included under nature and state of a system depends on the particular problem. The two aspects may overlap and a different distinction is then more appropriate. We consider a system with several characteristic parameters and call extent any particular combination of them. The extent to which exact knowledge is renounced determines the amount of information that can be derived from the system. We want to show a relation between this extent and methods of observation

of the system. We have an ensemble of chains of CH^2 units. The angle ϕ between two adjacent bonds connecting units is allowed to take certain values and the sequence of all angles is the conformation of the chain. In a small angle X-ray experiment, the scattered intensity I is averaged over all unit positions, implying a renouncement of the exact knowledge of conformations. An overall behavior, derived from the Ornstein-Zernicke theorem,[27] is given by

$$\lim_{b \to o} I = \overline{N^2(v)} - (\overline{N(v)})^2 \qquad \text{(II-1)}$$

where b is the momentum transfer and $\overline{N(v)}$ the average number of units in volume v.

In a neutron inelastic, incoherent scattering experiment we renounce to the exact knowledge of the proton spin states. The overall behavior which we derive is however the frequency distribution[12] weighted by the squared polarization vectors (with the notations of Ref. 12)

$$\sum_q \gamma_j^a(q)\, \gamma_j^{a'}(q)\, F(h\omega_j(q)) \qquad \text{(II-2)}$$

Relation (II-2) reflects the structure of the system in a less ambiguous manner than (II-1) and yields more information.

In the next chapters we shall calculate frequency distributions associated with given conformations and conversely derive the necessary information about chain structure from the frequency distribution. The hamiltonian of the system is

$$H(c) = H_p(c) + H_v(c) \qquad \text{(II-3)}$$

where c indicates the dependence in conformation; H_p is the sum of potential energies associated with each ϕ; H_v is the hamiltonian for harmonic vibrations.

If we isolate H_p, we call a conformation a state of the system. The thermodynamic behavior of a sample of chains is determined without exact knowledge of these states. It will however be seen in Chapter VI that the temperature dependence of the thermodynamic functions yields information on the ordering in the sequence of angles ϕ.

When we consider the harmonic activity, the state of the system is the set of occupation numbers for each frequency and the frequency distribution. These depend on conformation which in some sense belongs to the nature of the system. In principle, the frequency distribution is observable to any degree of accuracy, independently of what is known about conformations. The problem is to derive information about the conformations from a measurement of the frequencies.

Problems described above have received considerable attention under the name of spectrum of random matrix. The matrix elements are scalar products of the hamiltonian of the system in a convenient representation; the ensemble of matrices corresponds to the collection of systems.

A standard procedure is the following: one assumes a probability law for each matrix element over the set of elements identically labeled. One then determines the eigenvalue distribution, and compares it with the observed spectrum. The matrix element probability law is adjusted to provide a best fit between calculated and observed spectrum.

In the context of our problem the system is the chain of N points. To each j there corresponds a random variable ϕ_j from which the matrix elements are derived (see Chapter III). The set of allowed values of ϕ is S. The probability distribution of ϕ over the set Σ_j of points labeled j in the collection of chains is $P^{(j)}(t)$ for the continuous case, $P_k^{(j)}$ otherwise. As $N \to \infty$, $P^{(j)}$ tends towards the probability distribution of ϕ along the chain. Namely, "by an argument familiar in the statistical mechanics of systems containing many particles, the same frequency spectrum will be found for an arbitrary chain chosen out of the ensemble, except for an exceptional class of chains whose total probability tends to zero as $N \to \infty$."[28]

A well-known method to calculate the eigenvalue spectrum consists of integrating the joint eigenvalue distribution over all variables but one. This expression is well known if the matrix elements are independent gaussian random variables.[26]

Another method calculates the eigenvalues density as the (generalized) derivative of the ordering function O(x), which is the number of eigenvalues smaller than x. It has been applied in different ways to singly bordered or tridiagonal (or Jacobian, if symmetric) matrices and it is interesting to follow the evolution of the problem from Dyson[28] to Dean.[29]

Let the matrix elements a_{ii} of A be noted

$$a_{ii} = \alpha_i;\ a_{i,i+1} = a_{i+1,i} = \beta_i;\ a_{ij} = 0,\ |i-j| > 1 \qquad \text{(II-4)}$$

Dyson consideres matrices of order 2N-1, for which $\alpha_i \equiv 0$. This corresponds to the isotope defect in a linear chain ($\phi \equiv 0$) where β_i is inversely proportional to the mass at site i. The frequency distribution is derived from the ordering function $O_s(x)$ for the squared eigenvalues, i.e., $O_s(x)$ is the number of modes for which the squared eigenvalue are less than x. Dyson's result is:

$$O_s(1/x) = 1 - \mathrm{Re}\,[(i\pi)^{-1} \lim_{\epsilon \to 0} \Omega(-x + i\epsilon)] \qquad \text{(II-5)}$$

where $$\Omega(x) = \sum_{a=1}^{2N-1} \log\,[1 + \xi_a(x)]$$

and $$\xi_a(x) = \frac{x\beta_a^{\,2}}{1 + \xi_{a+1}(x)} \qquad \text{(II-6)}$$

The distribution $P^{(a)}$ of β over Σ_a yields the distribution W_a of $\xi(x)$ from relation (II-6). In the limit $N \to \infty$, W_a becomes $W_a\,[\xi_a(x),s]\,ds$ and is the probability that $\xi_a(x)$ be in the interval $(s, s + ds)$. If β_a is independent and if the range S of β_a is continuous, W_a satisfies the integral relation:

$$W_a[\xi] = \int_0^\infty W_a[\xi']\, P(\xi(1 + \xi')/x)((1 + \xi')/x)d\xi' \qquad \text{(II-7)}$$

If S is discrete, W_a satisfies a difference equation. An exact solution of the integral equation was found for the case $P(t) \simeq e^{-t}$. This is the heavy isotope problem, where the range of masses reaches to infinity. As a result, a considerable shift of the spectrum towards lower frequencies was found. This can be compared with the Brout and Visscher[30] discovery

of an approximate localized mode produced by a heavy isotope with mass ratio about 25.

In other cases Eq. (II-7) is solved by iteration. Dean[29] generalized Eqs. (II-5) and (II-6) to the case of the tridiagonal matrix A as in (II-4). His result also is the "direct" eigenvalue distribution (not the squared eigenvalue distribution). Later he gave a simpler result, which we shall use.

Schmidt[31] considers the matrix A such that:

$$a_{i,i-1} = a_{i,i+1} = \alpha_i$$

$$a_{i,i} = 2\,\alpha_i \qquad ; \; i = 1,\ldots,N.$$

This is also the isotope problem. He determines the eigenvalue distribution from the nonhomogeneous problem of order N + 1.

$$(\tilde{A} - x\,I)\,u = e \tag{II-8}$$

where $\tilde{A}$ is augmented from A with only one nonzero element $a_{n,n+1}$ and where e has all but its last components zero. The ratio of 2 successive components of u satisfies the recurrence relation

$$\frac{u_n(x)}{u_{n+1}(x)} = z_{n+1}(x) = \frac{1}{2-x/\alpha_n-z_n} \tag{II-9}$$

Equation (II-8) satisfies the eigenvalue problem

$$(A - xI)\,u = 0$$

for $\varphi_{N+1}(x)$ multiple of 2π , where $z_n = t_g(\varphi_n/2)$. Since $\varphi_n(x)$ is a monotonic nondecreasing function, $\varphi_{n+1}(x)$ counts the number of modes smaller than x. More precisely

$$O(x) = \frac{1}{2\pi}(\varphi_{N+1}(x) - \varphi_{N+1}(-\infty))$$

The evaluation of $\varphi_{N+1}(x)$ is made from the equality between the integer $[\varphi_{N+1}(x)/2\pi]$ and the number of pairs $(\varphi_k(x), \varphi_{k+1}(x))$ in the sequence $\{\varphi_\ell(x)\}$, $\ell = 1,\ldots, N$ which separate a multiple of 2π. Further, there is a one to one correspondence between any such pair and a negative $z_k(x)$. That there must be a negative $z_k(x)$ is seen from the condition $\varphi_{k+1}(x) - \varphi_k(x) < 2\pi$. Conversely, if there is such a $z_k(x)$, the relation (II-9) implies that $\varphi_k = 2\pi h + \pi$ be followed by $\varphi_{k+1} = 2\pi(h-1)$.

The number of roots smaller than x is then equal to the number of negative terms in the sequence $\{z_k(k)\}$, $k = 1,\ldots,N$. This result is however also a consequence of the fact that $\{u_k(x)\}$ is a Sturm sequence.[32]

For increasing N one introduces the density of $z_k(x)$, $W[z(x), s]ds$, the number of points along the chain for which $z(x)$ is in the interval $[s,s + ds]$. One has then:

$$O(x) = \int_{-\infty}^{0} W[z(x),s]ds \qquad \text{(II-10)}$$

By the argument quoted above, we also introduce

$$W_k\,[z_k(x),s]ds = W_k[z_k(x)]dz_k$$

the number of chains for which the points labeled k have a $z_k(x)$ in the interval [s,s + ds]. To determine W_k, Schmidt considered the set of chains having the same value α at point k. In this set

$$W_k[z_k(x)]dz_k = W_{k-1}[z_{k-1}(x)]dz_{k-1}$$

From relation (II-9) the change of variable z_{k-1} into z_k yields

$$W_k[z_k(x)] = \frac{1}{z_k^2(x)} W_{k-1}[2-x/\alpha - 1/z_k(x)]$$

In the limit $N \to \infty$, W_k tends towards W, for all k. If α_k is an independent random variable with probability P_j and values $\alpha^{(j)}$, we can write

$$W[z(x)] = \frac{1}{z(x)} \sum_{j=1}^{|S|} p_j W[2-x/\alpha^{(j)} - 1/z(x)]$$

from this equation Schmidt obtains W[z] and O(x). He calculated in this way the out of band distribution of electronic states.

Dean[29] considers the general tridiagonal matrix A. The sequence of principal minors of A,

$$\Delta_{j+1}(x) = (\alpha_j - x)\Delta_j(x) - \beta_j^2\Delta_{j-1}(x) \qquad \text{(II-11)}$$

with $\Delta_o(x) \equiv 1$, is a Sturm sequence. A root $\bar{x}$ of $\Delta_j = 0$ separates $\Delta_{j-1}(x)$ and $\Delta_{j-1}(\bar{x})$ with opposite signs. The number of roots of $\Delta_n(x) = 0$ smaller than x is the number of changes of signs in the sequence $\Delta_o, \Delta_1(x),\ldots,\Delta_n(x)$ or the number of negative terms in $\{y_j(x)\}$, where $y_j(x) = A_j + 1/\Delta_j$. Therefore $O(x) = \int_{\infty}^{0} W[y(x),s]ds$, where W is defined

as above. In Schmidt's derivation there is:

$$u_{n+1}(x) = (2 - x/\alpha_n)\, u_n(x) - u_{n-1}(x) \qquad \text{(II-12)}$$

Letting $U_1(x) = 1$ as a normalizing condition, $\{u_k(x)\}$ satisfies the conditions for Sturm sequences and property (II-10) follows.

Relation (II-12) is an ordering of eigenvectors, as pointed out in Ref. 32. Relation (II-11) is an ordering of eigenvalues. $\Delta_n(x)$ and $u_n(x)$ have the same number of zeros.

The previous argument for the determination of W from the probability law of (α_k,β_k) yields here

$$W[y(x)] = \sum_j p_j \frac{\beta^{(j)^2}}{(\alpha^{(j)}-x-y(x))^2}\, W\left[\frac{\beta^{(j)^2}}{\alpha^{(j)}-x-y(x)}\right] \qquad \text{(II-13)}$$

if the random variables are independent.

Schmidt has also considered correlation of neighbors; we apply his derivation to Dean's $W[y(x)]$.

Let $S = (\alpha_1,\beta_1),(\alpha_2,\beta_2)$ be noted by 1,2. Consider next:

$E_j^{(1)}$, the set of chains with value 1 at points j

$E_j^{(2)}$, the set of chains with value 2 at points j

$W_1[y_j(x)]$, the probability distribution of negative $y_j(x)$ over $E_j^{(1)}$

$W_2[y_j(x)]$, the probability distribution of negative $y_j(x)$ over $E_j^{(2)}$

p_{11} the probability that 1 in j-1 be followed by 1 in j

p_{12} the probability that 1 in j-1 be followed by 2 in j, etc.

One has:

$$W_1[y_j(x)] = p_{11}\, W_1[y_{j-1}(x)] + p_{21}\, W_2[y_{j-1}(x)]$$

$$W_2[y_j(x)] = p_{12}\, W_1[y_{j-1}(x)] + p_{22}\, W_2[y_{j-1}(x)] \qquad (II\text{-}14)$$

if the variable y_{j-1} is changed into y_j, each W on the right side has a form similar to right side of Eq. (II-13).

The effect of the correlation is to change (II-13) into a vector relation; when the range of the random variable is infinite, (II-14) is an integral relation.

Numerically however the determination of $O(x)$ is much more accessible by counting the negative elements in $\{y_k(x)\}$ obtained from the recurrence (II-11). Tridiagonal matrices of order 10^5 have been treated in this manner.[33]

Dean[34] has extended the method of Sturm sequences to any symmetric matrices. The idea is to partition the matrix into 4 blocks, whereby the block matrix is tridiagonal

$$A - x\,I = \begin{pmatrix} X & \vdots & y \\ \cdots & \vdots & \cdots \\ y^T & \vdots & z \end{pmatrix}$$

The partitioning can be done in N - 1 ways. However, one of these is found to be the most convenient. The negative eigenvalue theorem (NET) states that the number $\eta(x)$ of negative eigenvalues* of $(A - x\,I)$ is:

$$\eta(x) = \eta(X) - \eta(L)$$

where $\eta(X)$ is the number of negative eigenvalues of X and $\eta(L)$ is the number of negative eigenvalues of

$$L = z - y^T X^{-1} y$$

One recognizes the previous pattern. L is of reduced order; $\eta(L)$ can again be calculated as the sum of 2 contributions, and so on until exhaustion of matrix elements.

Let N_1 be the order of X; if $N_1 = 1$ the number of steps is N-1, however each one involves trivial operations. For $N_2 = 2$, the number of steps is N/2 but the auxiliary calculations grow in importance.

For numerical purposes, the Givens[35]-Sturm procedure competes with the NET. We compare both methods for the case of a matrix A of order N with no zero elements. Givens' method transforms A into a tridiagonal (singly bordered) matrix T by (N-1) (N-2)/2 successive rotations. Each rotation involves 18 (N-k) operations, where k is the index of the line at which the transformation occurs. The frequency distribution is thereafter obtained by counting the negative terms in the continued fractions (II-10) applied to elements of T. If the frequency range is divided in M intervals, there are 4MN additional operations to perform.

The application of the NET requires on the other hand N-1 steps per interval and $2(N-k)^2$ operations per step, where k = 1,..., N.

Comparing the numbers

---

*Number of eigenvalues of A smaller than x.

$$9(N-1)\,(N-2)\sum_{k=1}^{N}(N-k) + 4MN = 4.5\,N(N-2)(N-1)^2 + 4MN$$

and

$$2MN\sum_{k=1}^{N}(N-k)^2 = 0.33\,N^2(2N-1)(N-1)M$$

we find that Givens' procedure is more advantageous, especially since M is only proportional to the first power of N.

In most problems the nonzero elements are scarce and somewhat ordered diagonally. In this respect, Dean and Bacon[34] pointed out that the multiplication may involve less operation than $(N-k)^2$ at step k, for certain types of matrices.

In applying both methods, we found that Givens' transformation gives the result faster. This was however to be expected since we did not take special provision for zero elements.

The advantage in the treatment of Jacobian matrices is that the elements need not be stored in memory. They are generated as the line progresses. If this procedure could be reproduced at least partially in the application of the NET or in Givens' transformation, the effects of complicated orderings could be obtained for more realistic models of the chain.

Givens' method provides a direct proof that the degenerate modes are counted in the spectrum. The roots of A are the roots of T and a root of a Jacobian matrix is multiple only if some $a_{ii+i} = 0$. In that case we have the polynomials 1, $(a-x)$,$(a-x)^2$, etc., where for $x > a$, there

are 2 changes of sign.

The problem of the frequency spectrum has been solved by a perturbation method, where the parameter is the concentration of defects and where the modes are labeled by the phonon propagation vector k. Langer[36] pointed out that this technique has the advantage that it yields information on the phonon lifetime and the attenuation coefficient of the localized modes. The assumption here is that the phonon is a meaningful object of measurement, since it has a pseudo momentum k; and a "measurement[37] that fixes k will yield a spread in frequency." Calculations were made for mass defects[36] and spring impurities,[37] which give the width Γ_k. Also an experiment was suggested to measure the lifetime of an approximate localized mode.[30] The perturbation method is restricted to small defect concentration. We shall however consider disorders such that the pseudo momentum k is no more meaningful. Meaningful experiments are then observation of the spectrum and thermodynamical measurements, where only the distribution of the modes is relevant.

The moments method has also been applied to order-disorder problems. The usual objection to this method is that our out of band modes and singularities in general do not emerge clearly. However, it was pointed out that the Padé approximate of the moment expansion could yield precise information on the location of these singularities. (See also Refs. 38, 39, and 40 kindly communicated by Professor L. Cesari.)

In the next chapters we use the Sturm sequence method and its application in the NET and Givens' transformation.

The third step in the standard procedure consists of adjusting the matrix element probability law to conform to an observed spectrum. Here the matrix elements depend on the conformation of the chain (see Chapter III). Consider a sequence of carbon atoms j = 1,..,N. We say that the carbon atom j is in transconfiguration if it is in the plane of its 3 predecessors. Otherwise it is in gauche configuration. The conformation is then the sequence TG, etc.; such a sequence is called diastereosequence when the equivalence relation is tacticity.

We start by enumerating types of order along linear chains, as given in the literature. Thereafter we consider the relation between a particular order and the vibrational frequency distribution. Let N_o be the number of T's and N_1 of G's. The concentration of T's is then $p_o = N_o/(N_1 + N_o)$.

For $p_o = 0.5$, the short range[41] order parameter σ_B is defined from the probability P_s of occurrence of unlike pairs as

$$\sigma_B = 2 P_s - 1 \qquad \text{(II-15)}$$

The value $\sigma_B = 0$ indicates disorder. $\sigma_B < 0$ indicates a clustering of T's (and consequently of G's). $\sigma_B > 0$ indicates a tendency for alternation of T and G. The notion of short range order can also be extended to concentrations $P_o \neq 0.5$.

The sequence is called Markovian of order n_o, if n_o is the smallest n such that the conditional probability for configurations at any j is independent of configurations beyond $j \pm n$. A formulation[42] of this con-

dition is that for all m,n

$$P_{n,n_o}\left\{U^{(n)}|V^{(n_o)}\right\} \equiv P_{n,n_o+m}\left\{U^{(n)}|V^{(n_o)}\ W^{(m)}\right\} \qquad \text{(II-16)}$$

where $U^{(n)}$ is a sequence of n configurations, $V^{(n_o)}$ an adjoining sequence, $V^{(n_o)}\ W^{(m)}$ the joint sequences $V^{(n_o)}$ and $W^{(m)}$; $P_{n,n_o}\{U^{(n)}|V^{(n_o)}\}$ is the conditional probability that a given $V^{(n_o)}$ is followed by $U^{(n)}$.

A sequence of n_o vertices of the chain is called a cell; a sequence of configurations $U^{(n_o)}$ is called a state of the cell.

Properties of Markov chains are derived from the transfer matrix τ relating the states of 2 adjoining cells. The matrix elements of τ are the conditional probabilities mentioned above for the case $n = n_o$; they are noted P_{ij} where i,j label one of the 2^{n_o} states. The states of 2 cells r -apart are related by:

$$U^{(j+r)} = \tau^r\ U^{(j)} \qquad \text{(II-17)}$$

where $U^{(j)}$ is written in form of a 2^{n_o} components vector. As n increases $U^{(j+u)}$ tends towards the eigenvector t associated with the eigenvalue $\lambda = 1$ if λ is simple and of greatest module. A sufficient condition for this property is that τ be irreducible and primitive (theorem[43] of Perron-Frobenius). A matrix is primitive (or 1-cyclic) if the greatest common denominator of the length of all cycles

$$p_{j\ell_1},\ p_{\ell_1\ell_2},\ldots,p_{\ell_q j} \qquad \text{for any } q = 1,\ldots,N;\ \text{any } j = 1,\ldots,N.$$

of nonzero elements is unity. If the matrix is irreducible and p cyclic, there are p eigenvalues of module 1. In this case, the order depends on an initial state. This is called long range order.

Long range order based on the degeneracy of $\lambda = 1$ plays an important role in the theory of phase transition (Ising model). Phase transitions however are only considered at the limit $n_o \to \infty$, ruling out one-dimensional problems.

Long range order associated with finite matrices and multiplicity in module has not been considered as a meaningful model. A requirement for degeneracy in module is, for instance, that all diagonal elements of the transfer matrix be zero (otherwise the g.c.d. is 1) and there is no reasonable justification to introduce this value. Also, transitions from order to disorder are not associated with one-dimensional models (with the exception of molecular field theory).

For small n_o, a component t_j is easily calculated as the cofactor of any matrix element in the j column of $(I-\tau)$. The expansion of the determinant of this matrix is namely:

$$\sum_j \tilde{p}_{ij} C_{ij} = 0 \quad , \quad \text{for all } i$$

where $\tilde{p}_{ij}$ is the (i,j) element of $(I-\tau)$. The component t_j is interpreted as the rate of occurrence of the state labeled j in a cell. For example, with $n_o = 1$, if $p_{11} = 1 - AM$ is the conditional probability that T follows T, $p_{21} = 1 - BM$ that T follows G, we have:

$$
\begin{aligned}
t_1 &= \alpha(1\text{-}BM) \qquad \text{where } \alpha \text{ is a normalization factor.} \\
t_2 &= \alpha\, AM \\
N_o/N_1 &= (1\text{-}BM)/AM \\
p_o &= N_o/(N_1 + N_o) = (1\text{-}BM)/(1\text{-}BM+AM) \\
p_1 &= N_1/(N_1 + N_o) = AM/(1\text{-}BM+AM)
\end{aligned}
\qquad \text{(II-18)}
$$

The rate of occurrence of doublets TT, GG, etc., is given by multiplying $p_o(p_1)$ by the appropriate matrix element.

For $N_o = 2$, there are four states: TT, GG,TG, GT. When n_o increases, the number of matrix elements becomes prohibitive (namely 2^{2n_o}). It is however possible to construct a reduced transfer matrix τ_R with knowledge of the conditional probabilities that a state is followed either by a T or a G configuration. The order of τ_R is still 2^{n_o}, but the number of nonzero elements is only 2^{n_o+1}. The relation between τ and τ_R is

$$\tau = \tau_R^{2^{n_o}}$$

The case $n_o = 0$ describes the random or Bernoulli process. $n_o = 1$ is called simple Markov order. When for $n_o = 1$, $p_{11} = p_{21}$ (which implies $p_{12} = p_{22}$) the simple Markov order degenerates into a Bernoulli process. The case $p_{11} = p_{22}$ is confusing for both interpretations are valid. There is an example in the literature where this order is random (Bernoulli) for some authors and simple Markov for others. It concerns the interpretation of the famous Bovey and Tiers report[44] that free polymerization of methyl-methacrylate is describable by a single parameter α,

whereas anionic polymerization is not. Consider the sequence[42] of methyl groups:

$$\begin{bmatrix} H & H \\ C & C \\ H & R \end{bmatrix} - \begin{bmatrix} H & H \\ C & C \\ H & R \end{bmatrix} - \begin{bmatrix} H & R \\ C & C \\ H & H \end{bmatrix} - \begin{bmatrix} H & H \\ C & C \\ H & R \end{bmatrix}$$

They can be labeled according to the stereoconfiguration of each group

$$\ell \quad \ell \quad d \quad \ell$$

if we assume that the conditional probability that ℓ follows ℓ is α, that d follows d is α, that ℓ follows d is $1 - \alpha$, and that d follows ℓ is $1 - \alpha$, the process is indeed Markovian of order 1 with the transfer matrix (Price[45])

$$\tau = \begin{pmatrix} \alpha & 1 - \alpha \\ 1-\alpha & \alpha \end{pmatrix}$$

If we introduce the tacticity as a relationship between neighboring groups, the same sequence is written as

$$1 \quad s \quad s$$

where I (for isotactic) indicates that the 2 groups have some stereoconfiguration and S (for syndiotactic) that the two groups have opposite configurations. The rate of occurrence of I is α, the rate of occurrence of S is $1 = \alpha$, the process is of the Bernoulli type (Coleman[42]). (See also Figure II-1.) We recognize in $1-\alpha$ the parameter σ_B in Behte's short range order. This process is nothing but a degenerate simple Markov or Bernoulli process.

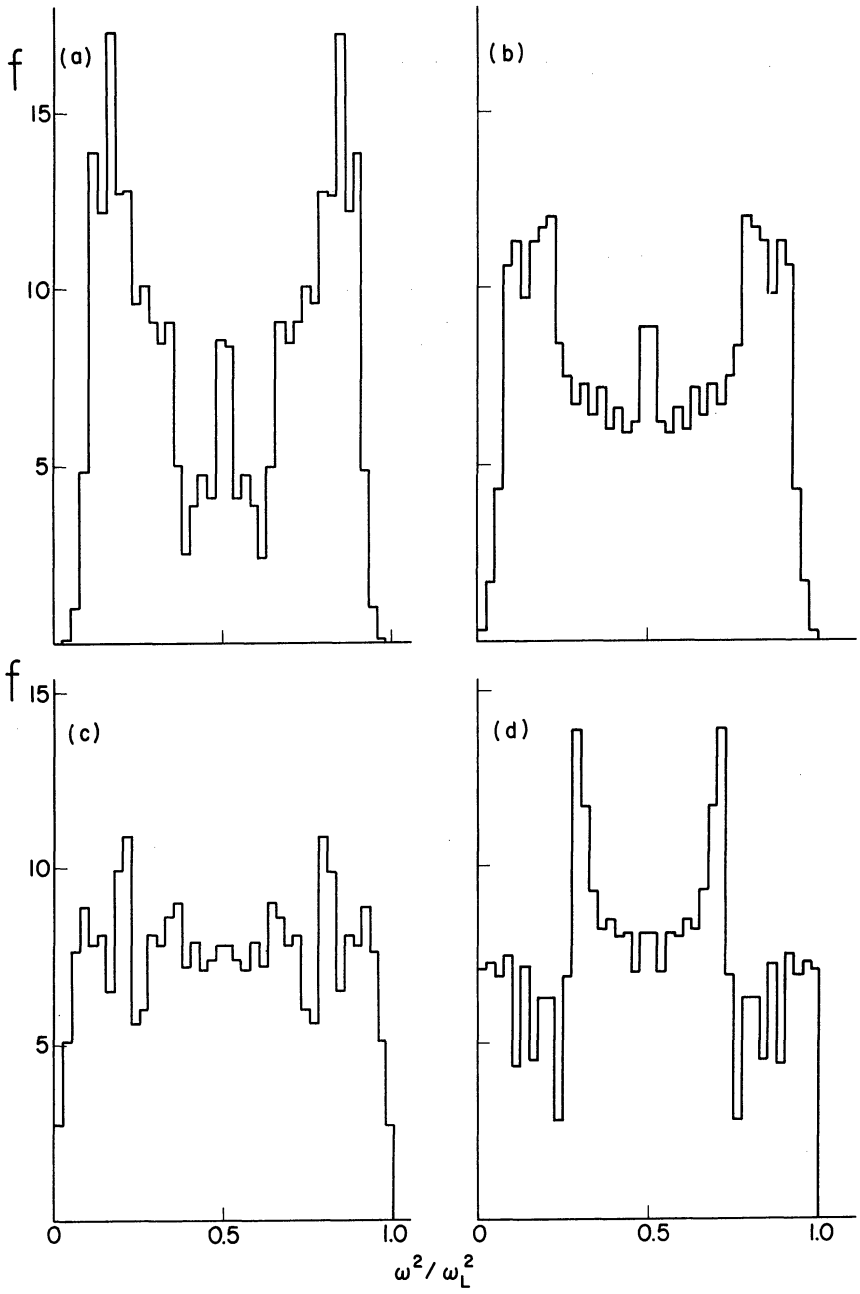

Figure II-1. Squared frequency distribution for simple chains with equal concentration of T and G configurations. The short range order parameter σ is defined in (II-15); AM, BM are the transfer matrix elements or conditional probabilities as defined in (II-18). The order of the T, G sequence is simple Markovian; the order of the complementary sequence (s,d) where s indicates similar and d dissimilar pairs, is however random (Bernoulli). Compare with the random T, G distribution on Figure III-6, Chapter III.

(a) σ = 0.6 ; AM = 0.8 ; BM = 0.2
(b) σ = 0.2 ; AM = 0.6 ; BM = 0.4
(c) σ = -0.2 ; AM = 0.4 ; BM = 0.6
(d) σ = -0.6 ; AM = 0.2 ; BM = 0.8

$N_o/N_1 = 1$; $n_o = 1$

The concept of short range order is readily extended to a nondegenerate Markov process. We have namely:

$$\alpha = p_o\, p_{o1} + p_1\, p_{1o}$$

for a Bernoulli process:

$$\bar{\alpha} = 2\, p_o(1-p_o)$$

The short range order is defined as:

$$\sigma_B = 2(\alpha - \bar{\alpha})$$

Anticipating the results of Chapter III we count the number of the classes of states, for a given n_o, that are invariant under circular permutation. From the cycle index, we get typically:

$$\kappa(n_o = 4) = \frac{1}{4}\,(x_1^4 + x_2^2 + 2x_4^1)_{x=2} = 6$$

the total number of states being $2^4 = 16$.

For the first few integers we have:

n_o	$\kappa(n_o)$	2^{n_o}
1	2	2
2	3	4
3	4	8
4	6	16
5	8	32
6	18	69
7	20	128

We shall note that the normal frequency distribution associated with a

Markovian order n_o is approximatively decomposed into $\kappa(2n_o)$ frequency distributions components corresponding to each class.

If one distinguishes between even and odd vertices of the chain, the Bragg-Williams long range order parameter S is defined as

$$S = 2 P_L - 1$$

where P_L is the probability that T belongs to an even vertex. $S = 0$ is a random (Bernoulli) process. $S > 0$ indicates a preference for even, and $S < 0$ a preference for odd vertices.

Such a long range order is, for example, meaningful in a lattice of even sites and a superlattice of odd sites. It indicates the placement preference of (T,G) with respect to the 2 frames of reference. This interpretation may not agree[27] with the ordering of conformations. However the reference frame need not be geometric: Coleman and Fox[44] have described a polymerization mechanism in which a "growing chain has two reactive states, capable of adding a monomer each with its own stereospecificity." Here P_L would be the probability that T is associated with one of these states. This mechanism is non Markovian. It provides an interpretation anionic polymerization, recognized as being of a non Bernoulli type.

The treatment of semi crystalline polymers by Tobolsky and Gupta[8] uses the same concept. The chain is in one of the two states—crystalline or amorphous; there are here, however, two independent parameters:

α , probability of persistence in a crystal.

p , probability that it escapes into an amorphous region.

These authors describe their mechanism as Markovian, they obtain crystallinity percentage, average sequence length in crystalline and in amorphous region as a function of (α, p).

An obvious example of non Markovian order is the non-self-intersecting chain. If a chain satisfies the volume exclusion, the number of ways for adding a new link decreases as its length grows; in fact "almost all configurations[10] permitted by the unrestricted theory are ruled out."

The evaluation of the numbers C_n of such non-self-intersecting walks of n steps has at present only been approximately determined. It has been proven that the limit

$$\mu = \lim_{n\to\infty} \frac{C_{n+1}}{C_n} \qquad \text{exists.}$$

Temperley[10] has conjectured that μ is related tothe "corresponding limiting ratio to the terms in the expansion of the Ising partition function" (with the notations of Ref. 16)

$$Z(T) = 2^N (\cosh K)^{NC/2} \sum_r n(r) \tanh^r(K)$$

where $K = J/kT$. It was asserted that

$$\mu = \lim_{r\to\infty} \frac{n(r+1)}{n(r)} = \coth K_c$$

where T_c is the Curie temperature. In a discussion of the Faraday Society, Fisher[47] showed however that because of the contribution of S shaped walks

$$\mu > \coth K_c$$

The issue here is to determine how closely the results of the Ising model fit to the problem of nonintersecting chains.

Another problem is to decide whether a chain occupies all possible sites. If the volume exclusion is satisfied, voids may appear. In the graph theory,[48] a walk going exactly through each vertex is a Hamiltonian circuit. Whether a graph process is such a circuit depends on the degree of each vertex. A lattice is crystalline when these degrees are equal. Otherwise the lattice is amorphous. The condition that a set of vertices form a lattice is that[27]

$$\frac{\overline{N^2(v)} - (\overline{N(v)})^2}{N(v)} = c$$

is independent of the regular[27] volumes v.

Coleman and Fox[42] pointed out that in the absence of information about order, it is appropriate to derive such characteristics as concentrations of T, G and departure from randomicity, from calculations that do not imply Markovian order. Statistics of non Markovian chains are also valid for Markovian order. In view of Chapter III, we shall use their theorems II and III: we consider successively closed sequences of G's and T's. The quantity of interest is, for the first sequences:

$$f_n = P_{n,1}\{TG^{n-1}|T\}$$

which is the probability that the recurrence time for T has length n. The mean recurrence time is $\chi(T) = \sum_{n=1}^{\infty} n f_n$. Theorem II states:

$$\chi(T) = \frac{1-q}{p_o}$$

where $q = \lim_{n\to\infty} p_n\{T^n\}$, assumed to be zero, and where p_o is the occurrence probability of T. Theorem III determines the mean length $\mu(T)$ of closed sequences of T. It states:

$$\mu(T) = \frac{p_o - q}{p_1 - p(GG)}$$

where p_1 is the probability for occurrence of G, and p(GG) for occurrence of the doublet GG. For a Bernoulli process, $\mu_B(T) = 1/p_1$. Coleman and Fox define the persistence ratio,

$$\rho = \frac{\mu(T)}{\mu_B(T)}$$

and the "statistical after effect" $\rho - 1$, which gives a measure of the departure from randomicity.

Given a certain order, the above formula allows the calculation of characteristics such as:

- concentration of singlets T, G
- concentration of doublets TT, TG, etc.
- concentration of multiplets.

In the inverse problem one infers order from the knowledge of these characteristics. There are known techniques to determine the latter from a frequency distribution, or other observables. There is a smallest number of characteristics required to specify order. We consider here the example of Bovey and Tiers[44]; the rates R of occurrence of the following triplets of α methyl groups are given:

$$R_1 \left\{ \begin{matrix} \ell\ell\ell \\ + \\ ddd \end{matrix} \right\} \quad ; \quad R_2 \left\{ \begin{matrix} \ell d\ell \\ + \\ d\ell d \end{matrix} \right\} \quad ; \quad R_3 \left\{ \begin{matrix} \ell dd + dd\ell \\ \\ +\ell\ell d + d\ell\ell \end{matrix} \right\}$$

where ℓ, d are the 2 configurations of a group. An identical representation of this table is:

$$R_1 \left\{ \begin{matrix} I\ I \\ + \\ I\ I \end{matrix} \right\} \quad ; \quad R_2 \left\{ \begin{matrix} S\ S \\ + \\ S\ S \end{matrix} \right\} \quad ; \quad R_3 \left\{ 2SI + 2IS \right\}$$

where I, S indicate the tacticity of a doublet. To infer that the (I,S) sequence is random (Bernoulli) the rates must be in the proportion

$$R_1 = \sigma^2 \quad ; \quad R_2 = (1-\sigma)^2 \quad ; \quad R_3 = 2(\sigma-\sigma^2)$$

This was verified for methyl methacrylate polymerized from free radical monomers. The data of anionic polymerization did not fit with this pattern. It was therefore concluded that the (I,S) sequence is not of the Bernoulli type. Coleman and Fox argue that the data are not sufficient to decide whether the order is simple Markov or not. Indeed if the transition matrix is

$$\tau = \begin{pmatrix} p_{11} & p_{12} \\ p_{21} & p_{22} \end{pmatrix}$$

R_1 yields p_{11}; R_2, p_{22}; R_3, $p_{12} + p_{21}$.

If the order is simple Markovian,

$$p_{12} = 1-p_{11} \quad ; \quad p_{21} = 1-p_{22} \quad ; \quad p_{12} + p_{21} = 2-p_{11}-p_{22}$$

It is seen that R_3 could be equal to $2-R_1-R_2$ without p_{21} and p_{12} satisfying the above requirements. Hence nothing more can be inferred.

If a process is known to be Markovian of order n_o, $(2^{n_o} - 1)\, 2^{n_o}$ elements are to be specified. Otherwise the $2^{n_o} \times 2^{n_o}$ elements are needed to infer that the process is Markovian of order n_o.

Dean[49] has given a method to derive rates of occurrence of multiplets from the harmonic frequency distribution of simple systems. In this method we suppose, for example, that the concentration of T is smaller than the concentration of G, and that a T yields out of band modes. From the property of ordering of out of band modes in terms of typical T, G sequences, a relation is established between areas of the frequency distribution and rate of occurrence of these sequences. In Chapter III we use the Green's function method to perform the identification. Determination of some transfer matrix elements from the frequency distribution is then possible.

CHAPTER III

FREQUENCY DISTRIBUTIONS OF SIMPLE CHAINS

Here we consider a sequence of mass points $j(j=1,\ldots,N)$ joined by bonds of length ℓ. The bonds are not necessarily aligned. The complement of the angle $(j-1, j, j+1)$ is the configuration of $(j-1, j, j+1)$ and is noted ψ_j. The sequence

$$\{\psi_j\} \quad , \quad j = 1,\ldots,N.$$

is the conformation of the chain. A special case is the regular conformation $\psi_j \equiv \tilde{\psi}$, for all j. When $\tilde{\psi} = 0$, the chain is extended. Notice that the conformation does not specify completely the structure of a chain since a configuration ψ_j is invariant under a rotation about the j-1, j axis.

We suppose that the chain is maintained in a given conformation by a potential V. If we insert springs of force constant γ between each successive pair, a longitudinal vibration can take place. We may also imagine that the springs act perpendicularly to the bonds, in which case the vibrational motion is transverse.

Simple chains provide a model[50] for the harmonic activity of long molecules in the frequency range where the grouping of several atoms into one, is valid. The frequency distribution for regular conformations with cyclic boundaries is given by the inverse square root law. The

squared frequencies for regular conformation have been related to the zeros of Gegenbauer[50] polynomials, where the result is applicable to free and fixed boundaries. In general the squared frequency distribution is identical[51] to the eigenvalue distribution of a tridiagonal or singly bordered matrix. Ordering of eigenvalues of such matrices is easily performed on a digital computer.[49] It leads to the eigenvalue distribution as defined in Chapter II. Calculations have been made for the isotope and spring defects on a regular chain. Calculations as a function of conformation seem however not to have appeared in the literature (except in Ref. 52).

We first consider qualitative results from a regular chain with a single "defect," i.e., a value $\psi_j \neq \tilde{\psi}$; this is called a singly folded chain. It is natural to distinguish the cases where the reference value is $\tilde{\psi} = 0$ from the case $\tilde{\psi} \neq 0$; namely, in the first, the defect value $|\psi_j|$ can only be greater than $\tilde{\psi}$, whereas in the second $|\psi_j|$ can be greater or smaller than $\tilde{\psi}$. We shall see that the absence or presence of out of band modes is related to this distinction.

The case $\tilde{\psi} = 0$ is easily solved. Figure III-1 shows the dynamical matrix A in Cartesian and in internal displacements coordinates. For cyclic boundaries A^i is of order one less per fold than A^c; the extra mode corresponds to a zero frequency motion in the y-direction.

If $M_o(\omega^2) = A_o^i - \omega^2 I$, where A_o^i is the dynamical matrix of the extended structure with cyclic boundary conditions, there corresponds to the singly folded chain a matrix M which, according to the Green's function

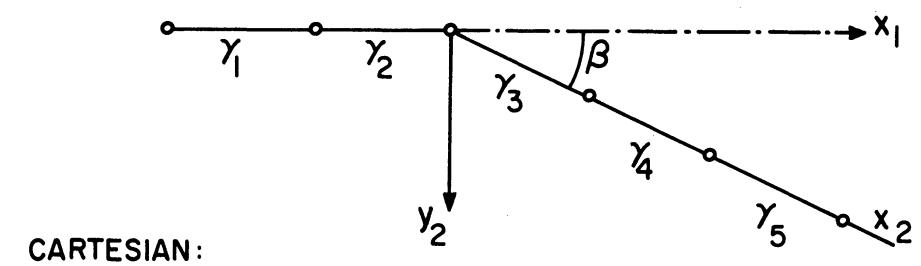

CARTESIAN:

$$A^c = \begin{vmatrix}
\gamma_1 & -\gamma_1 & & & & & \\
-\gamma_1 & \gamma_1+\gamma_2 & -\gamma_2 & & & & \\
 & -\gamma_2 & \gamma_2+\gamma_3\cos^2\beta & -\gamma_3\cos\beta & 0 & +\gamma_3\cos\beta\sin\beta & \\
 & & -\gamma_3\cos\beta & \gamma_3+\gamma_4 & -\gamma_4 & -\gamma_3\sin\beta & \\
 & & 0 & -\gamma_4 & \gamma_4+\gamma_5 & 0 & -\gamma_5 \\
 & & +\gamma_3\cos\beta\sin\beta & -\gamma_3\sin\beta & 0 & \gamma_3\sin^2\beta & 0 \\
 & & & & -\gamma_5 & 0 & \gamma_5+\gamma_6 \quad -\gamma_6 \\
 & & & & & & -\gamma_6 \quad \text{etc.}
\end{vmatrix}$$

INTERNAL:

$$A^i = \begin{vmatrix}
2\gamma_1 & -\gamma_2 & & & & \\
-\gamma_1 & 2\gamma_2 & -\gamma_3\cos\beta & & & \\
 & -\gamma_2\cos\beta & 2\gamma_3 & -\gamma_4 & & \\
 & & -\gamma_3 & 2\gamma_4 & -\gamma_5 & \\
 & & & -\gamma & 2\gamma_5 & \\
 & & & & \text{etc.} &
\end{vmatrix}$$

$$B = \begin{vmatrix}
-1 & 1 & & & & & \\
 & -1 & 1 & & & & \\
 & & -\cos\beta & 1 & & \cdots & -\sin\beta \\
 & & & -1 & 1 & & \\
 & & & & -1 & 1 & \\
 & & & & & \text{etc.} &
\end{vmatrix}$$

Figure III-1. Dynamical matrix for the harmonic activity of a simple chain with a single fold, in Cartesian (A^c) and in internal (A^i) displacement coordinates. The B matrix transforms the Cartesian displacement vector y into the internal displacement vector ℓ. The equations of motion are given in (IV-1). The angle is noted β instead of ψ_j in view of later application.

method,[53] is written as:

$$M(\omega^2) = M_o(I + M_o^{-1} D)$$

The frequencies are the roots of:

$$|I + M_o^{-1}(\omega^2)D| = 0 \qquad \text{(III-1)}$$

The "defect" matrix has the form

$$D = \begin{pmatrix} \vdots & \vdots \\ \cdots 0 & d_{j-1,j}\cdots \\ \vdots & \\ \cdots d_{j,j-1} & 0\cdots \\ \vdots & \vdots \end{pmatrix}$$

where

$$d_{j-1,j} = d_{j,j-1} = \gamma_t(1 - |\cos \psi_j|) \qquad \text{(III-2)}$$

The elements of the matrix M_o^{-1} are the Green's function of the extended conformation; they are written

$$M_{o\ ij}^{-1} = g^{(n)} \quad , \quad n = |i-j|$$

In this case:

$$g^{(n)} = -\frac{\text{cotg } N\theta/2}{2\ \gamma_b \sin\theta} \cos n\theta - \frac{\sin|n|\theta}{2\gamma_b \sin\theta}$$

$$\omega^2/\omega_L^2 = \sin^2\theta/2 \quad ; \quad \omega_L^2 = 4\gamma/M$$

For the extended structure the squared frequency distribution is:

$$G_o = 1/\omega_L \, \omega(1-\omega^2/\omega_L^2)^{1/2} \qquad \text{(III-3)}$$

A single fold introduces a correction to the squared frequency distribution of the form (Figure III-2)

$$\Delta G = f\, G_o - 1/N\,(\delta(\omega^2-\omega_L^2) + \delta(\omega^2)) + \begin{cases} 0 \;, & \nu < 0 \\ \frac{2(1+\nu)}{N}\,\delta(\omega^2-(\omega^2/2)(1+(1+\nu/2)(1+\nu)^{-1/2})), & \nu > 0 \end{cases}$$

so that the squared frequency distribution of a singly folded chain is:

$$G = G_o + \Delta G$$

where $f = (1+\nu/2)\,\nu/N\pi(\nu^2 + 32\,(\omega^2/\omega_L^2)(1+\omega^2/\omega_L^2))$

and $\nu = \cos^2 \psi_j - 1$

hence a fold from the extended chain connot produce an out of band (or localized) mode. Its effect is to attenuate the transmission of the motion by a factor proportional to $|\cos \psi_j|$. When ψ_j reaches $\pi/2$, the two half chains are independent and the defect is analogous but not equivalent to the infinite mass isotope. The difference lies in the boundary condition.

Brout and Visscher[30] have found an "approximate" localized state for the very heavy isotope case, which decays into the continuum at a

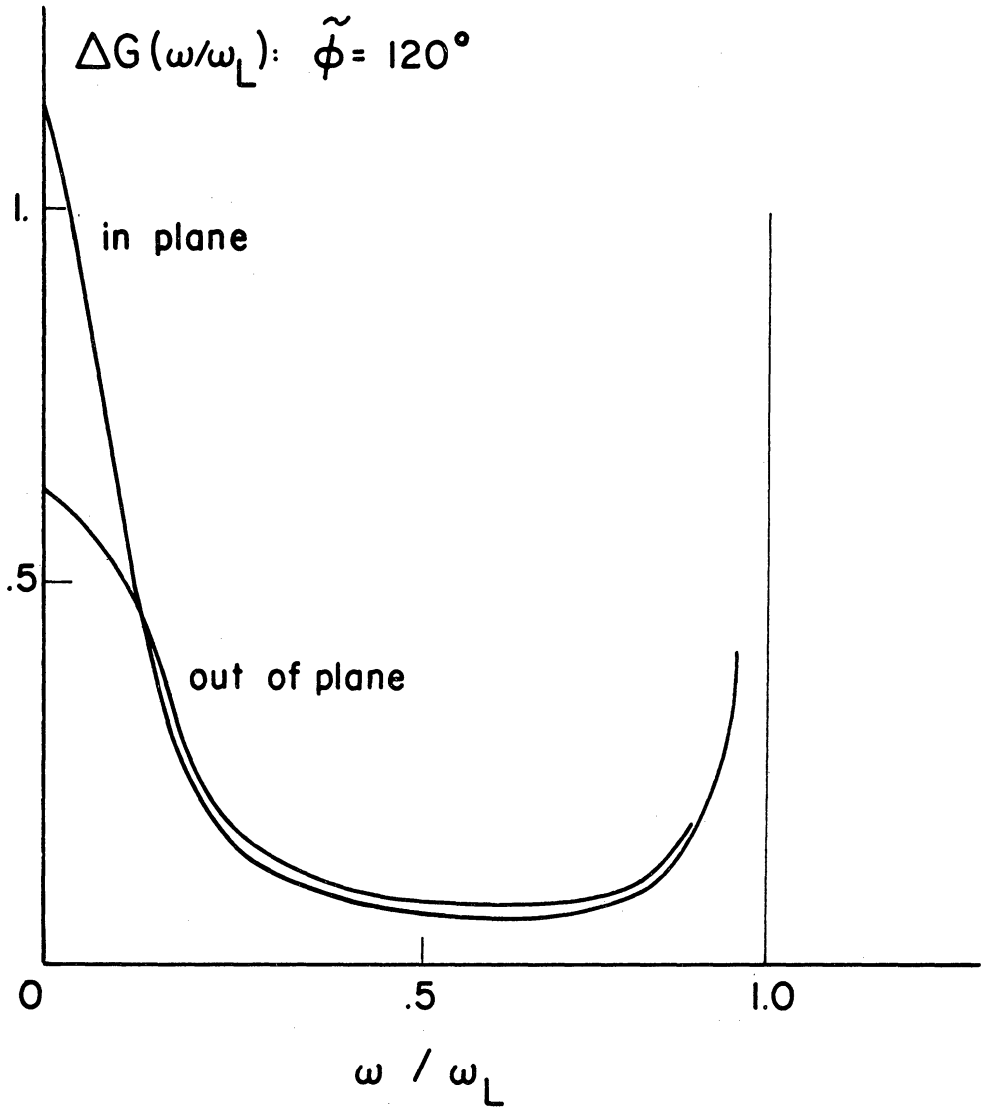

Figure III-2. Correction to the frequency distribution for a single fold, calculated by the Green's function method. The exact normalization of these curves is given by Eq. (III-4).

rate slow enough to be observed. It corresponds to a complex root

$$\omega_o + i\epsilon$$

of the determinantal equation

$$|I + M_o^{-1} D| = 0 \qquad \text{at the limit } N \to \infty .$$

There is a similarity between the heavy isotope and the fold defects in the aligned chain. The determinantal equation for the latter is written as

$$(1 + dg(1))^2 - d^2 g(0) = 0$$

where $d = d_{j-1,j}$

$$d^2(g^2(1) - g(0)) - 2d\, g(1) + 1 = 0$$

$$d_{\pm} = (g(1) \pm g(0))^{-1}$$

Inserting the definition of d and g(n), we get:

$$(\cos\theta \pm 1)\frac{\text{Cotg } N\theta/2}{2\sin\theta} = \left(\frac{1}{1-\cos\psi_j} - \frac{1}{2}\right)$$

$$\left.\begin{aligned} -\epsilon_f \cot g\, \theta/2 &= \operatorname{tg} N\theta/2 \\ \epsilon_f \operatorname{tg}\, \theta/2 &= \operatorname{tg} N\theta/2 \end{aligned}\right\} \qquad \text{(III-5)}$$

where $\epsilon_f = \dfrac{\cos\psi_j - 1}{\cos\psi_j + 1}$ (III-6a)

For the mass defect, the determinantal condition reduces to[54]:

$$\epsilon_m \operatorname{tg} \Theta/2 = \operatorname{tg} N\Theta/2 \qquad \text{(III-7)}$$

where $$\epsilon_m = 1 - M'/M \qquad \text{(III-6b)}$$

The sharp resonance in the continuum reported by Brout and Vischer[30] would be observed for values of ϵ_m lower or equal to -25. From (III-6a) it is seen that ϵ_f cannot be lower than -1. Hence we argue that the effect of a single fold in the extended conformation is not observable by a resonance as in the case of the very heavy isotope.

Using the transformation[55]

$$\omega^2 = \frac{\omega_L^2}{2} (2 - \xi - \xi^{-1})$$

the determinantal condition for the isotope defect is then:

$$1 - \epsilon_m (2 - \xi - \xi^{-1}) (\xi - \xi^{-1})^{-1} = 0 \quad , \quad |\xi| < 1$$
$$1 - \epsilon_m (2 - \xi - \xi^{-1}) (\xi - \xi^{-1})^{-1} = 0 \quad , \quad |\xi| > 1$$

for the fold defect it is:

$$1 + \nu\, \xi(\xi - \xi^{-1})^{-1} = 0 \quad , \quad |\xi| < 1$$
$$1 + \nu\, \xi(\xi - \xi^{-1})^{-1} = 0 \quad , \quad |\xi| > 1$$

We note that in neither case is there a complex root in the physical ξ sheet.

We now turn to the more general case $\tilde{\psi} \neq 0$; the two half chains may decrease or increase their fold angle as reflected by the sign of $\psi_j - \tilde{\psi}$. The dynamical matrix is:

$$
\begin{array}{ccccccc}
\ldots 2\gamma & -\gamma\cos\tilde{\psi} & & & & & \\
-\gamma\cos\tilde{\psi} & 2\gamma & -\gamma\cos\tilde{\psi} & & & & \\
 & -\gamma\cos\tilde{\psi} & 2\gamma & -\gamma\cos\psi_j & & & \\
 & & -\gamma\cos\psi_j & 2\gamma & -\gamma\cos\tilde{\psi} & & \\
 & & & -\gamma\cos\tilde{\psi} & 2\gamma & \ldots & \\
 & & & & -\gamma\cos\tilde{\psi} & \ldots &
\end{array}
$$

where ψ_j is the "defect" value.

We use again relation (III-1). The Green's function, however, has an additional factor cos $\tilde{\psi}$ in the denominator which modifies the integration path given in Mahanty, et al.[55]

The Fourier transform of the squared frequency distribution is determined in this reference from:

$$\Delta F(\alpha) = \int_C e^{i\alpha\omega^2} \, d \log |I + M_o^{-1} D| \qquad \text{(III-8)}$$

The appropriate change of variable is here:

$$\omega^2 = (\omega_L^2/4)\,(2-\cos\tilde{\psi}(\xi - \xi^{-1})) \qquad \text{(III-9)}$$

The correspondence is given in Figure III-3 and Table III.

An out-of-band mode above the continuum arises from the Γ_5 integration, and another below the continuum arises from the Γ_6 integration. Thus, the Green's function is

TABLE III

CORRESPONDENCE BETWEEN ω AND ξ

ω^2	ξ	Contour
0 to $(\omega_L^2/2)$ $(1 - \cos\tilde{\psi})$	$1/\cos\tilde{\psi} \pm (1/\cos^2\tilde{\psi} - 1)$ to 1	Γ_6, Γ_7
$(\omega_L^2/2)$ $(1 - \cos\tilde{\psi}\cos\Omega)$	$e^{i\Omega}$; $0 \leq \Omega \leq \pi$	Γ_1, Γ_2, Γ_3, Γ_4
$(\omega_L^2/2)$ $(1 + \cos\tilde{\psi})$ to ∞	-1 to 0^-	Γ_5

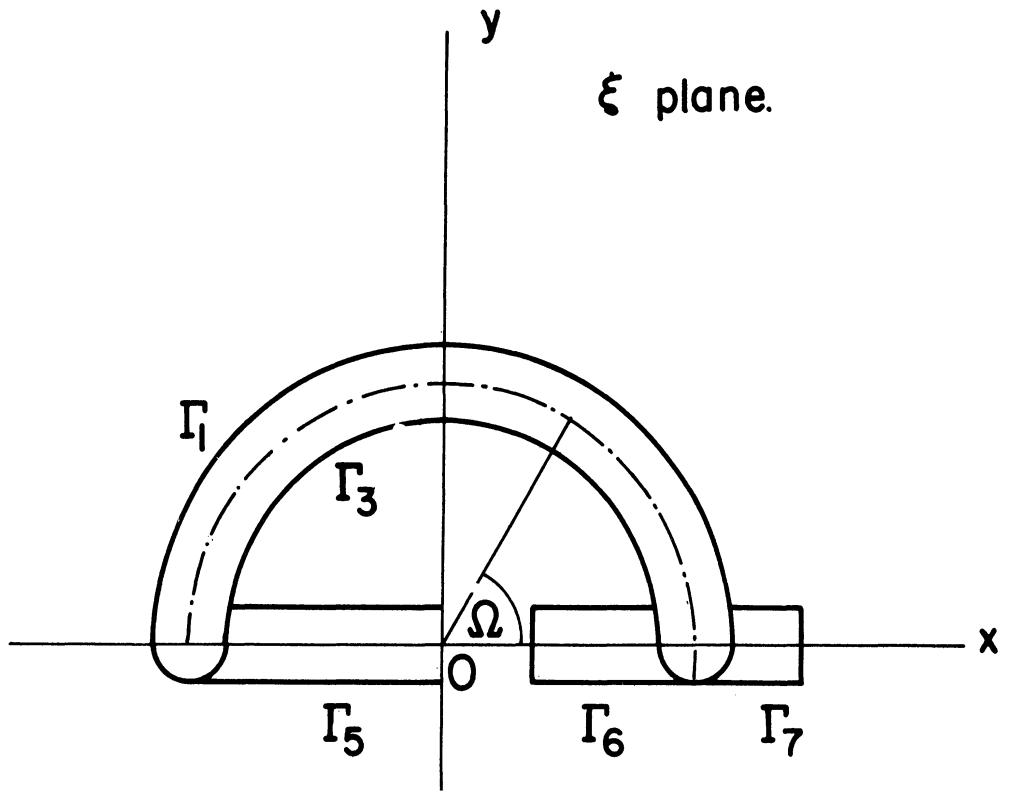

Figure III-3. Integration contour in the ξ plane to determine the density of modes ω (Eq. (III-9)). The difference between this and the isotope problem is in the contribution of a portion of the positive real axis.[55]

$$g(n) = \begin{cases} -\frac{1}{\gamma \cos\tilde{\psi}} \frac{\xi^n}{\xi - \xi^{-1}}, & |\xi| < 1 \\ -\frac{1}{\gamma \cos\tilde{\psi}} \frac{\xi^{-n}}{\xi^{-1} - \xi}, & |\xi| > 1 \end{cases}$$

The squared frequency distribution of the unperturbed chain is

$$G_o = \frac{1}{\pi\omega_L^2} (\cos^2\tilde{\psi} - (1-2\omega^2/\omega_L^2)^2)^{-1/2}$$

The additional term due to the defect is

$$\Delta G = fG - \frac{1}{2N} (\delta(\omega^2-\omega_L^2(1+\cos\tilde{\psi}) + \delta(\omega^2-\omega_L^2(1-\cos\tilde{\psi})))$$

$$+ \begin{cases} 0, & \mu < 0 \\ \frac{2(1+\mu)}{N} \left[\delta(\omega - \frac{\omega_L^2}{2} (1 + \cos\tilde{\psi}(1+\mu/2)(1+\mu)^{-1/2}) \right. \\ \left. \quad + \delta(\omega - \frac{\omega_L^2}{2} (1-\cos\tilde{\psi}\ (1+\mu/2)(1+\mu)^{-1/2}) \right], & \mu > 0 \end{cases}$$

$$f = -(1+\mu/2)2\mu/N(\mu^2+(8/\cos^2\tilde{\psi})(\cos^2\tilde{\psi} - (1-2\omega^2/\omega_L^2)^2)$$

$$\mu = (\cos^2\psi_j/\cos^2\tilde{\psi}) - 1$$

Then μ the squared frequency distribution for a singly folded chain is

$$G = G_o + \Delta G$$

For $\psi_j > \tilde{\psi}$, the defect reduces the singularities at $(\omega_L/2)\ (1 \pm \cos\tilde{\psi})$. In the range $\psi_j < \tilde{\psi}$ two out-of-band modes appear: one lower than the lowest, the other higher than the greatest cut off. The separations $(\omega_o/\omega_L)^2$ are given as a function of ϕ_j in Figure III-4. The presence of these modes

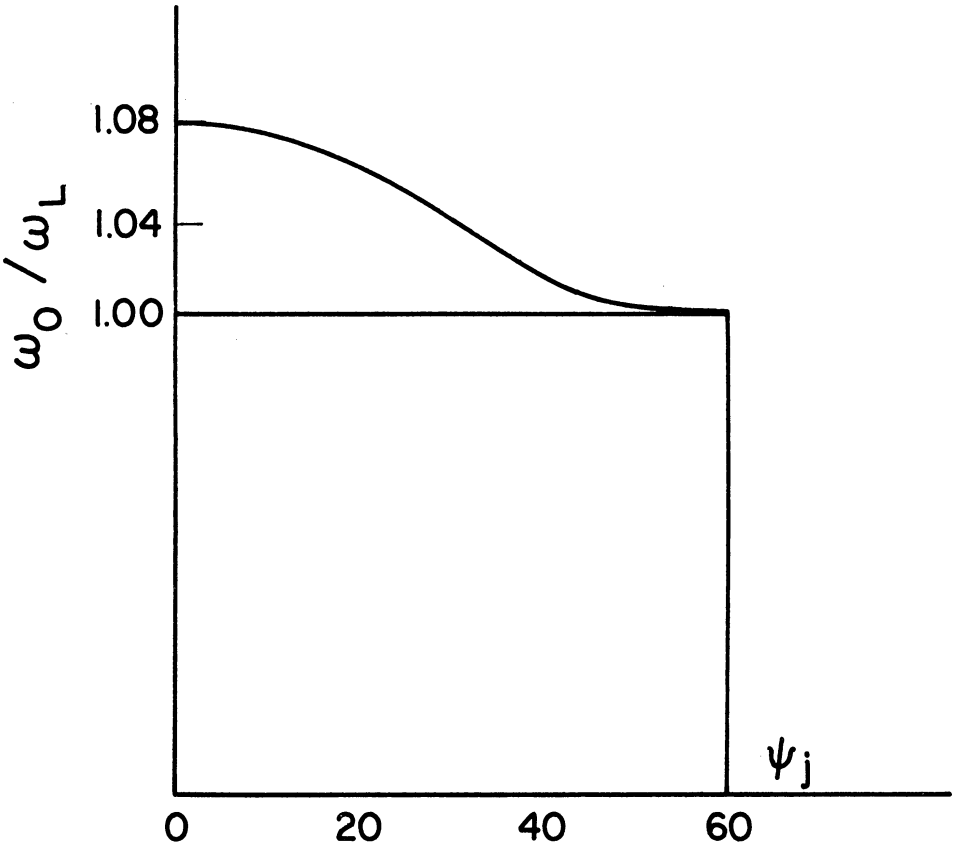

Figure III-4. Separation of the upper (or lower) out-of-band mode from the continuum as a function of ψ_j, calculated by the Green's function method. There is one such curve for each $\tilde{\psi}$ (Eq. III-13).

could have been conjectured using Hadamard circles (see Chapter IV) centered about the a_{jj} and $a_{j+1\ j+1}$ matrix elements of A^i. Their radii increase as ψ_j moves away from $\pi/2$ providing an increased "allowed" region for eigenvalue location. Conversely, when ψ_j moves toward $\pi/2$, these 2 circles shrink, forbidding any eigenvalue to escape from the continuum.

Two other out-of-band modes appear below this continuum for fixed boundaries. Again, a prediction could have been made. The mechanism is different however since the radii associated with first and last rows are not modified. Here the centers of the 2 circles are displaced from a_{11} to $a_{11}/2$ and a_{nn} to $a_{nn}/2$. The necessary condition for appearance of these modes is then

$$2\,a_{11} - 2\,a_{11}\cos\tilde{\psi} > 0$$

$$a_{11} - a_{11}\cos\tilde{\psi} < 2\,a_{11} - 2\,a_{11}\cos\tilde{\psi}$$

which is always verified for $\tilde{\psi} \neq 0$.

In Reference 54 the importance of out-of-band modes is illustrated by the evaluation of the vibrational self-energy, i.e., the difference between the sum of all frequencies (square roots of eigenvalues) in the perfect and the defect states. The in band modes are shifted by an amount proportional to ω_L/N, where ω_L is the largest unperturbed eigenmode. A localized (out-of-band) mode ω_o contributes to $(\omega_o - \omega_L)$, which is an order of magnitude greater than ω_L/N.

We determine now the harmonic frequency spectrum of a simple chain in a given conformation, and inversely from a given spectrum we derive the characteristics of the family of conformations with which it is associated.

The frequency distribution, subsequently noted F.D., is in fact a distribution averaged over an ensemble of chains. It also is the F.D. of a typical chain as $N \to \infty$. Hence a formulation of the inverse problem is to determine the configuration distribution (C.D.), which is the probability that the angle ψ of a given vertex lies in a certain interval. Two characteristics of the C.D. are:

- the range of possible ψ values at each vertex
- the ordering of ψ along the chain, in the sense of Chapter II.

One appropriate case in the study of the carbon backbone is the discrete range $(0,\overline{\psi})$. The value $\overline{\psi}$ is given by the tetrahedral geometry and the type of motion considered. For the longitudinal motion, one has (see Figure IV-1):

$$\cos \tilde{\psi}_{\ell} = 1 - \sin^2\alpha \, (1 - \cos \phi) \qquad \text{(III-11)}$$

where 2α and ϕ are respectively the valence and internal rotation angle. For the transverse motion one has

$$\cos \tilde{\psi}_{t} = \cos \phi \qquad \text{(III-12)}$$

At low temperatures the internal rotation angle is restricted to one of the 3 angles $0, 2\pi/3, 4\pi/3$. Since the 2 last configurations yield the

same cos ψ, we restrict ourselves to the two values of $\psi = (0, \tilde{\psi}_{\ell t})$ also denoted (T,G) for trans and gauche configurations. The effects of various values of $\bar{\psi}$ and various ordering of (G,T) are seen in Figures (III-5, III-6, III,7). The pure G frequency continuum has a width equal to cos $\bar{\psi}$ and is centered at $\omega^2/\omega_L^2 = 1/2$. Figure III-6 shows the F.D. for various concentractions of G configurations randomly distributed (Bernoulli type). One can see three components in these F.D.: the pure T continuum for $p < 0.4$; the 2 branches of the periodic TG conformation for $0.4 < p < 0.6$; the pure G conformation for $p > 0.6$. In Figure II-1 and Figure II-7 the order is Markovian simple. It is measured by the parameter σ_B defined in Chapter II. The effect of σ_B is to enhance one or two of the above components, with respect to the Bernoulli case ($\sigma_B = 0$).

The inverse problem is solved in two steps. The first is the identification of "structures" in the F.D., in terms of sequences of configurations. By "structure," we mean a typical frequency pattern in a certain frequency interval. Only certain sequences of T,G can be identified with structures. For instance for $p > 0.5$, the configuration T produces a localized mode $\tilde{\omega}$, but the sequence TT produces the mode $\tilde{\omega} + \Delta\tilde{\omega}$, $\tilde{\omega} + \tilde{\omega}_2$. There is no meaningful identification of $\tilde{\omega}$ in terms of T since the mode associated with T depends on the configurations in the vicinity of T. Dean[49] found however that sequences of the type:

GTF, GGTGG, GGGTGGG,

where T is bordered with an equal number of G configurations, can be iden-

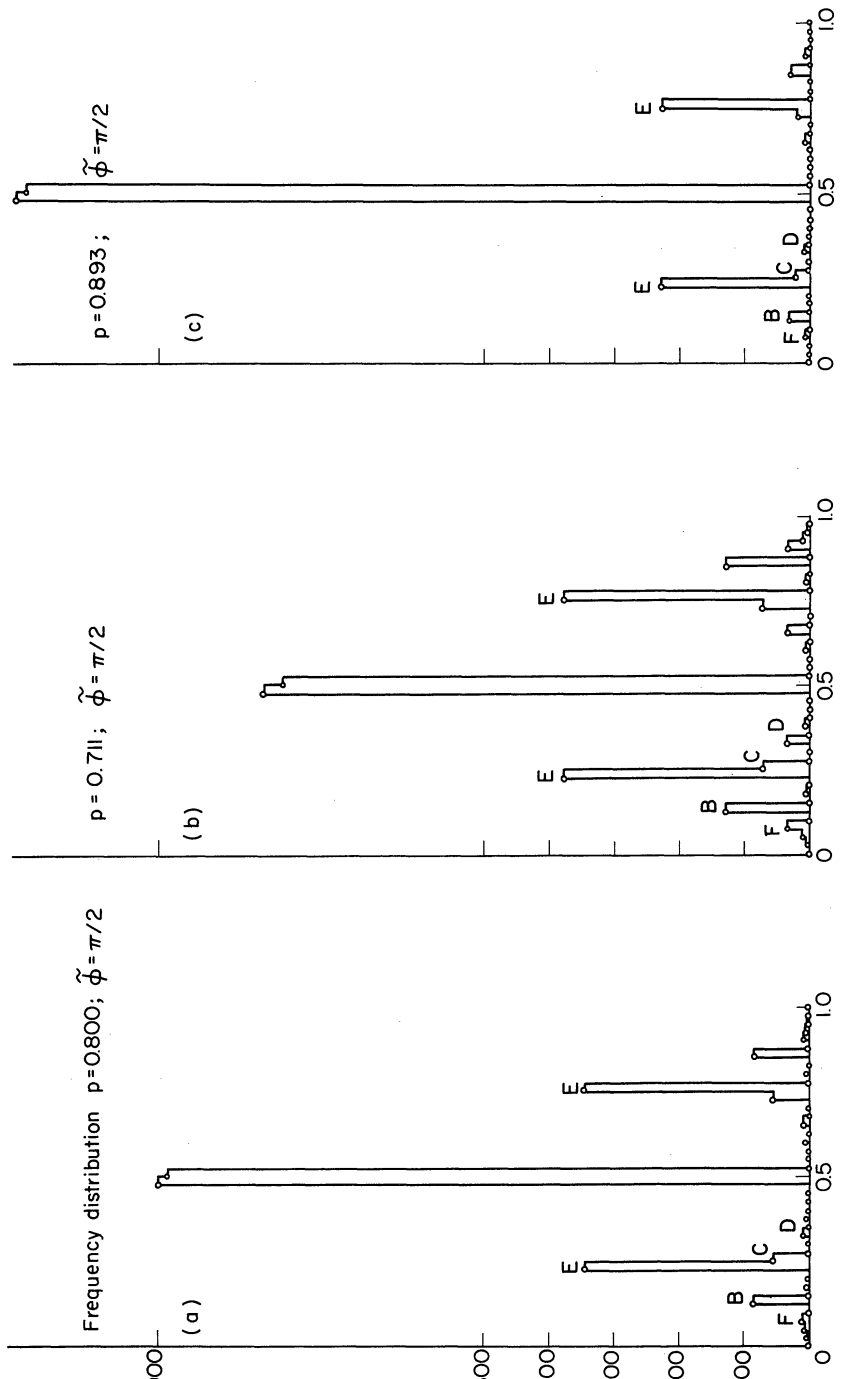

Figure III-5. Squared frequency distribution for 3 concentrations p of randomly distributed folds $\psi_j = \pi/2$. The reference chain is extended. The ω^2/ω_L^2 interval is partitioned in 40 intervals; the number of squared frequency in each interval is given by the corresponding ordinate f. The concentration p is the number of folds divided by the number N of mass points (N = 3000). The case p = 0 yields the inverse square root law over the interval (0,1); the case p = 1 yields the singular point at $\omega^2/\omega_L^2 = 1/2$. In the three intermediate cases given here, modes are scattered around $\omega^2/\omega_L^2 = 1/2$ in peaks labeled E,B,C, etc. These peaks are the contribution of typical islands of T (extended) configurations.

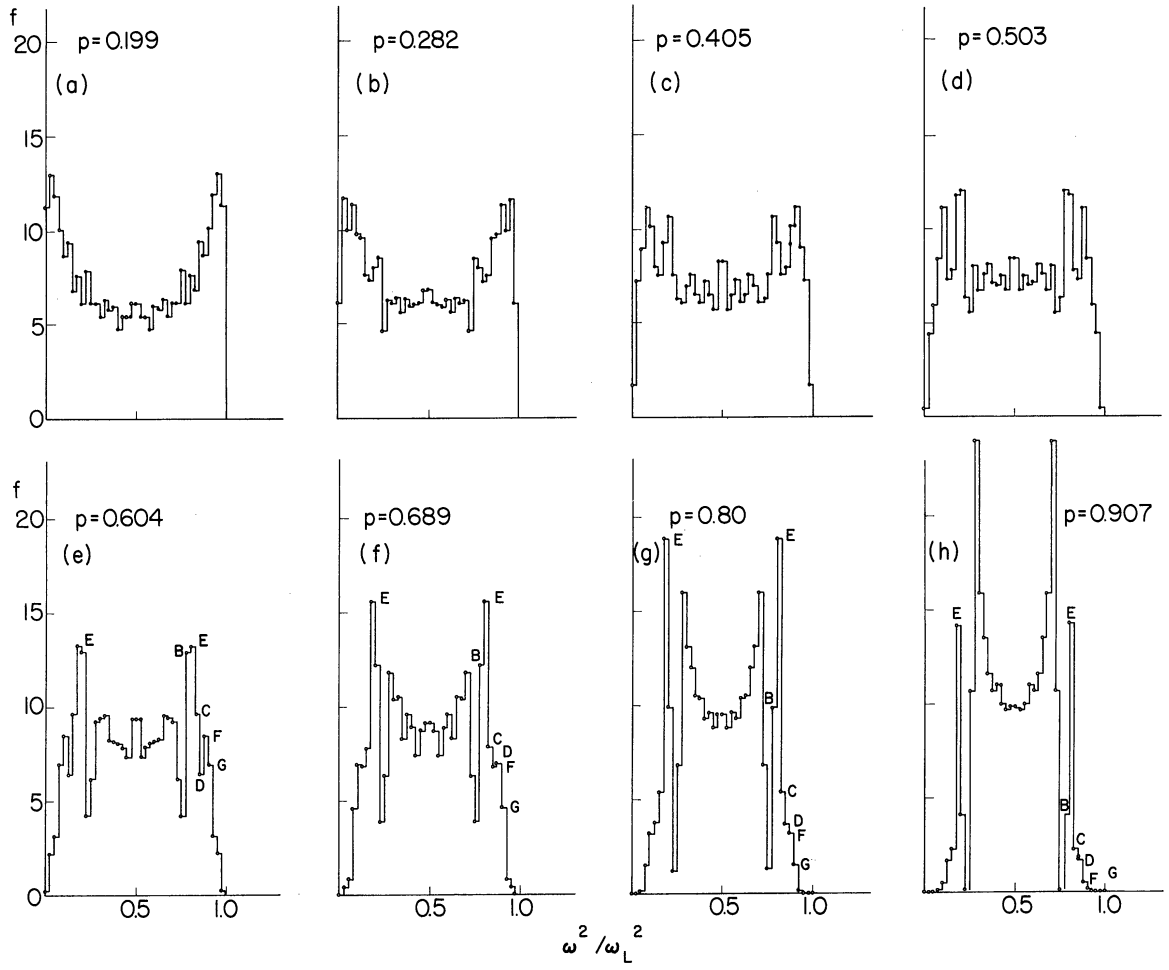

Figure III-6. Squared frequency distribution for 8 concentrations p of randomly distributed folds $\psi_j = 2\pi/3$. The remarks of Figure III-5 apply here; however the case p = 1 corresponds to the inverse square root law distribution, centered about $\omega^2/\omega_L^2 = 1/2$ in the range (1/4, 3/4). The intervals (0,1/4) and (3/4,1) are the "forbidden" gaps; these are gradually filled as p departs from 1. The structures in the forbidden gaps (labeled E,B,C,etc.) are associated with "islands" of T structures as in Figure III-5; their association is however more ambiguous because of the relatively smaller width of the forbidden gaps.

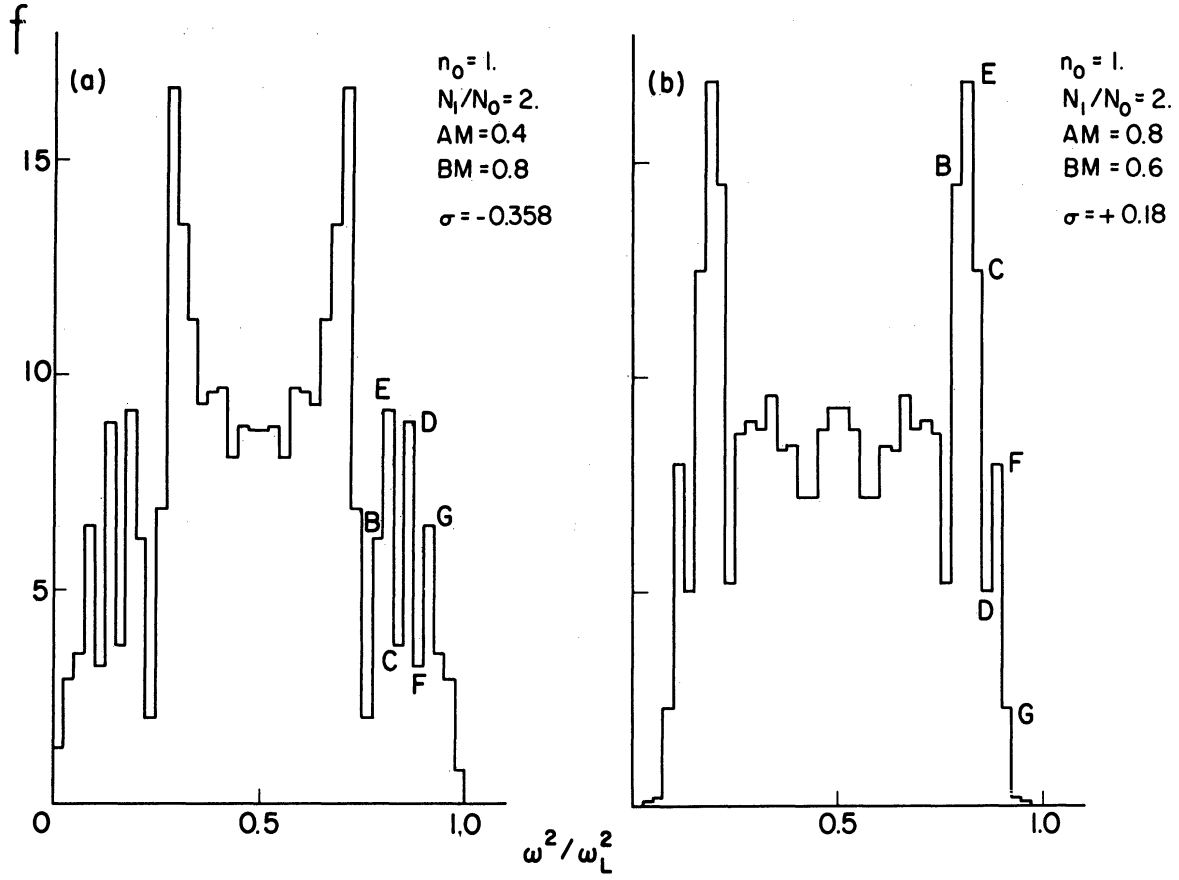

Figure III-7. Squared frequency distribution for simple Markovian chains. The fold angle is $\psi_j = 2\pi/3$. N_0 is the number of T configurations, N_1 of G configurations. The relation with p is:

$$p = \frac{1}{1 + N_1/N_0} ,$$

which equals 0.666 in this case. The short range order σ_B is defined in Chapter II. Case (a) is more ordered than (b) and corresponds to a concentration of T and G's respectively: this can be interpreted on the frequency distribution by the superposition of the two inverse square root laws centered about the same point but extending over different intervals: the smaller corresponds to G clusters and the other to T concentrations.

tified with $\tilde{\omega}$. The number of G necessary to establish a definite correspondence depends on the problem. In the case $\tilde{\psi} = \pi/2$, the first of these sequences is found meaningful, whereas for $\tilde{\psi} = 2\pi/3$ only the third is identified. Such sequences are called T "islands." If a sequence is an island, all those obtained by bordering this sequence with G configurations are equivalent. The problem of identification is to find the smallest typical sequence for a given island. The out-of-band mode $\tilde{\omega}$ associated with a single T defect is calculated from (III-10)

$$\tilde{\omega}^2 = \frac{\omega_L^2}{2}\left(1 + \cos\tilde{\psi}\,(1 + \mu/2)(1 + \mu)^{-1/2}\right) \qquad \text{(III-13)}$$

This mode is a function of the configuration angle $\tilde{\psi}$ of the regular conformation and of the defect angles ψ.

$$\mu = (\cos^2\psi_j / \cos^2\tilde{\psi}) - 1 \qquad > 0$$

$$\omega_L^2 = 4\,\gamma/M.$$

For $\tilde{\psi} = 120°$ and $\psi = 0$, we identify $\tilde{\omega}$ with the mode of a T island bordered with an infinite number of G configurations. The other T islands (i.e., bordered with a number of G configurations greater than the characteristic minimum) yield modes in a vicinity of $\tilde{\omega}$.

Equation (III-13) allows the identification of the E peak, for given $\tilde{\psi}$. (Figure III-4, III-5, III-6.) Conversely from a known E peak, the value of $\tilde{\psi}$ can be determined by (III-13). In the case $\tilde{\psi} = 120°$ we have $\tilde{\omega}^2 = 0.812\ \omega_L^2$. For $\tilde{\psi} = 90°$, we have $\tilde{\omega}^2 = 0.75\ \omega_L^2$.

The second step is the relation of the area under a frequency structure and the rate of occurrence of the associated island. The one is proportional to the other. Characteristics of the configuration distribution are then derived from the rates of occurrence of all islands identified in the F.D.

We first consider the problem where the concentration p of G configurations is greater than 0.5. In this case the T configurations produce structures in the forbidden gap and these are better identified than structures in the allowed interval. A reason for this situation is the interaction effect of 2 defects. It is well known that 2 defects far apart yield out-of-band modes that coalesce. As the distance between the T configurations decreases, these modes split. Hence clustered out-of-band modes indicate isolated T's whereas spread out modes indicate clustered T's. The identification proceeds on this basis. An important feature in the counting of T configurations is the following relation: for low T concentrations $\bar{p} = 1 - p$, every T configuration transfers 2 modes from the continuum into the forbidden gaps. This result was derived in the last paragraph for single defect and is readily visualized in the example ($\tilde{\psi} = \pi/2$) corresponding to a fold of a regular degenerate chain:

$$
\begin{array}{ccccccc}
\ldots & 2 & 0 & & & & \\
 & 0 & 2 & -1 & & & \\
 & & -1 & 2 & 0 & & \\
 & & & 0 & 2 & \ldots &
\end{array}
$$

The Hadamard circles of lines 2 and 3 have finite radii and yield each

a mode outside the continuum. This proposition is not valid for large $\bar{p}$ since at the limit $\bar{p} = 1$ there would be twice as many modes as degrees of freedom. Hence some T in closed sequences as GGTTT...TGG yield modes in the pure G continuum; at this stage it becomes more relevant to count the number of changes of species T,G in the conformation.

We now identify the peaks labeled E, B, C, etc., on Figures III-5, and III-6. In order to proceed the concentration of G configurations and their ordering must be given. Here the order is random (Bernoulli). We try successively the sequences:

$$GTG \quad , \quad GGTGG \quad , \quad etc$$

for the T island, and the sequences

$$GTTG \quad , \quad GGTTGG \quad , \quad etc$$

for the TT island. The rate R of occurrence is determined by the concentration $\bar{p}$ of T. For GTG we have:

$$R_{12} = (\bar{p} - 1)^2 \bar{p}$$

(The first index indicates the number of T's, the second the number of G enclosing the "island".) In general

$$\begin{aligned} R_{1,2n} &= (\bar{p} - 1)^{2n} \bar{p} \\ R_{22} &= (\bar{p} - 1)^2 \bar{p}^2 \quad etc \end{aligned} \tag{III-14}$$

Let S_E/S_T be the ratio of the area of one of the E peaks to the total area—the other E peak is left out to avoid double counting. Other ratios such as S_B/S_T are defined similarly. Tracing the curves S_E/S_T,

etc, measured on the F.D., as a function a $\bar{p}$, we compare them to the $R_{ij}(\bar{p})$ curves. If a peak X corresponds to one single island the S_X/S_T ratio should match a predicted $\bar{p}$ dependence. The labeling of a peak is made by best fit of S_E/S_T S_B/S_T, etc., with model behavior. Figure III-8 gives evidence that the observed ratios reproduce a predicted $\bar{p}$ dependence in a certain interval. Coincidence is imperfect: first, the modes labeled under one peak may belong to 2 islands because of a particular partition of the frequency interval; also the modes attached to a certain island may spread over a frequency interval overlapping frequencies of different assignments. Next, there are contributions of "imperfect islands" where the defects are not symmetrically bordered. For instance the sequences GTGGG and GGGTG occur at the same rate as GGTGG in the random model, and would produce modes similar to those of GGTGG; the latter configurations are seen to be equivalent in the case $\bar{\psi} = \pi/2$ Figure III-8. They are not equivalent in the case $\bar{\psi} = 2\pi/3$, as indicated by the $\bar{p}$ behavior. In general, a frequency peak is a superposition of contributions of several islands, with however one dominant island. It is remarkable that one actually emerges, as shown in Figure III-8.

Using these assignments (see Figure III-8), we may derive the ordering associated with a F.D. Hence from Figure III-5a we measure S_B/S_T and we read the concentration $\bar{p}$ on the R_{22} curve in Figure III-8a. To test whether the order is random (Bernoulli), we calculate the persistence ratio (see Chapter II):

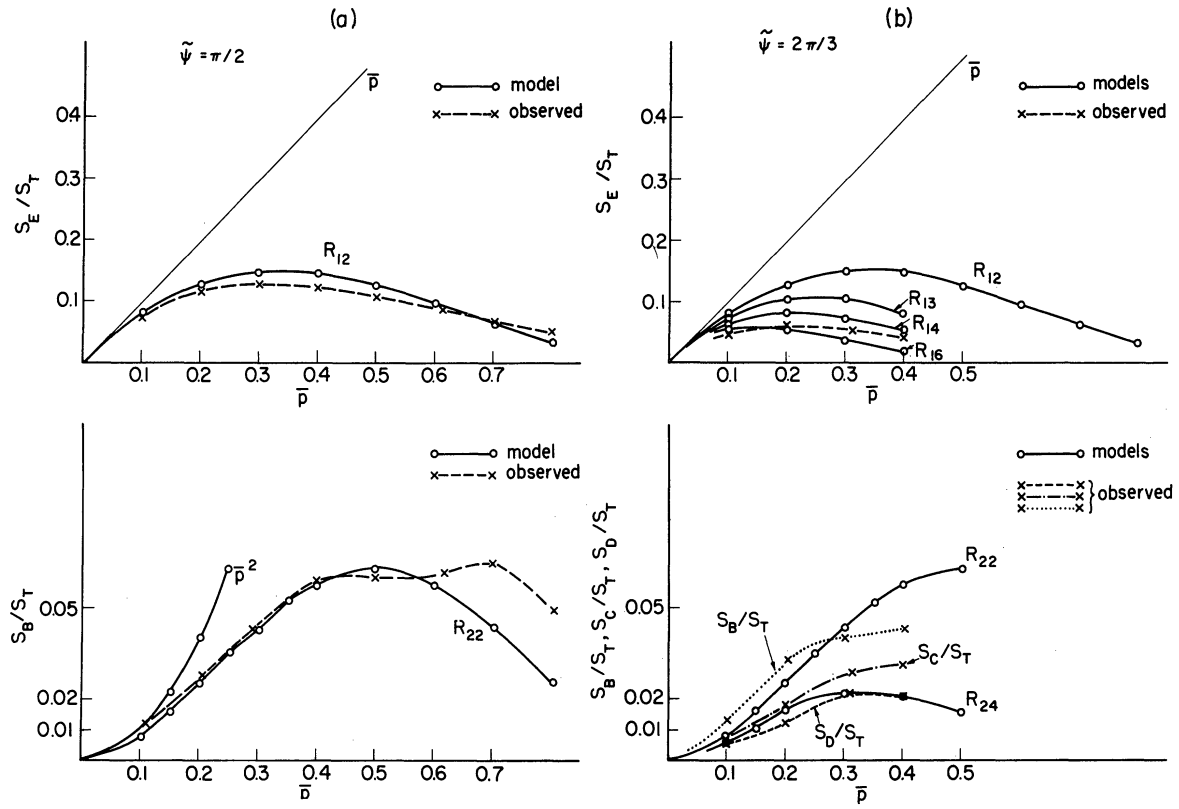

Figure III-8. Ratio S_E/S_T and S_B/S_T, etc., as a function of the concentration $\bar{p}$ of T configurations. S_E is the surface under one of the peaks labeled E; S_B is the surface under one of the peaks labeled B; S_T is the total surface. The broken curves are the quotients as measured on Figures III-5 and III-6. The plane lines are the quotients predicted by models R_{ij}, Eq. (III-14).

(a) $\bar{\psi} = \pi/2$ (see Figure III-5). The E peak is identified with the island described by R_{12}, i.e., GTG. The measured S_E/S_T is lower than the assigned ratio for $\bar{p} < 0.675$: hence some GTG islands produce modes elsewhere. The B peak is identified with the island described by R_{22}, i.e., GTTG. The measured S_B/S_T is higher than the predicted ratio, for $\bar{p} < 0.43$; hence some other island than GTTG contributes to this particular squared frequency interval.

(b) $\psi = 2\pi/3$ (see Figure III-6). The E peak is identified with the island described by R_{16}, i.e., GGGTGGG. The D peak is identified with the island described by R_{24}, i.e., GGTTGG.

$$\rho = \mu(G)\,\bar{p}$$

where $$\mu(G) = \frac{p}{\bar{p} - p_2(TT)}$$

and $p_2(TT)$ equals the rate of occurrence of TT. The latter is obtained from S_B/S_T:

$$p_2(TT) = R_{22}/p^2 = 0.043/0.51 = 0.085$$

hence $$\rho = \frac{0.711 \times 0.289}{0.289 - 0.085} = 1.005$$

which indicates a random order with an one per thousand error. From Figure III-6f, we measure $S_D/S_T \doteq 0.021$. This value yields $\bar{p} \cong 0.3$ on the R_{24} curve. Further, one has

$$p_2(TT) = R_{24}/p^4 = 0.021/0.24 = 0.88$$

and $$\rho = \frac{0.3 \times 0.7}{0.3 - 0.88} = 0.99$$

which indicates a random order within an error of 1%.

However in Figures III-7a,b, we find respectively $S_D/S_T = 0.029$ and 0.0165. The first of these values is not reached by the R_{24} curve on Figure III-8b. The second yields $\bar{p} = 0.2$, hence $p_2(TT) = 0.115/0.41 = 0.04$ and $\rho = 0.82$, which also indicates that we cannot use the assumptions of curve (Figure III-8b). In both cases the "statistical after effect" is recognized.

Can we assert from the F.D. of Figure III-7a,b that the order is simple Markovian? We write the rate of occurrence of "islands" in terms of the matrix elements of the transfer matrix τ. These are also the conditional probabilities that a configuration be followed by another. Using the notation of Chapter II we have:

Islands	Rate of Occurrence for a Simple Markovian	Assigned Structure Surface
GGGTTGGG	$p\ p_{22}^{4}\ p_{21}\ p_{12}$	S_E
GGTTGG	$p\ p_{22}^{2}\ p_{21}\ p_{11}\ p_{12}$	S_D
GGTTTGG	$p\ p_{22}^{2}\ p_{21}\ p_{11}\ p_{12}$	S_G
GGTGTGG	$p\ p_{22}^{2}\ p_{21}\ p_{12}^{2}$	S_X

From the quotients of these rates we get:

$$p_{11} = S_G/S_D$$

$$p_{22}^{2} = (S_E/S_D)p_{11}$$

$$p_{12}\ p_{21} = (S_X/S_D)p_{11}$$

It is seen that because of the symmetry of islands, p_{12} and p_{21} appear always paired and that there is no way of determining anything else but their product raised to some power. Hence in order to proceed further, the "island" technique must be complemented by some information concerning the off diagonal matrix elements. For example the rate of occurrence of GT or TG would yield: $p\ p_{21} + (1 - p)\ p_{12}$, from which the desired result could be obtained.

For the evaluation of the labeling accuracy we compare some measured versus calculated quotients:

Figure	σ	Measured S_E/S_o	Calculated $p_{22}^2/p_{11} = \frac{BM^2}{1-AM}$	Measured S_E/S_o	Calculated $p_{22}/p_{11}^2 = (\frac{BM}{1-AM})^2$
III-7a	-0.358	1.06	1.07	1.45	1.78
III-7b	0.18	3.4	1.8	7.5	9

We see that E and D in Figure III-7a are correctly assigned. The other results do not match particularly well; they could be improved by decomposing the surface of a peak into contributions of the several islands. These are determined by numerical experimentations as described in Ref. 49.

In view of the above difficulty, we consider the information yielded by the area S_f of the total structure in one of the forbidden gaps. We had seen that S_f is less than or equal to the number of folds:

$$S_f/S_T < \bar{p}$$

A lower bound of this quantity is the number of unlike pairs. There are at least 2 out-of-band modes per unlike pair TG. In the Bernoulli process we have:

$$\bar{p}(1-\bar{p}) \leq S_f/S_T \leq \bar{p} \qquad \text{(III-15)}$$

For a simple Markov chain

$$\bar{p}\, p_{12} \leq S_f/S_T \leq \bar{p}$$

Inequality (III-15) corresponds to the shaded area on Figure III-9. The measured S_f/S_T curve for $\bar{\psi} = \pi/2$ conforms to the inequality; but the curve $\bar{\psi} = 2\pi/3$ is systematically below the unlike pair line, which indicates that the width of the forbidden gap, a function of $\bar{\psi}$, was chosen too narrow in the measurement of S_f. The ratio S_f/S_T follows a pattern that can be empirically reproduced by a polynominal in $\bar{p}$ (or p) (for example Figure III-10).

$$\frac{S_T - 2\,S_f}{S_T} = \frac{S_{in}}{S_T} = p_o(\tilde{\psi}) + (1 - |\cos\bar{\psi}|)p/2(1 + p) \qquad \text{(III-16)}$$

where S_{in} is the frequency area in the interval

$$(1/2\,(1-\cos\tilde{\psi}) \quad , \quad 1/2(1+\cos\tilde{\psi}))$$

which is the support of the continuum for p = 1 (i.e., the allowed gap at that value); $p_o(\psi)$ is the ratio S_{in}/S_T at p = 0.

The use of these curves requires knowledge of the ordering (which is random for the curves in Figure III-9) and of the angle $\tilde{\psi}$. They could be used in the range $p < 0.5$, where the "island" technique fails for lack of out-of-band modes. This is also an attempt to decompose a given spectrum into components associated with basic orders such as pure T and pure G. Generally it looks as if the F.D. for random order has three main components: the two quoted above and the alternation GT (or TG).

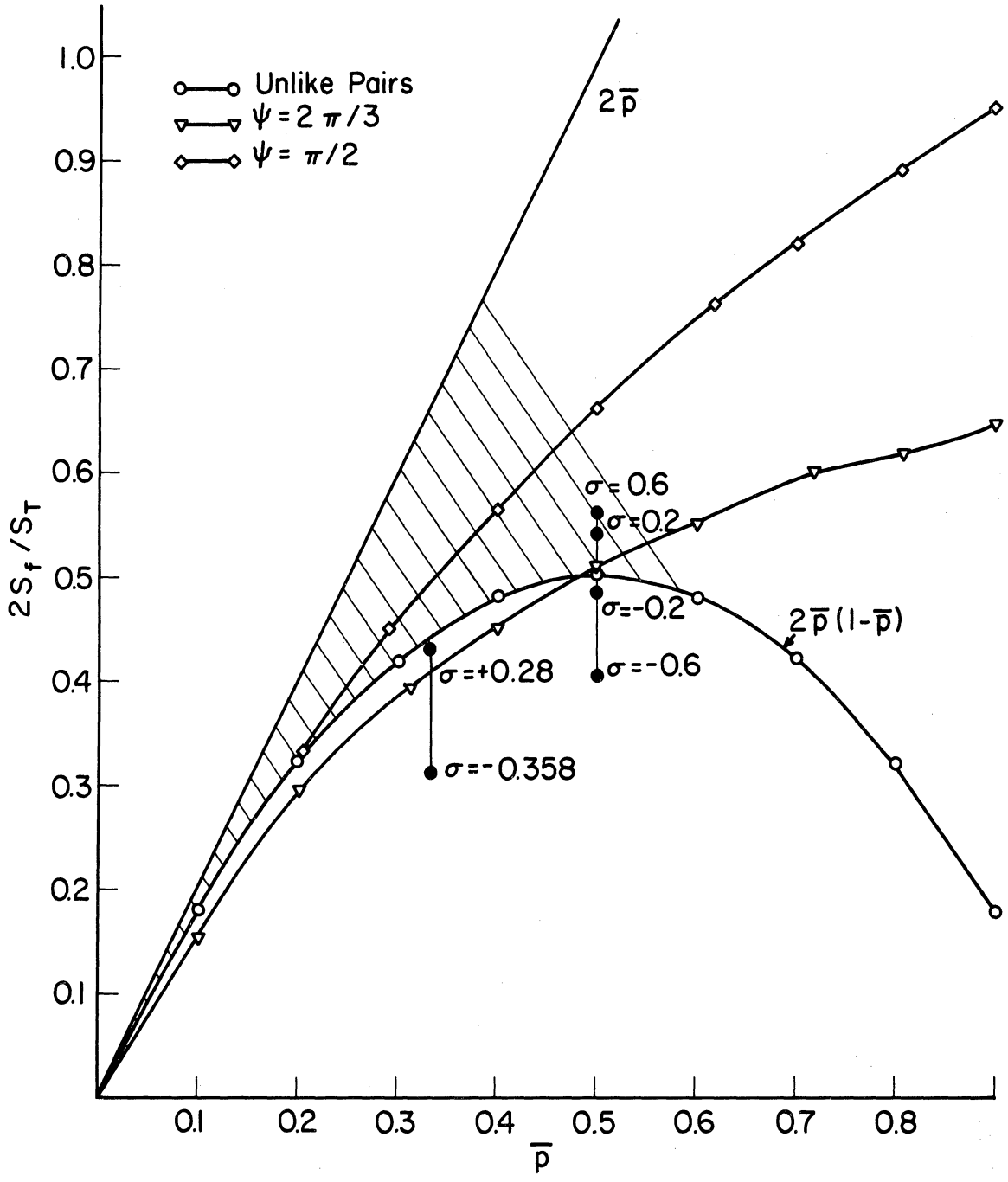

Figure III-9. Ratio of out-of-band modes to total frequency surface as a function of $\bar{p}$ (concentration of T configurations). S_f measures the surface of the structure in one of the forbidden gaps; 2 S_f is then the total contribution. The shaded area is an allowed region for S_f/S_T; it is bounded from below by the "unlike pair" concentration and from above by twice the T concentration (to account for the fact that each T produces 2 out-of-band modes for $\bar{p} \ll 1$). The curve associated with $\psi = 2\pi/3$ is below the allowed area because the out-of-band gaps were chosen too small.

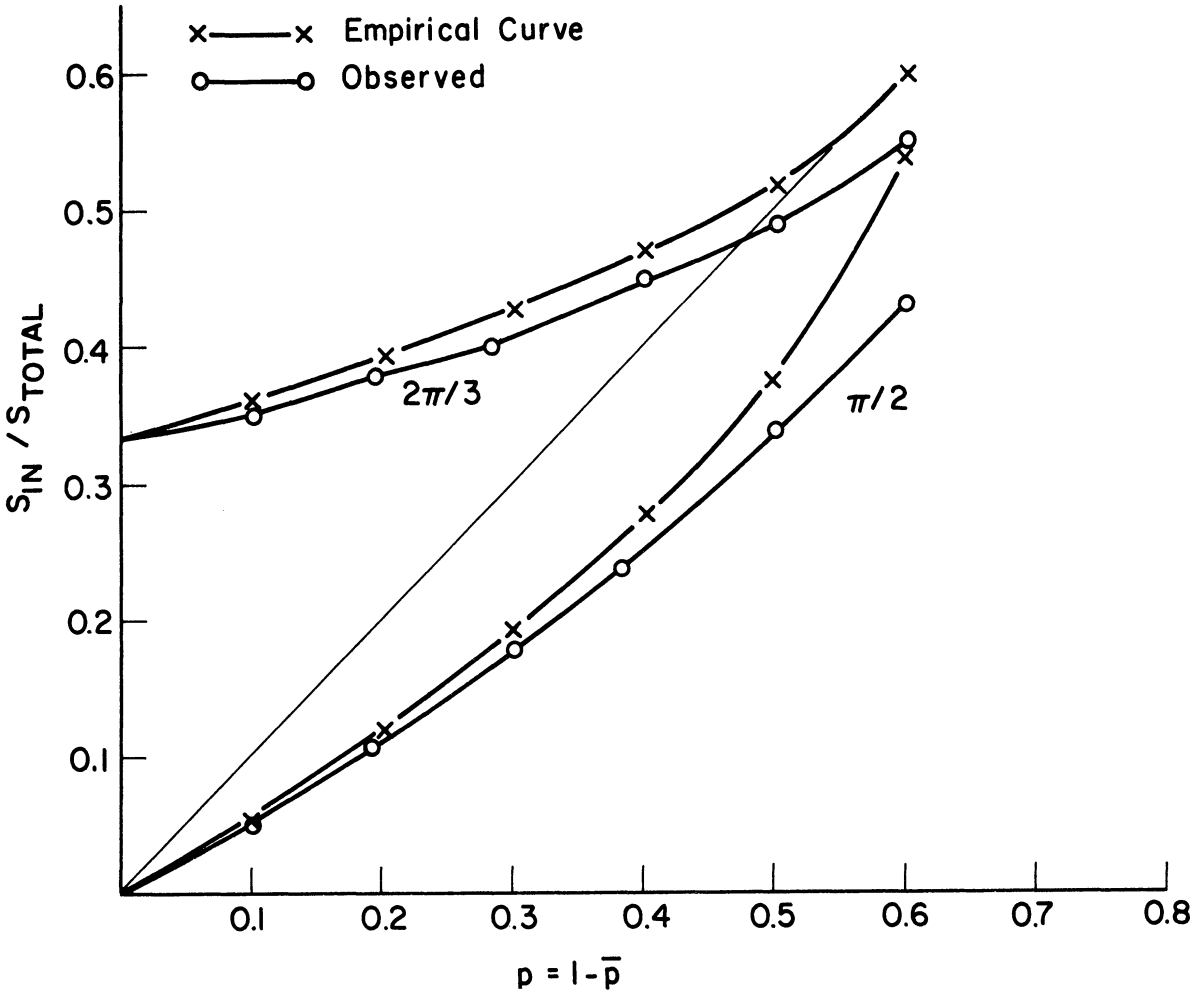

Figure III-10. Empirical curves for the measurement of concentration of G configurations in a random chain, for two values of $\bar{\psi}$ ($p < 0.5$).

In the previous sections, the range R_j of ψ values had two elements only. By extending R_j to the entire $(0,2\pi)$ interval, the frequency distribution for random order shows a typical behavior, as seen in Figure III-11. The cut-offs are smoothed and the frequency peaks are displaced towards the center of the interval. In these calculations ϕ is taken as the random variable. The dependence of the configuration angle on ϕ is given by Eqs. (III-11, III-12). Two types of dependencies are considered: one for the in plane motion, the other for the "out of plane" motion. The 2 problems show distinct characteristics; in the first case, the matrix elements

$$a_{i,i+1} = -\gamma_b(1 - \sin^2\alpha\,(1 - \cos\phi\,)) \qquad \text{(III-17)}$$

vary in the interval $(\gamma_b,\ \gamma_b(1 - \sin^2\alpha))$; in the second case, the matrix elements

$$a_{i,i+1} = -\gamma_t \cos\phi \qquad \text{(III-18)}$$

vary over the wider relative range $(\gamma_t,0)$.

We recognize in Figure III-11a the central peak as the contribution of $\phi = \pi/2$ and the E peaks as the contribution of $\phi = 0, \pi$, in analogy with Figure II-5 where $\tilde{\psi} = \pi/2$. This central peak does not appear in the planar motion F.D., for the matrix elements do not reach the value 0. One notices also the difference in curvature between the 2 peaks.

We have seen that the frequency distribution is sensitive to the parameters considered, in two ways: appearance of typical mode accumula-

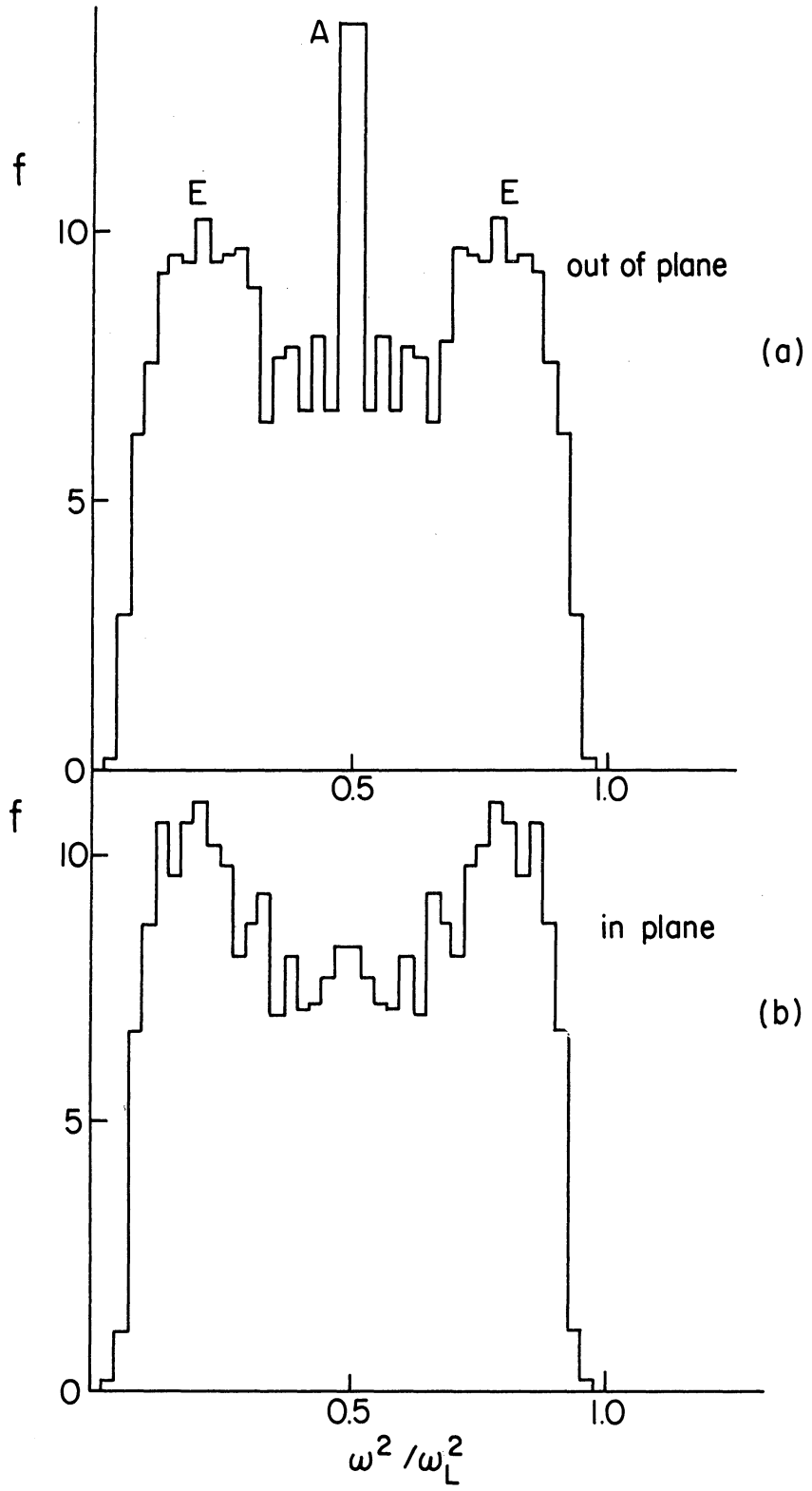

Figure III-11. Frequency distribution for a range R = (0, 2π) of the random variable ϕ. The dependencies of the "in plane" and "out of plane" matrix elements on ϕ are not the same; they are given in Eqs. (III-17, III-18).

tions in the forbidden gap ($p > 0.5$) and redistribution of modes in the continuum. Quantitative interpretation of the spectrum usually involves the analysis of out-of-band modes. Progress in this interpretation is however made difficult by superposition of the effects to be singled out. It is felt that more empirical techniques in relation to the shape of the continuum could be developed.

CHAPTER IV

INTERACTION OF LONGITUDINAL AND TRANSVERSE MODES

We have considered a chain composed of mass points with one degree of freedom, longitudinal or transverse. In this case the only effect of a fold is the attenuation or enhancement of the transmitted motion. We will call this the self-effect. When two degrees of freedom are combined, this effect applies independently to each one. In addition however a local coupling of the 2 modes occurs. We will now determine the joint effects on the F.D. (We shall however not be able to treat the complicated conformations as in Chapter III.)

In order to provide a model for a polyethylene backbone, two simple chains will be incorporated in a ribbon like structure, with two rows of respectively even and odd numbered mass points, distributed as in Figure IV-1. Each point is also connected to its two nearest neighbors on the opposite row. The "in plane" motion of the structure is the superposition of three independent motions—two longitudinal along even and odd rows respectively and one zigzag along the diagonals. The out of plane motion is the superposition of the two independent transverse motions of even and odd rows.

The equations of motion for the planar conformation are, in internal displacement coordinates:

$$m \ell_j = -\gamma_b \ell_{j-2} + 2\gamma_b \ell_j - \gamma_b \ell_{j+2} \qquad \text{(C-C-C bending)}$$

$$m\ddot{s}_j = -\gamma_s s_{j-1} \cos 2\alpha + 2\gamma_s s_j - \gamma_s s_{j+1} \cos 2\alpha \quad \text{(C-C stretching)}$$

$$m\ddot{t}_j = -\gamma_t t_{j-2} + 2\gamma_t t_j - \gamma_t t_{j+2} \quad \text{(out of plane motion)}$$

(IV-1)

γ_b, γ_s, γ_t are the force constants for the bending, stretching, and out of plane motions; 2α is the valence angle.

We allow the ribbon to fold along any diagonal bond. The angle of "rotation" ϕ_j is the angle between the normals to the (j-2, j-1, j) and (j-1, j, j+1) planes. Any nonzero angle ϕ_j produces the following effects:

- attenuation of the longitudinal motion (angle β)
- attenuation of the transverse motion (angle ϕ_j)
- interaction between longitudinal and transverse motions (angle δ)
- interaction between transverse and zigzag motions (angle ξ).

The following geometrical relations will be needed for the equations of motion in any conformation. At every vertex j, we constuct a right handed Cartesian coordinate system whose x axis is aligned with (j-2,j); whose y axis is perpendicular to the plane (j+2, j+1, j) and directed through the plane of the figure, when unfolded at $\phi = o$. Considering the vertex j-1, we first express β,δ,ξ as functions of ϕ and α.

Isolating the configuration j-1, j+1, j+3*, j from Figure IV-1, we find:

$$2\ell^2 \sin 2\alpha\,(1-\cos\phi_j) = 2d^2(1-\cos\beta)$$

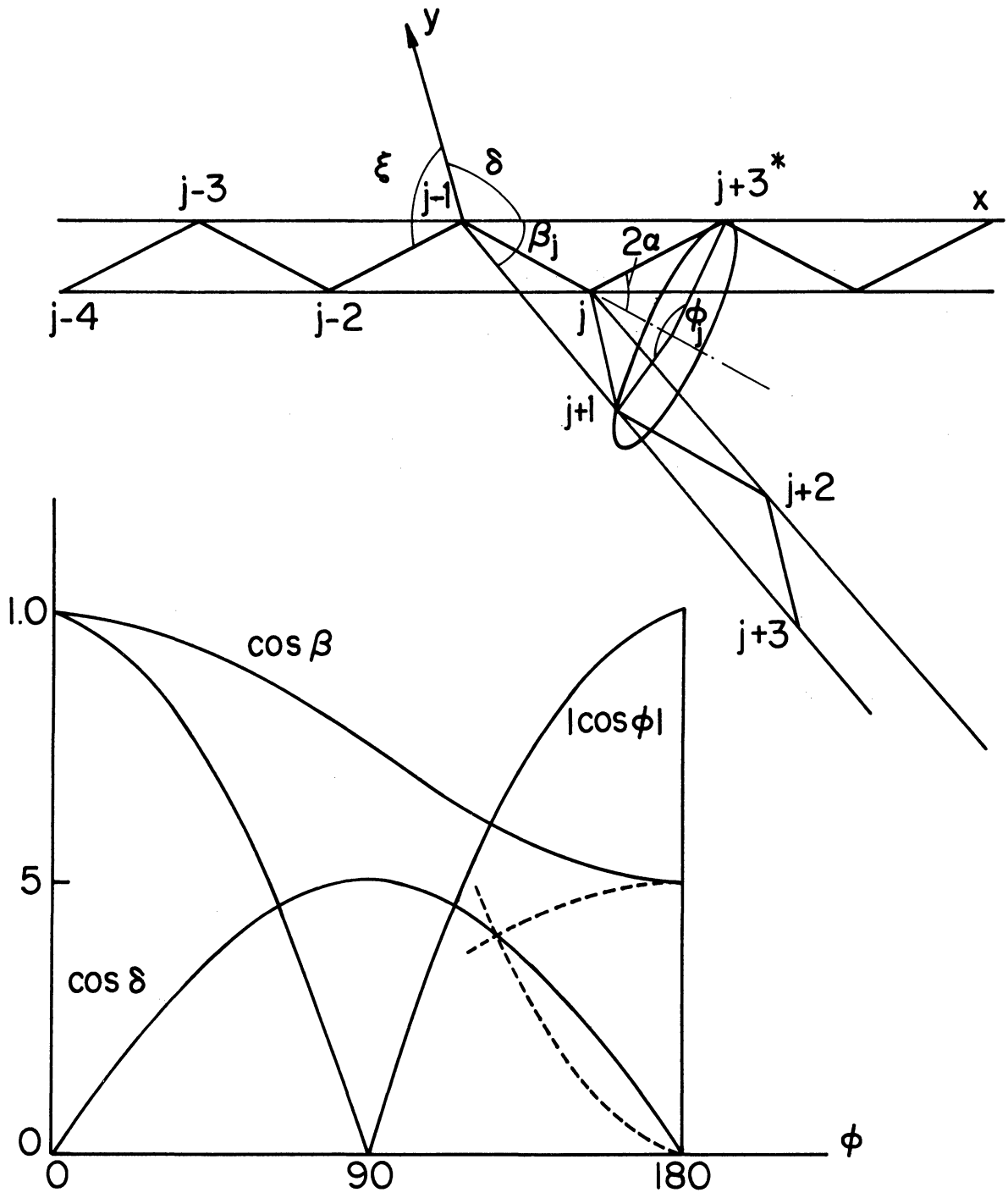

Figure IV-1. Trans and gauche configurations of the carbon skeleton for $2\alpha = 60°$. The diagram at the bottom is the variation of force orientations as a function of internal rotation angle ϕ ; the dotted lines are drawn symmetrically to cos β and $|\cos \phi|$, respectively, and intersect on the cos δ curve (see Eq. (IV-6)).

where ℓ, d are the distances (j-1,j) and (j-1,j+1) respectively. The relation between β and ϕ_j is

$$\cos\beta = 1 - \sin^2\alpha\,(1-\cos\phi_j)$$

The attenuation coefficient for the longitudinal motion is cos β. For the transverse motion it is cos ϕ_j. Notice the latter goes to zero for $\phi_j = \pi/2$ and that the former reaches a minimum at $\phi_j = \pi$ (see Figure IV-1).

Isolating the plane P(j-1,j,j+3*) from Figure IV-1 (see Figure IV-2), we consider the normal y, to P through j-1 and the axis y associated with vertex j-1. By definition y is orthogonal to (j-1,j). Constructing A such that (j-1,B) is of unit length, we have:

$$\cos\delta = q^2 + 1 - p^2$$

$$q = \frac{\sin\alpha}{\sin\phi_j} \text{ and } p^2 = \cos^2\alpha + q^2\cos^2\phi_j$$

$$\cos\delta = \sin\alpha\sin\phi_j \qquad \text{(IV-2)}$$

The bending-torsion interaction coefficient is cos δ.

Isolating the plane P(j-1,j,j+1) in Figure IV-1, we consider the normal y to (j-2, j-1, j) and the perpendicular M in P to (j-1,j); then (see Figure IV-2b)

$$\cos\xi = (1 + x^2 - p^2)/2x = \sin2\alpha\sin\phi_j \qquad \text{(IV-3)}$$

The stretch-torsion interaction coefficient is cos ξ.

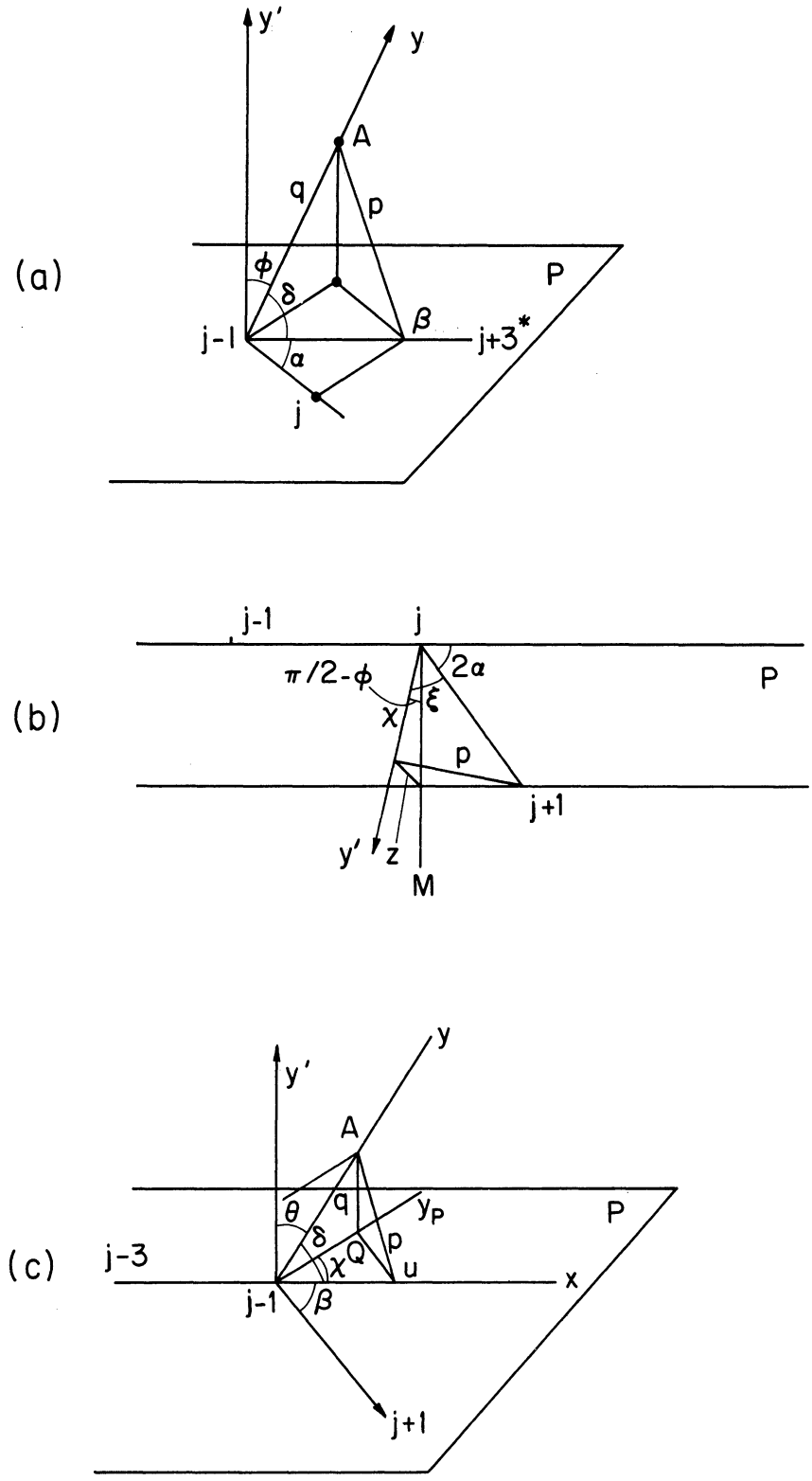

Figure IV-2. Three-dimensional geometrical relations taken from Figure IV-1 (top):

(a) between cos δ and (ϕ,α),
(b) between cos ξ and (ϕ,α),
(c) between cos δ and (θ,X).

It will be useful to establish the following relation between 2 reference systems at vertex j-1: the first is the Cartesian system associated to vertex j-1; the other has the same x axis, but its y' is orthogonal to the (j-3, j-1, j+1) plane P. In this frame, the direction of y is given by (0,X) which we want to express as a function of (ϕ_j,α) (see Figure IV-2c). Let (j-1,u) have unit length; consider the projection y_p of y on P and construct the projection Q of U on y_p. From Q, the normal to P intersects y in A. We then have:

$$\cos \delta = (1 + q^2 - p^2)/2q$$

$$q = \frac{\cos \chi}{\sin \theta} \; ; \; p^2 = \sin^2\chi + \cos^2\chi \, \frac{\cos^2\theta}{\sin^2\theta} \qquad \text{(IV-4)}$$

hence $\cos \delta = \cos \chi \sin = \sin \phi_j \sin \alpha$, which is the wanted relation. Further we have that:

$$\chi + \beta = \pi/2$$

since y is orthogonal to j-1, j+1; hence

$$\cos \chi = \sin \beta \qquad \text{(IV-5)}$$

sin θ is derived from (IV-4) and (IV-5).

A geometrical property of the cos β, cos δ, cos ϕ functions is (see Figure IV-1, bottom): for any $0 < \alpha \leq \pi/2$ there is a triple crossing point, i.e., a value ϕ_j^* such that

$$1 - |\cos\phi_j^*| = 1 - \cos [\beta(\phi_j^*)] = \cos [\delta(\phi_j^*)] \qquad \text{(VI-6)}$$

Namely, letting $z = |\cos \phi_j^*|$ and supposing that $\pi/2 < \phi^* < \pi$, we have:

$$1 - z = \sin^2\alpha(1 + z) = \sin\alpha\sqrt{(1-z)(1+z)}$$

$$\frac{1 - z}{1 + z} = \sin^4\alpha\left(\frac{1 + z}{1 - z}\right) = \sin^2\alpha$$

let $q = \frac{1-z}{1+z}$; if $q = \sin^2\alpha$, then $q = \frac{\sin^4\alpha}{q}$

which proves the assertion.

It is remarkable that for $\alpha = 34°$, $\phi^* = 120°$ which is the angle of the gauche conformation. One notices that at this particular value the self coefficients for bending and transverse motions are greater than the interaction coefficient.

The equations of motion will be derived from the simpler case where 3 rows L_1, L_2, L_3, of longitudinally oscillating masses branch at vertex j. The connection with our problem will be recognized immediately (see Figure IV-3).

The reference system at vertex j is the x axis aligned with L_1 and the z axis orthogonal to the (L_1, L_2) plane. The orientation of L_3 in this frame is (Θ, X). With this notation, we can write the bond length variation at the branching point as:

$$\Delta\ell_{j,j+1} = x_{j+1} - (x_j \cos\beta + y_j \sin\beta)$$

$$\Delta\ell_{j,t+1} = x_{t+1} - (x_j \cos\chi + y_j \sin\chi) \sin\Theta - z_j \cos\Theta$$

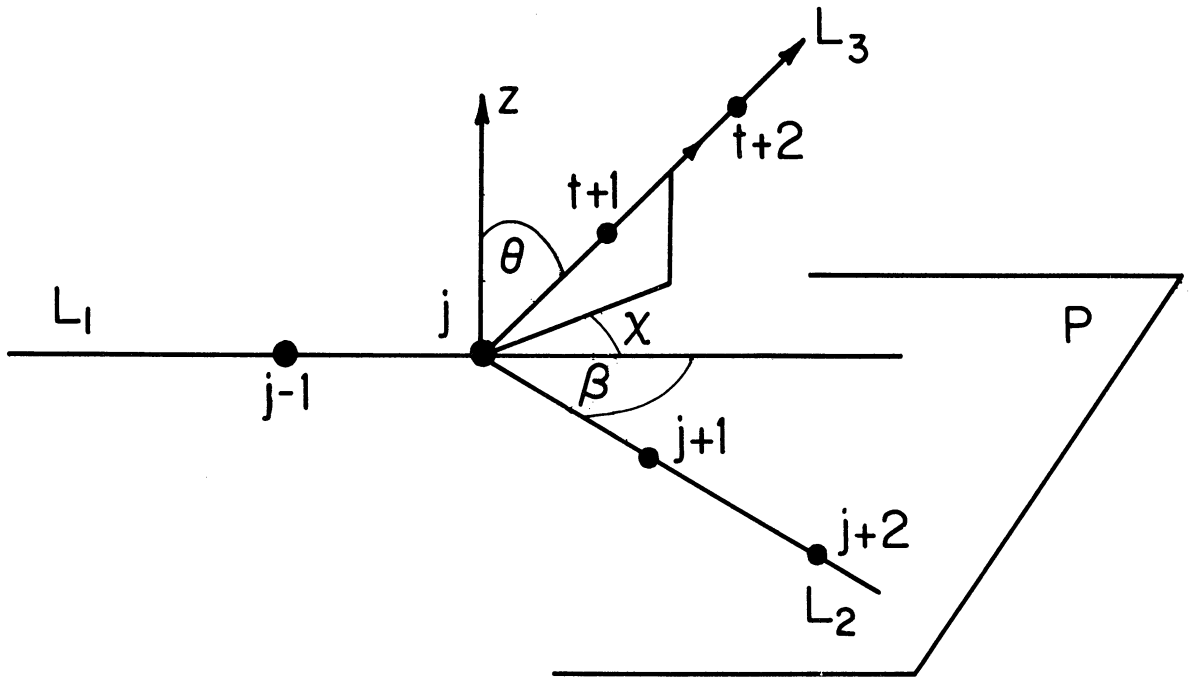

Figure IV-3. Geometry of 3 branched lines L_1, L_2, and L_3.

For nearest neighbor interaction, the dynamical matrices A^c and A^i (in Cartesian and internal displacement coordinates respectively) are given in Figure IV-4. The B matrix has two zero energy independent eigenvectors (free boundary conditions) where p, z are parameters.

$$\begin{pmatrix} p\cos\beta \\ p\cos\beta \\ p \\ p\sin\beta \\ 0 \\ 0 \\ 0 \\ p \end{pmatrix}, \quad \begin{pmatrix} 0 \\ 0 \\ 0 \\ 0 \\ z \\ z\cos\Theta \\ z\cos\Theta \\ 0 \end{pmatrix}$$

There is only one "zero mode" degree of freedom in this L_1, L_2 plane. We have used the relation

$$\cos(\beta + \chi) = 0$$

which L_3 as transverse to L_1. Adding a fourth branch L_4, orthogonal to L_1, we complete the model for bending and transverse motions in a folded chain. Figure IV-5 gives the dynamical matrices A^c and A^i in Cartesian and internal coordinates respectively. There are three noteworthy differences between A^c and A^i:

- A^i is not symmetric; the dissymmetry is introduced by the difference in transverse and longitudinal force constants.
- A^i is of order one less than A^c per fold
- there are 4 nonzero matrix elements a_{ij} such that $|i-j| > 1$, per fold in the internal coordinate reference, compared to 20 in the Cartesian.

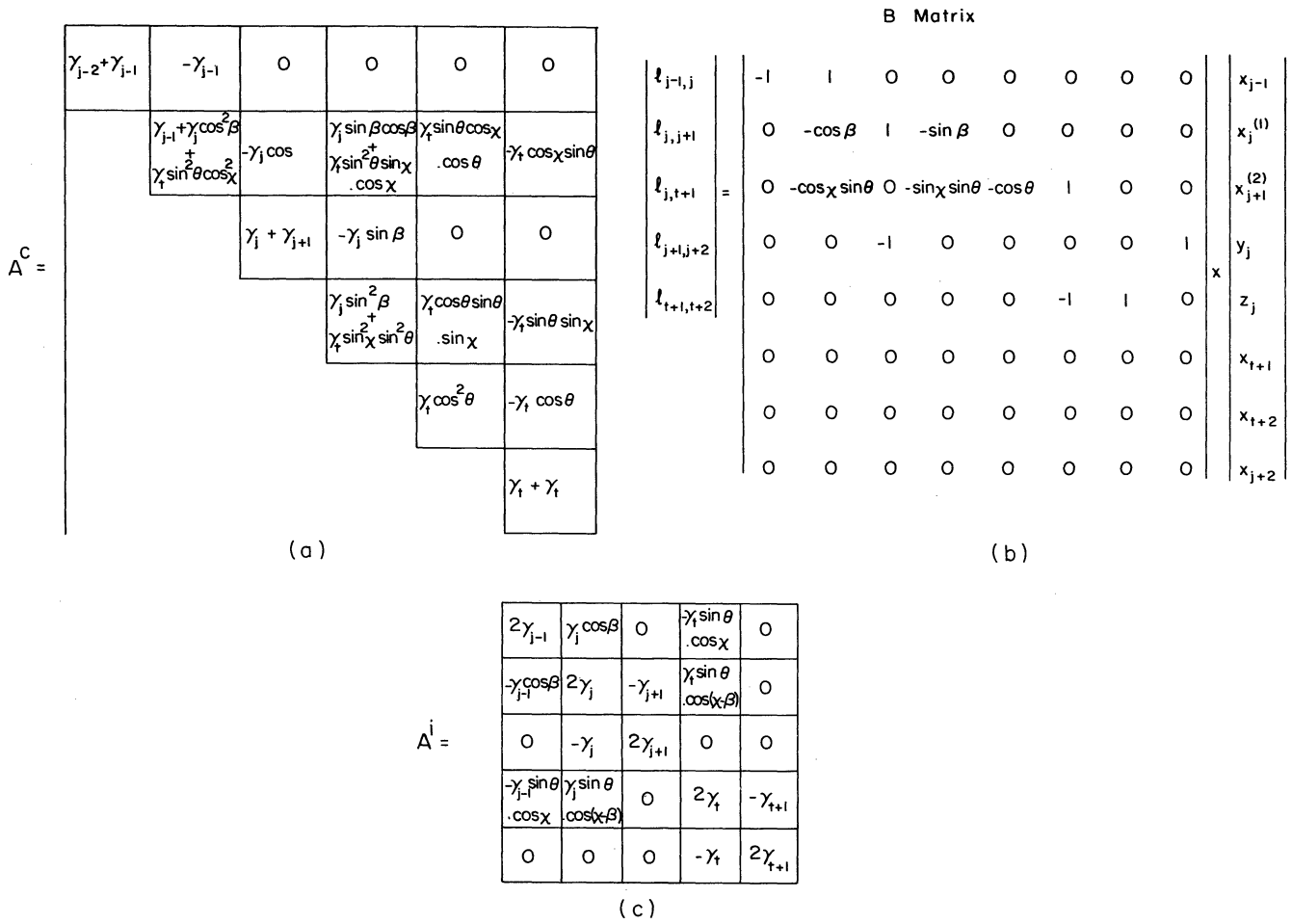

Figure IV-4. Dynamical matrix for the 3 branched lines:
(a) in Cartesian displacement coordinates,
(b) B matrix,
(c) in internal displacement coordinates.

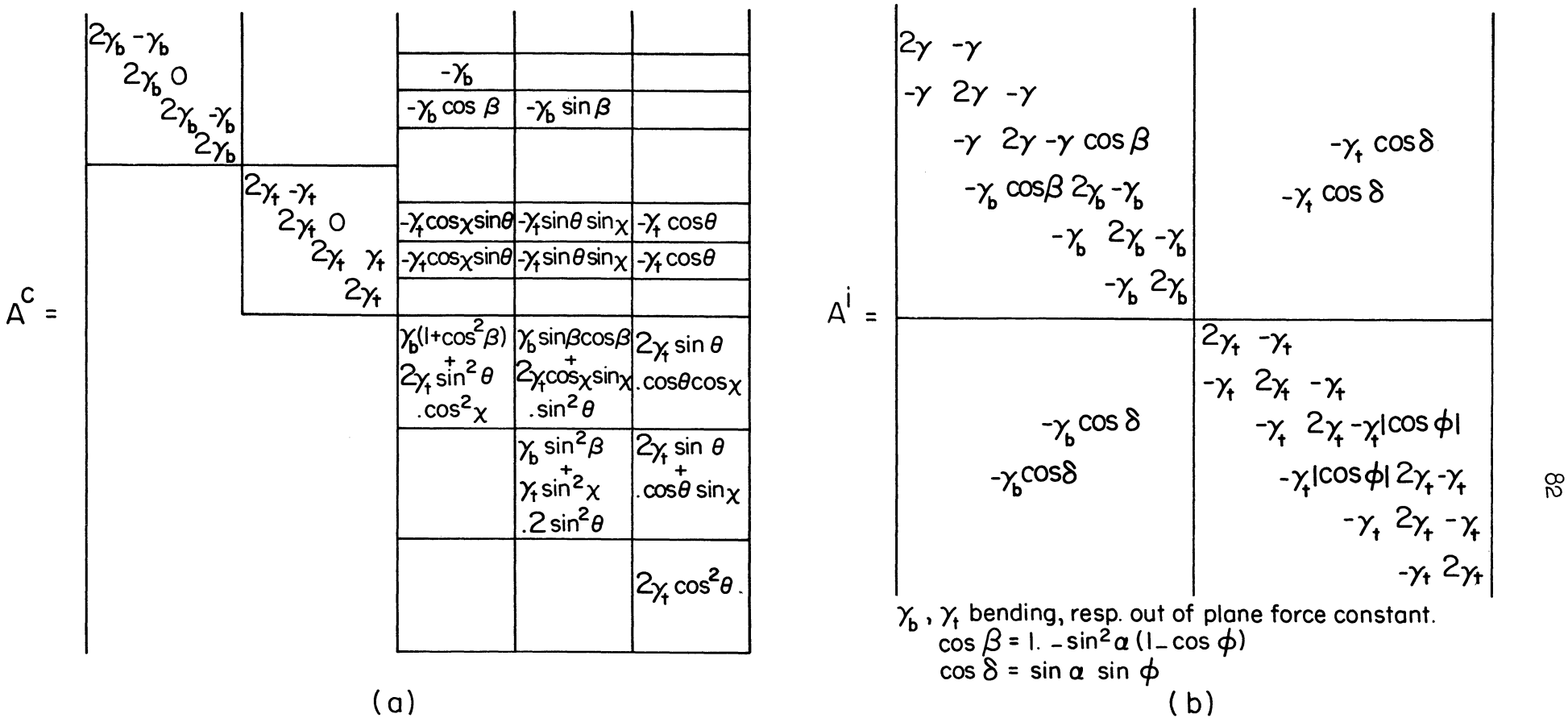

Figure IV-5. Dynamical matrix for a singly folded chain with interaction between bending and out of plane motions and self-effect:

(a) in Cartesian coordinates,
(b) in internal coordinates.

One would consider A^i for calculation of the eigenvalue spectrum rather than A^c; however because of the dissymmetry, A^i does not qualify for the Sturm theorem. More precisely, if D_n is the principal minor of order n of the matrix A - νI, the recurrence relation[56] $D_n D_{n-2} = C_{n-1,n-1} D_{n-1} - C_{n,n-1} C_{n-1,n}$ is generally valid. However $\{D_n\}$ is a Sturm sequence only if $C_{n,n-1}$ has the same sign as $C_{n-1,n}$. This is the case for symmetric matrices. It also is true for tridiagonal matrices such that sign (a_{ij}) sign (a_{ji}), $i \neq j$. Little can be said in the general case, but there is no reason for $C_{n-1,n}$ and $C_{n,n-1}$ to have same signs, for all n. Calculations will therefore be made in Cartesian coordinates.

Useful information can be derived from A^i, both in the special case of equal force constants $\gamma_t = \gamma_b$ and in the general case: we may for instance use the Green's function method for the singly folded chain at vertex j. The defect matrix is

$$\begin{pmatrix}
\vdots & \vdots & \vdots & \vdots & \\
\cdots\ 0 & d_{j-1,j} & \cdots\ 0 & d_{j-1,j+N} & \cdots \\
\cdots\ d_{j,j-1} & 0 & \cdots\ d_{j,j-1+N} & 0 & \cdots \\
\vdots & \vdots & \vdots & \vdots & \\
\cdots\ 0 & d_{j-1+N,j} & \cdots\ 0 & d_{j-1+N,j+N} & \cdots \\
\cdots\ d_{j+N,j-1} & 0 & \cdots\ d_{j+N,j-1+N} & 0 & \cdots \\
\vdots & \vdots & \vdots & \vdots &
\end{pmatrix}$$

where $d_{j-1,j} = -\gamma_b(\cos\beta - 1)$; $d_{j-1,j+N} = \gamma_t \cos\delta$

$d_{j-1*N,j} = -\gamma_b \cos\delta$; $d_{j-1+N,j+1} = -\gamma_t\,(|\cos\phi_j| - 1)$

The longitudinal motions are labeled by j = 1, ..., N; the transverse, by j+N = N+1,..., 2N. Next we can write:

$$K = I + M_o^{-1} D = \begin{pmatrix} I + K_{11} & K_{12} \\ K_{21} & I + K_{22} \end{pmatrix}$$

where the K_{ij} are 2 x 2 matrices. In particular

$$K_{12} = \begin{pmatrix} g(1)\, d_{j,j+N-1} & g(0)\, d_{j+1,N+j} \\ g(0)\, d_{j,j+N-1} & g(1)\, d_{j-1,N+j} \end{pmatrix}$$

K_{21}, K_{12} correspond to the interaction effect; K_{11}, K_{22} correspond to the attenuation effect, derived in the last paragraph. The calculation in closed form of ΔG, the correction to the frequency distribution, cannot be done from $|K| = 0$ with the technique used previously. This is a limitation of the Green's function method. We consider therefore the approximate problem

$$\tilde{K} = \begin{pmatrix} I & K_{12} \\ K_{21} & I \end{pmatrix}$$

where the attenuation effect is neglected. Using the transformation (III-9) and specializing for the case $\gamma_b = \gamma_t$ we have:

$$\Delta(\xi) = 1 - \cos^2\delta \; \frac{\xi^2}{(\xi^2-1)^2} \left(\xi^2(2-\cos^2\delta) + 2\right)$$

There is an out-of-band mode corresponding to the root:

$$\xi_o = \frac{\cos\delta - 1}{1 - \cos^2\delta}$$

$$\omega^2_{out} = \frac{\omega_L^2}{2}\left(2 - \frac{(\cos\delta-1)^2 + (1-\cos^2\delta)^2}{(1-\cos^2\delta)(\cos\delta-1)}\right) \qquad \text{(IV-7)}$$

(see Figure IV-6)

It is present in the entire ϕ interval. For the more realistic case $\gamma_b \neq \gamma_t$ it is calculated from the root

$$-1 < \xi_o < o \qquad \text{of}$$

$$\xi^4(1 + \epsilon \cos^2(\cos\delta-2)) + \xi^3 \cos^2\delta\,(\epsilon - 1)$$

$$-2\,\xi^2\left(\cos^2\delta\left(1 + (1-\epsilon)\cos^2\delta\left(\frac{\cos^2\delta-1}{2}\right)\right) + 1\right) + 1 = 0$$

where $\epsilon = \gamma_t/\gamma_b$

The appearance of the out-of-band mode is characteristic of the bending-torsion interaction and can be contrasted to the attenuation or self-effect. These two effects work somewhat in opposition. When both are present, the separation from the continuum is less pronounced, and in part of the ϕ interval the out-of-band mode rejoins the continuum. This behavior is shown in Figure IV-6. (For the symmetric case $\gamma_t = \gamma_b$, the calculation is made from the negative eigenvalue theorem; A^i is partitioned in submatrices of equal order.) We need to invert X only for 2 of its element, in the case of a single fold (see Chapter II).

Prediction of out-of-band modes can also be made from the norm of the dynamical matrix. More precisely, the eigenvalues are known[57,58] to belong to the intersection of two families of circles D_1 and D_2 (also

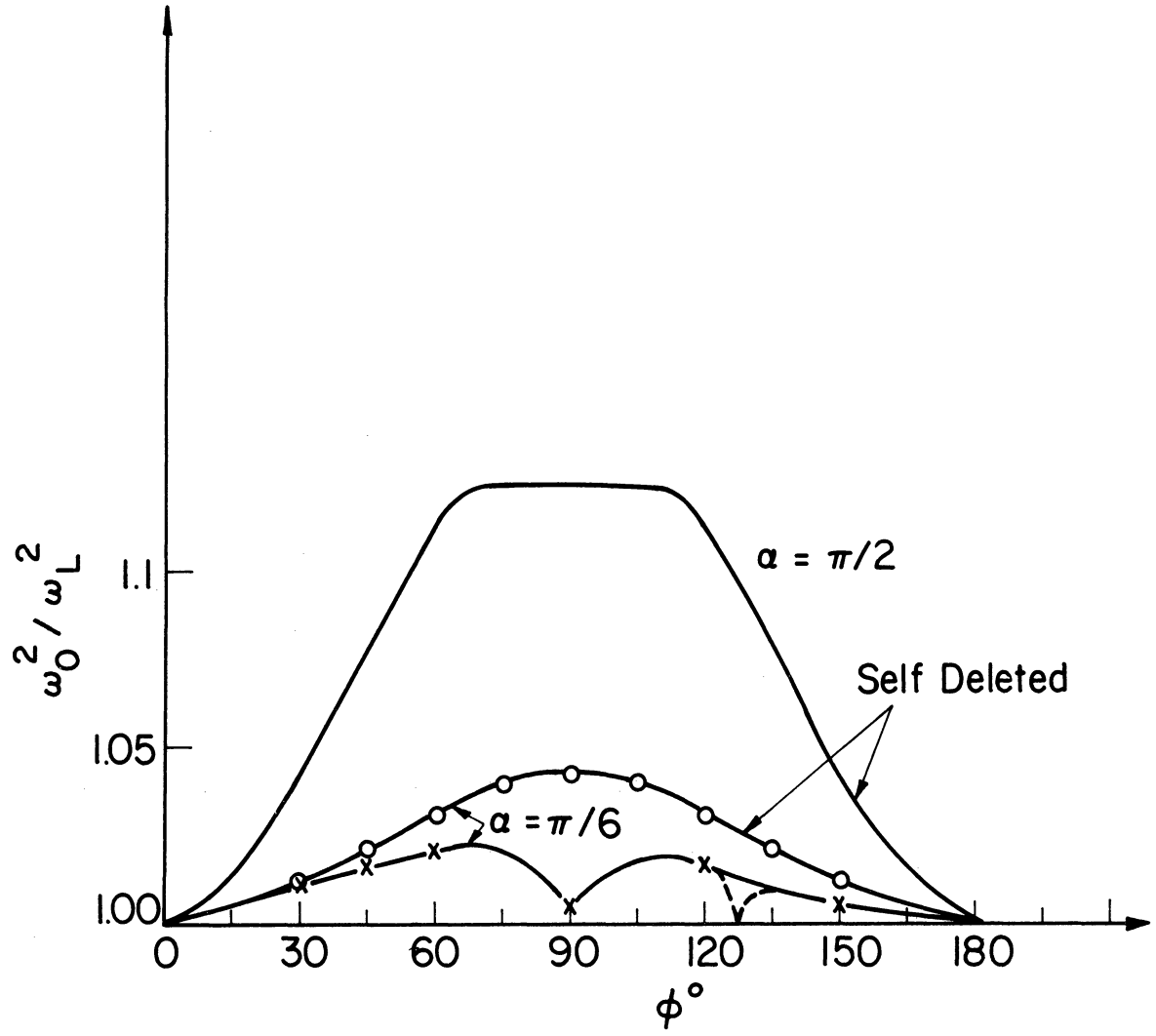

Figure IV-6. Out-of-band mode for bending and transverse motions described in Figure IV-5, as a function of ϕ, for $\gamma_t = \gamma_b$. The two top curves are derived from the Green's function method on a model deleting the self effect (see Eq. (IV-7)). The bottom curve takes self and interaction effects into account.

called Hadamard circles) where

D_1 = union of all circles of center a_{ii} and radius

$$d_i = \sum_{j \neq i} |a_{ij}|$$

D_2 = union of all circles of center a_{ii} and radius

$$f_i = \sum_{j \neq i} |a_{ji}|$$

We consider the matrix elements of A^i (Figure IV-5 as a function of ϕ. The circles are centered around $2\gamma_b$ and $2\gamma_t$. These centers are independent of ϕ, but some radii (lines 3,4,9,10) depend on ϕ; there are actually two radii for each diagonal element, one calculated from the row, the other from the column. If the smallest circle of such a pair overlaps the position of the highest uperturbed (ϕ = o) mode, an out-of-band mode can appear. Whether it actually does is not decided so easily. Calculations tend however to show that separation occurs when allowed.

When $\gamma_t/\gamma_b \ll 1$, clearly only the circles centered around $2\gamma_b$ need to be considered; conversely for $\gamma_t\gamma_b \gg 1$, only the circles centered around $2\gamma_t$ are relevant. In the vicinity of $\gamma_t/\gamma_b = 1$ the circles of lines 3, 4 and 9, 10 compete for a possible out-of-band mode. We consider these cases successively.

For $\gamma_t/\gamma_b \ll 1$, the condition for separation from the continuum is:

$$\text{column:} \quad \gamma_b(1 + \cos\beta) + \gamma_b \cos\delta \geq 2\gamma_b$$

$$\text{row:} \quad \gamma_b(1 + \cos\beta) + \gamma_t \cos\delta \geq 2\gamma_b \qquad \text{(IV-8)}$$

We use a two-parameter $(\phi, \gamma_t/\gamma_b)$ representation of these inequalities (Figure IV-7). The first inequality requires ϕ to be on the left side of line L; the second further requires (γ_t/γ_b) to be above the S line. We notice here the role of the dissymmetry in matrix elements: it provides two separate conditions where one is a refinement of the other. In the case of a symmetric matrix (such as A^c, which is equivalent to A^i) rows and columns yield identical information; the latter is however expressed in a more complex form than the elementary dependence on the parameters in either row or column of the dissymmetric matrix: the dissymmetry performs a decomposition.

Similarly for $\gamma_t/\gamma_b \gg 1$, one has to consider:

$$\text{column:} \quad \gamma_t(1 + |\cos\phi|) + \gamma_t \cos\delta \geq 2\gamma_t$$

$$\text{line:} \quad \gamma_t(1 + |\cos\phi|) + \gamma_b \cos\delta \geq 2\gamma_t \qquad \text{(IV-9)}$$

Here ϕ is to be on the right side of L and (γ_t/γ_b) below the S line.

As (γ_t/γ_b) approaches 1 from above, circles centered about $2\gamma_b$ as well as circles centered about $2\gamma_t$ may overlap the highest unperturbed $(\phi = 0)$ mode:

$$2\gamma_b + \gamma_b(1 + \cos\beta) + \gamma_b \cos\delta \geq 2\gamma_t + \gamma_t(1 + |\cos\phi|) + \gamma_b \cos\delta \qquad \text{(IV-10)}$$

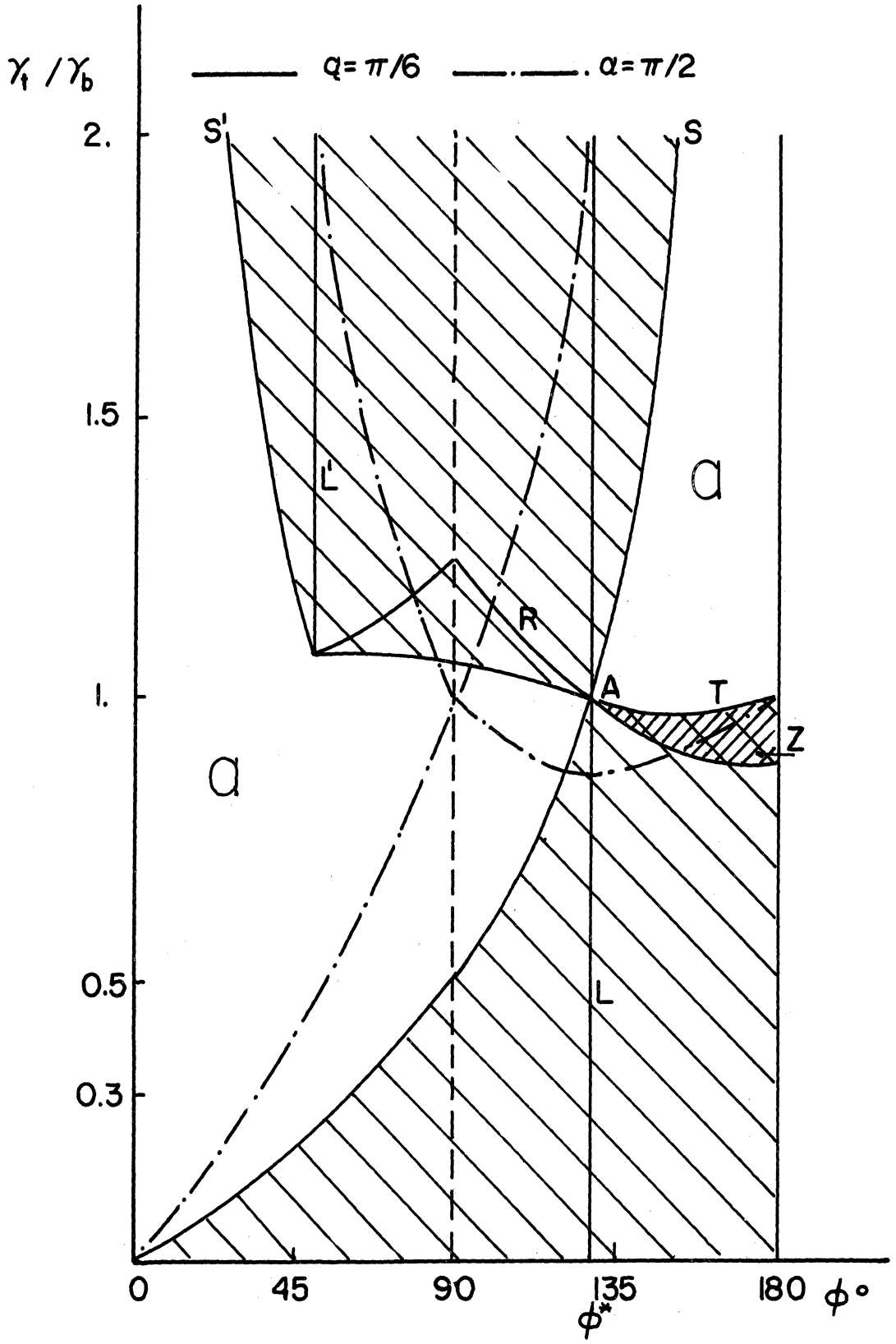

Figure IV-7. Allowed regions for out-of-band modes in the bending-transverse motion model, derived from matrix A^i in Figure IV-5. See Eqs. (IV-8) and (IV-12).

or $$\gamma_t/\gamma_b \leq \frac{3 + \cos\beta}{3 + |\cos\phi|} \qquad \text{(line R)}$$

The forbidden region is now shifted above line R, left of L, provided that the norm of the matrix is greater than its value at $\phi = 0$

$$\gamma_b(1 + \cos\beta) + \gamma_b \cos\delta + 2\gamma_b \geq 4\gamma_t \qquad \text{(IV-11)}$$

or $$\gamma_t/\gamma_b \leq \frac{3 + \cos\beta + \cos\delta}{4} \qquad \text{(line T)}$$

The provision does not hold in region z which must be subtracted from below R.

Approaching $(\gamma_t/\gamma_b) = 1$ from below, the two requirements are:

$$2\gamma_t + \gamma_t(1 + |\cos\phi| + \gamma_t \cos\delta \geq 4\gamma_b$$

$$2\gamma_t + \gamma_t(1 + |\cos\phi| + \gamma_t \cos\delta \geq \gamma_b(1+\cos\beta) + \gamma_t \cos\delta + 2\gamma_b \qquad \text{(IV-12)}$$

They correspond to lines T and R on the right hand side of L.

We notice that there is only one angular value ϕ^* for which no out-of-band mode can appear, irrespective of the γ_t/γ_b ratio, and that it is the point of triple crossing (Figure IV-1).

At $\gamma_b/\gamma_t = 0.3$, which is an acceptable value for polyethylene, a separation from the continuum occurs only in the interval $0 \leq \phi \leq \pi/3$. This is far from the actual value $\phi = 120°$ and leads to conjecture that the interaction is then small compared to the self-effect. We shall evaluate this assertion with numerical results.

The behavior of the out-of-band mode in Figure II-6 does not reflect the prediction of Figure IV-7 near point A. (Although the curve is slightly depressed in the right branch.) The smallest value for the out-of-band mode is registered at $\phi = \pi/2$, corresponding to the total attenuation of transverse motion.

STRETCH AND TRANSVERSE MODE INTERACTION

The actual ratio of stretch to torsion force constants is of order 10; the circles centered about $2\gamma_t$ and $2\gamma_s$ are disjoint, because of the $\cos 2\alpha$ attenuation in the stretch motion. This corresponds to a forbidden gap at $\phi = 0$. We consider only the case $\gamma_s/\gamma_t \gg 1$. From Figure IV-8, a mode may separate from the transverse continuum if

$$\gamma_t(1 + |\cos \phi| + \sin \phi \sin 2\alpha) \geq 2\gamma_t$$

For $2\alpha = 60°$ this inequality yields a small "forbidden" interval around $\phi = 90°$; $\phi = 120°$ is an allowed value.

Two modes may separate from the lower and upper bounds of the stretch continuum, respectively, if

$$2\gamma_s \cos 2\alpha + 2\gamma_t \sin \phi \sin 2\alpha \geq 2\gamma_s \cos 2\alpha$$

This condition is always satisfied because the stretch mode does not suffer attenuation under internal rotation ($\phi \neq 0$). Hence a single fold may yield 3 out-of-band modes. The interaction effect is best observed in the vicinity of the stretch continuum and the transverse-stretch forbidden

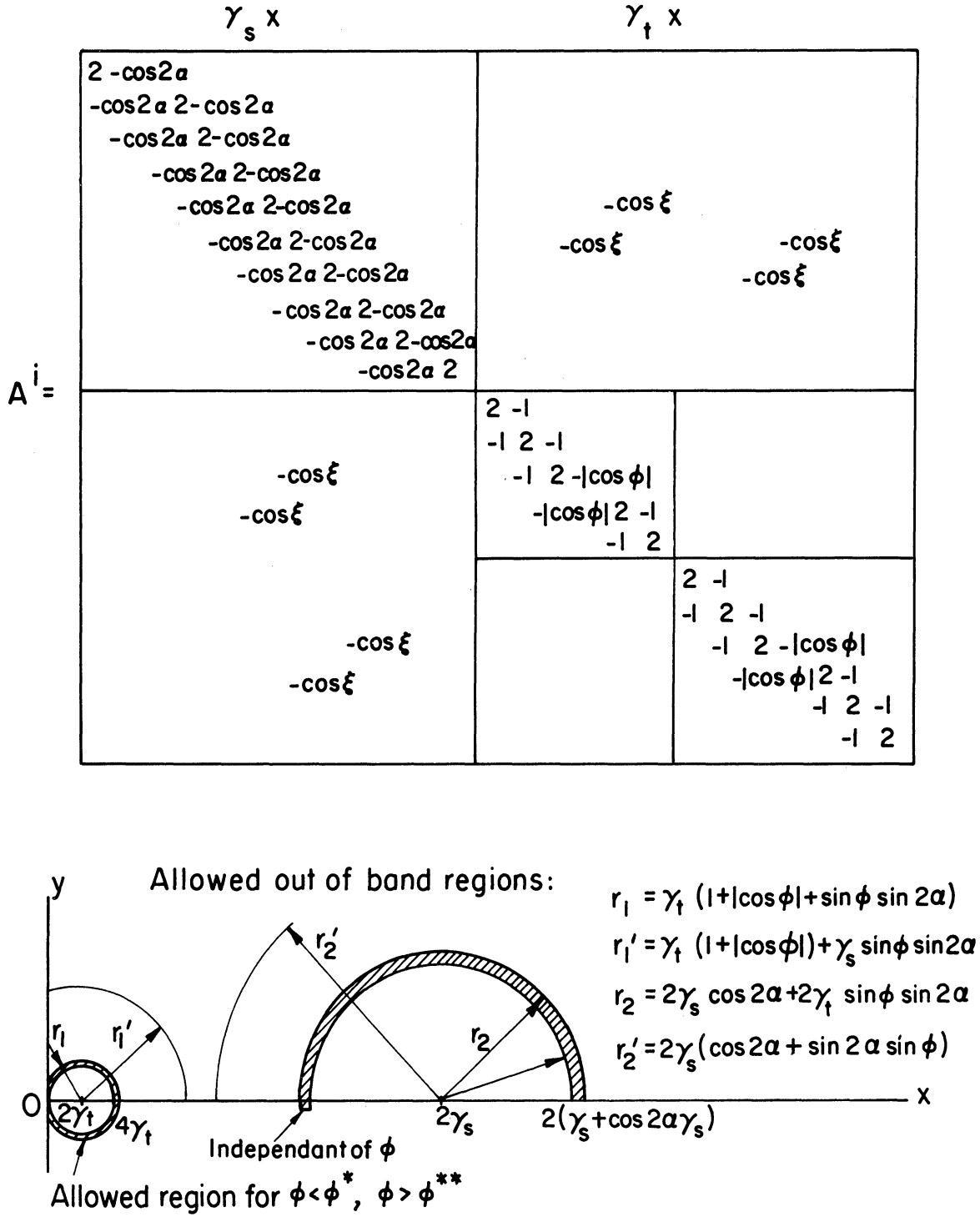

Figure IV-8. Interaction of stretch and transverse motions; dynamical matrix in internal coordinates for a singly folded chain. The shaded rings are differences between Hadamard circles at $\phi = 120°$ and $\phi = 0$.

gap. (If bending is superposed, the isolated mode separated from the transverse continuum joins the bending continuum.)

As a further consequence of the fold, even and odd rows are coupled through the transverse-stretch interaction.

CALCULATIONS FOR A 3-FOLDED CHAIN (Figure IV-9)

The frequency distribution of longitudinal and out-of-plane motions is calculated for a chain of 20 mass points and fixed boundary conditions. The Cartesian matrix is of order 2 x 20 + 3. The eigenvalue distribution is determined from the negative eigenvalue theorem, with the 1, n-1 partition. To evaluate the relative importance of interaction and attenuation (or self) effects, the same problem is also treated with the self-effect only (case S). The corresponding matrix is written in internal coordinates, is tridiagonal and of order 2 x 21. The object of the calculation is to determine the effect of the 3 fold separated successively by 5, 4, 3 and 2 coplanar units; the latter could map the folding of the chain at the crystallites surface.

In case S, the greatest change with respect to the planar configuration is the attenuation of the torsion and bending cut-off peaks: this is however related only to the concentration of the defects, not to their separation. The clustering of the folds seems to spread the excess modes from the bending peak uniformly into the continuum. This is not the case when motions are locally coupled. The excess modes concentrate then towards the end of the bending continuum. In this model clustering has a

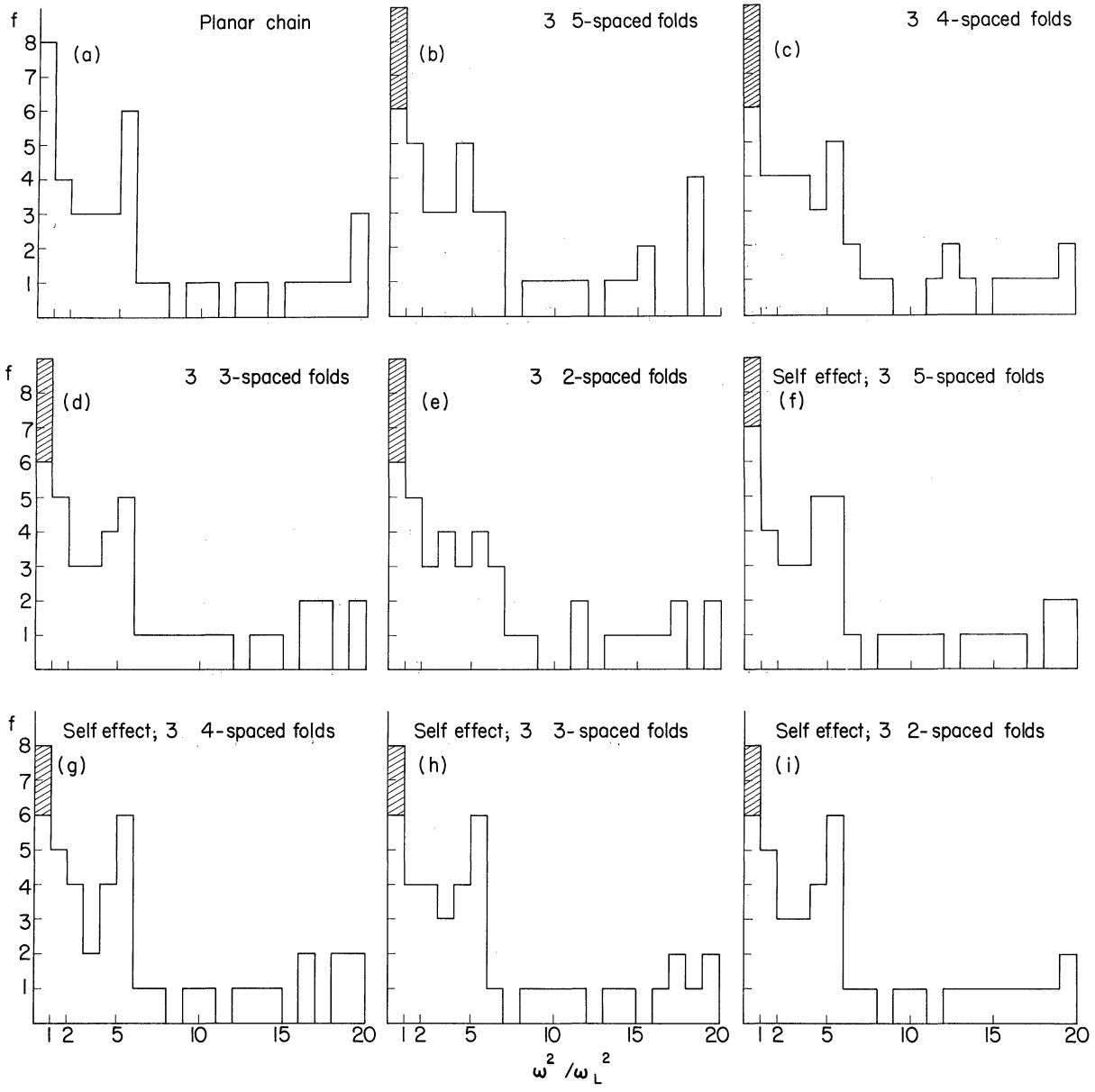

Figure IV-9. Squared frequency distribution for a chain of 20 mass points with longitudinal and transverse motion. The dynamical matrix is similar to Figure IV-5(a). The shaded areas are zero energy modes. Three folds are introduced with various separations:

(a) planar conformation,
(b) to (e) interaction and self-effect,
(f) to (i) self-effect only.

major effect, to wash out the torsion "cut off," where the excess modes fill the continuum on both sides. This does not agree with the observed results of Danner et al.,[7] for which the bending cut off is washed out. However, this experiment is very inaccurate at the energy of the bending continuum. Our result is that for a well separated fold distibution, the frequency pattern is dominated by the self-effect, whereas a clustered distribution yields a more typical interaction effect.

The gauche conformation ($\phi = 120°$ for $\alpha = 34°$) is certainly a remarkable angle*: at this value the self-effect essentially determines the F.D. for any ratio of the force constants. The coupling itself has two effects, it separates modes from the continuum and it redistributes the continuum. When competing with attenuation in the gauche conformation, only the second is discernible and this requires clustered folds. Attenuation does not occur in the stretch motion, hence all interaction effects will best be observed in that part of the spectrum.

*Though for $\gamma_t/\gamma_b = 1$, $\phi = \pi/2$ (total attenuation) seems more remarkable.

CHAPTER V

KIRKWOOD-PITZER MODEL

The dimension of the lattice and the range of forces are known to have considerable influence on the harmonic frequency distribution. We have considered simple chains of a one-dimensional type and with nearest neighbor interactions. The model of Chapter IV is "locally" three dimensional and has "locally" next to nearest neighbor forces, depending on the density of folds. In the Kirkwood model, the in plane motion is uniformly two-dimensional and has a next to nearest neighbor force range. A folding couples this motion with the out of plane mode, giving a local three-dimensional effect. The out of plane motion as described by Pitzer[18] has a force range of order 3. We will evaluate fold effects on the frequency distribution with this more realistic carbon zigzag backbone.

We let the reference system of vertex j have the x axis aligned with (j-2,j), the y axis in the (j-2,j-1,j) plane upward for odd j, downward for even j; the z axis is perpendicular to (j-2,j-1,j). The Kirkwood equations[15] at vertex j are (where we delete components of the same species with indices smaller than j, i.e., terms below the diagonal in matrix representation):

$$m\ddot{x}_j = \ldots 2(\gamma_b \sin^2\alpha + \gamma_s \cos^2\alpha)x_j - \gamma_s \cos^2\alpha\, x_{j+1}$$

$$-\gamma_b \sin\alpha\, x_{j+2} + (-1)^j \sin\alpha \cos\alpha \left\{ \gamma_1 y_{j-2} - (2\gamma_b - \gamma_s) y_{j-1} \right.$$

$$+ (2\gamma_b - \gamma_s)\, y_{j+1} - \gamma_b\, y_{j+2} \Big\} \qquad (V\text{-}1)$$

$$m \ddot{y}_j = \ldots 2(\gamma_s \sin^2\alpha + 3\gamma_b \cos^2\alpha) y_j - (\gamma_s \sin^2\alpha + 4\gamma_b \cos^2\alpha)\, y_{j+1} + \gamma_b \cos^2\alpha\, y_{j+2}$$

The dimensionality and range are reflected in the dynamical matrix which as a 2 x 2 block matrix is simply bordered (dimensionality effect) and where each block is doubly bordered (range effect).

The basic unit of the Pitzer model is a sequence of 4 neighboring vertices k,l,m,n. If z_k^{lmn} is the distance of vertex k to the (l,m,n) plane, the potential energy of torsional deformation is composed of all $(\gamma_t/2)\,(z_k^{lmn})^2$ terms, for all possible conformations. The equation at vertex j is:

$$m \ddot{z}_j = \ldots 4\gamma_t z_j - \gamma_t z_{j+1} - 2\gamma_t z_{j+2} + \gamma_t z_{j+3} \qquad (V\text{-}2)$$

the matrix is triply bordered.

We denote the matrix elements for the joint equations by a_{ij}

$$i,j = 1,\ldots,NC,\ NC+1,\ldots 2NC,\ 2NC+1,\ldots,3NC$$

where NC is the number of carbon atoms.

We impose cyclic conditions on each of the 9 block matrices separately; the corresponding dispersion relations are:

$$\omega^2 = \omega_o^2 \pm \sqrt{\omega_o^4 + \omega'^4} \qquad (V\text{-}3)$$

where $\omega_o^2 = \frac{\gamma_s}{M}(1 - \cos 2\alpha \cos\theta) + \frac{2\gamma_b}{M}(1 + \cos\theta)(1 + \cos 2\alpha \cos\theta)$

$$\omega'^4 = \frac{8\gamma_b\gamma_s}{M^2}(1 + \cos\theta)\sin^2\theta$$

for the torsional motion:

$$\omega^2 = \frac{8\gamma_t}{M}\sin^2\theta\,(1 \pm \cos\theta) \qquad \text{(V-4)}$$

We compare these relations with the model used in Chapter IV (Eq. (IV-1)). The points of comparison are the location of extreme values on the dispersion relations in Figures V-1, and V-2 and the curvature of these functions at these values. The latter indicates the degree of accumulation of modes at the singular points. By inspection of Figure V-1, we find a decrease of the stretch band and a corresponding increase of the stretch-bend forbidden gap (in Figure V-1 the valence angle α of the model (IV-1) has been adjusted to minimize the difference). The radius of curvature of the lowest singularity in each band is considerably greater. The lower singularity of the stretch band is split in two singularities, which a dimensional effect comparable to the one described in Ref. 21 (compare Figures V-1 and V-8).

The purpose of our calculation is to determine the effects of folds on the frequency distribution; more specifically the influence of these more complex dispersion relations on the disorder phenomena considered in the last chapter.

The matrix elements for a folded chain are the derivatives of the deformation potential energy with respect to Cartesian displacement com-

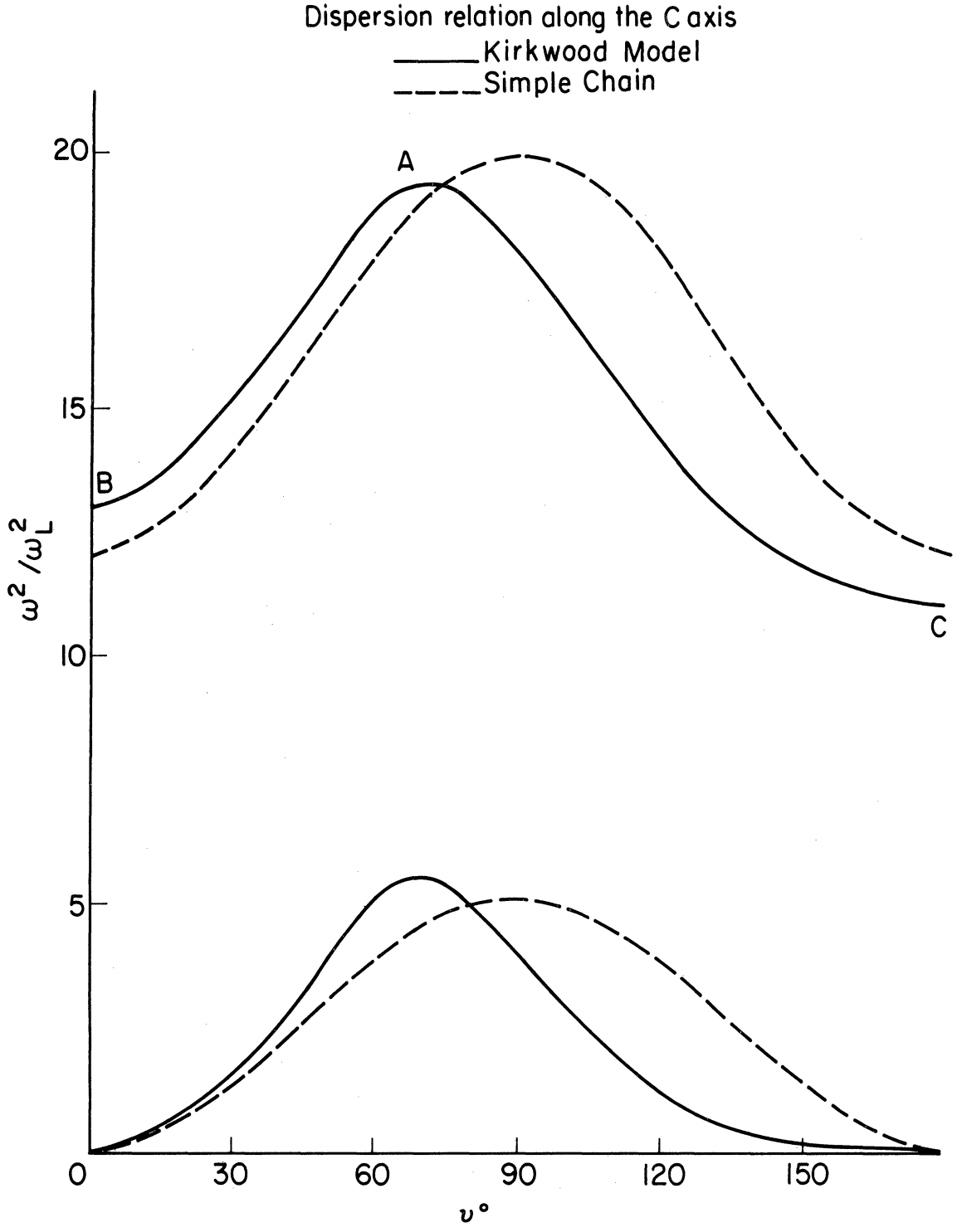

Figure V-1. Dispersion curve for the stretch bend motion of the Kirkwood model Eq. (V-1) and Eq. (IV-1b). The valence angle for the Kirkwood model is $2\alpha = 60°$.

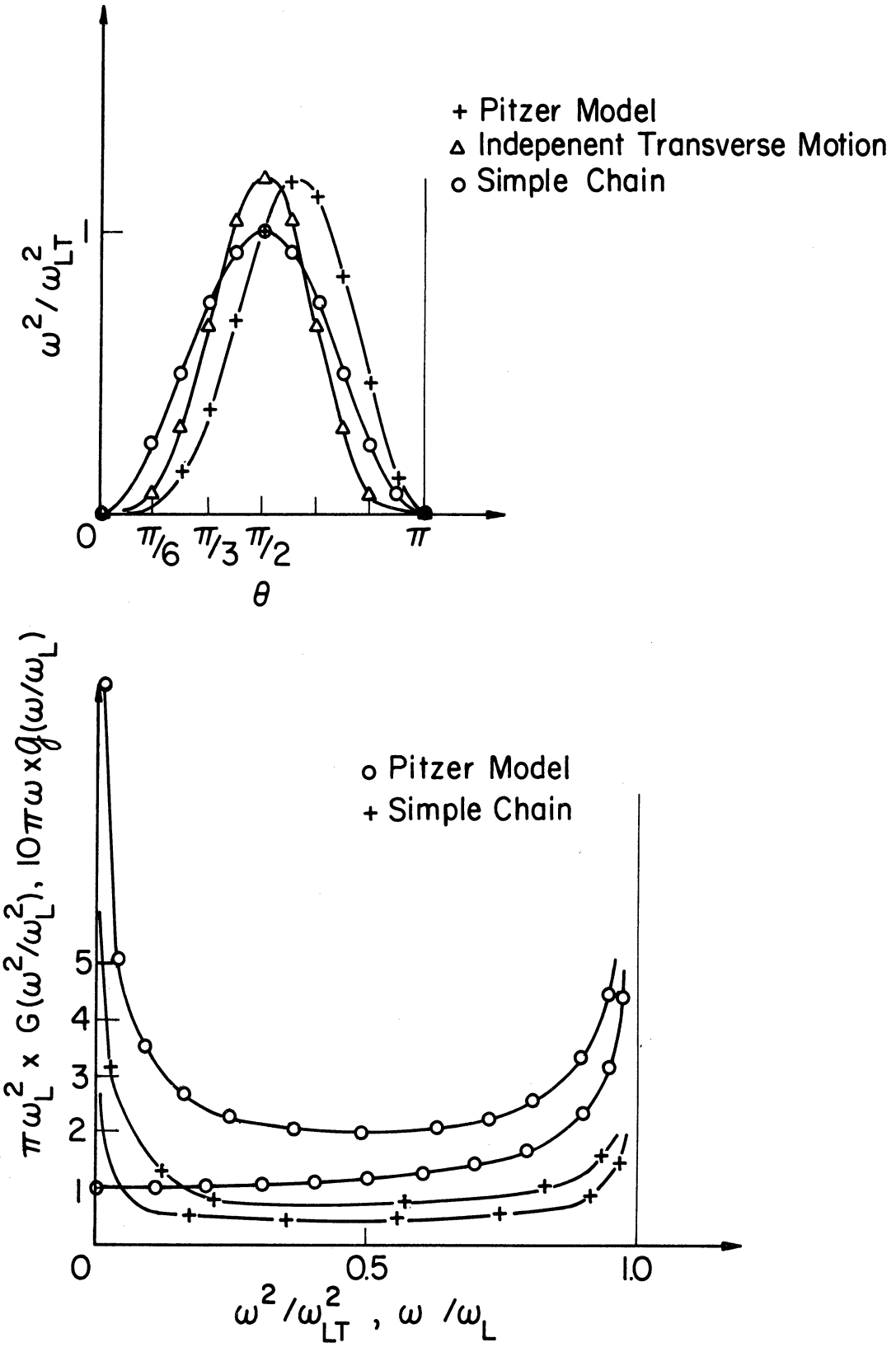

Figure V-2. Dispersion curves for the torsion modes of the Pitzer model Eq. (V-2) and Eq. (IV-1c). The corresponding frequency distributions are obtained graphically.

ponents. It is convenient to separate the contributions of stretching, bending, and torsion energies; the dynamical matrix for the folded chain is accordingly decomposed into:

$$A_f = A'_o + A_{fs} + A_{fb} + A_{ft} \qquad (V\text{-}5)$$

where A_{fs} is the matrix of all elements derived from stretch energy and modified by the fold; A_{fb}, A_{ft} are similarily defined, and A'_o includes all elements not affected by the fold. We consider a chain folded along the (j-1,j) axis.

CONTRIBUTION OF THE C-C STRETCH ENERGY

The potential energy is proportional to the sum of the squared bond length variation $\Delta\ell$ between nearest neighbor vertices. Among all such variations, the expression of $\Delta\ell_{j-1,j}$ only is affected by the fold

$$\Delta\ell_{j-1,j} = (x_{j+1}-x_j)\cos\rho\sin\mu + (y_{j+1} - y_j)\cos\mu + (z_{j+1} - z_j)\sin\rho\sin\mu \qquad (V\text{-}6)$$

(μ,ρ) are the polar coordinates of (j,j+1). From Figure V-3 one has:

$$\sin\mu\sin\rho = \sin 2\alpha \sin\phi$$

$$\cos\mu = \sin\alpha\cos 2\alpha - \cos\alpha\sin 2\alpha\cos\phi$$

One does not expect the stretch frequency distribution to depend on ϕ other than by coupling between bending and torsion modes through the folding.

From (V-6) we have the modified matrix elements:

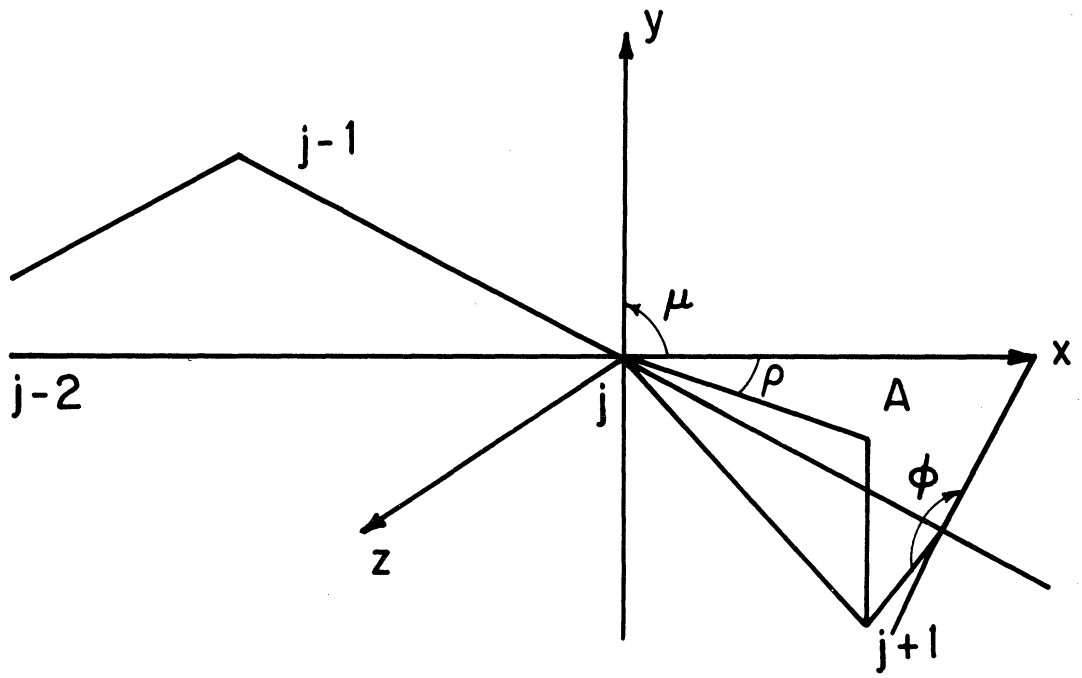

Figure V-3. Three-dimensional representation of vertices j, j+1, j-1 as a function of ϕ. A is the projection of j+1 on the x,y plane; μ,ρ are its polar coordinates.

$$a^s_{jj} = \gamma_s (\cos^2\rho \sin^2\mu + \cos^2\alpha)$$

$$a^s_{jj+1} = -\gamma_s \cos\alpha \cos\rho \sin\mu$$

$$a^s_{j,j+NC} = -\gamma_s(\sin\alpha \cos\alpha - \sin\mu \cos\mu \cos\rho)$$

$$a^s_{j,j+NC+1} = -\gamma_s \cos\rho \sin\mu \sin\alpha$$

$$a^s_{j,j+2NC} = \gamma_s \cos\rho \sin\rho \sin\mu$$

$$a^s_{j+1,j+NC} = -\gamma_s \cos\alpha \cos\mu$$

$$a^s_{j+1,j+2NC} = -\gamma_o \cos\alpha \sin\rho \cos\mu$$

$$a^s_{j+NC,j+NC} = \gamma_s(\cos^2\mu + \sin^2\alpha)$$

$$a^s_{j+NC,j+NC\neq1} = -\gamma_s \sin\alpha \cos\mu$$

$$a^s_{j+NC,j+2NC} = -\gamma_s \cos\mu \sin\mu \sin\rho$$

$$a^s_{j+NC+1,j+2NC} = -\gamma_s \sin\alpha \sin\mu \sin\rho$$

$$a^s_{j+2NC,j+2NC} = \gamma_s \sin^2\rho \sin^2\mu$$

in order to conform with Eq. (V-1), j is assumed even.

CONTRIBUTION OF THE BENDING ENERGY

For the planar chain the bending energy at vertex j is determined from the displacements of j-1, j+1 and j. We proceed here in the same manner (see Figure V-4). The problem is to express the relevant distance

in the appropriate coordinate system.

In the example of Figure V-4 only the displacements of vertices j-1 and j need to be rewritten. For j-1, we calculate the angular variation $\Delta\alpha$ of the projection P'_x of P_x on the plane (j-1, j, j+1); a displacement x_{j-1} of j-1 along x yields

$$\ell\, \Delta\alpha_x = -x_{j-1} \sin\alpha \cos\phi \qquad \text{(V-7)}$$

Similarily for y_{j-1}, z_{j-1} the contribution is:

$$\ell\, \Delta\alpha_y = -y_{j-1} \cos\alpha \cos\phi$$

$$\ell\, \Delta\alpha_z = -z_{j-1} \sin\phi$$

For j we calculate the projection of the displacement (x_j, y_j, z_j) along (A,j), where A is the projection of j on (j-1, j+1); the corresponding angular variations are

$$\ell\, \Delta\alpha_x = x_j \frac{\cos\alpha \sin^2\alpha\, (1-\cos\phi)}{L}$$

$$\ell\, \Delta\alpha_y = y_j \frac{\sin\alpha}{L} (\sin^2\alpha + \cos^2\alpha \cos\phi)$$

$$\ell\, \Delta\alpha_z = -z_j \frac{\sin\alpha}{L} \cos\alpha \sin\phi$$

where

$$L = \Big[\cos^2\alpha \sin^4\alpha\, (1-\cos\phi)^2 + \sin^2\alpha\, (\sin^2\alpha + \cos^2\alpha \cos\phi)^2 + \sin^2\alpha \cos^2\alpha \sin^2\phi\Big]^{1/2}$$

The modified matrix elements for bending energy are then:

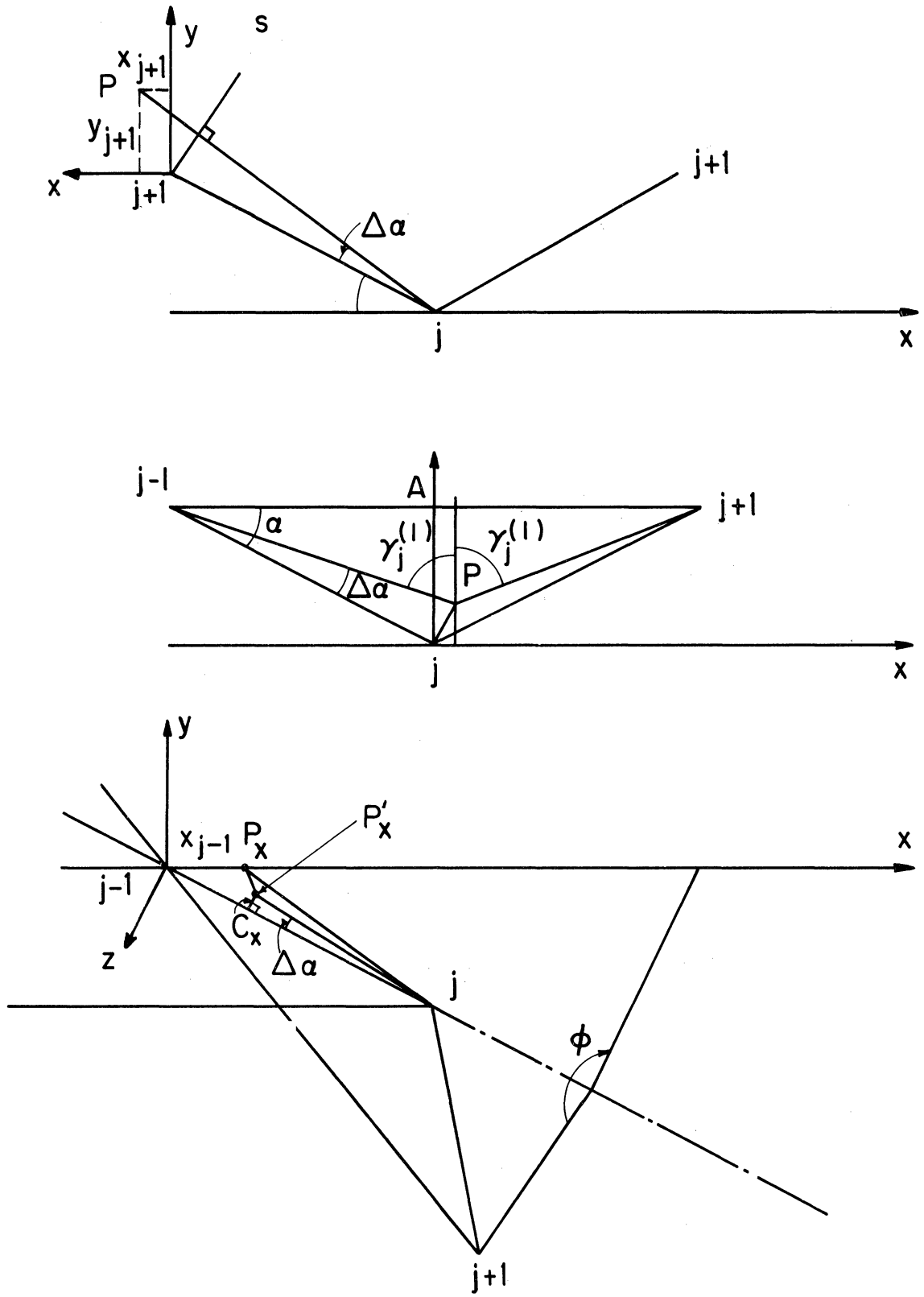

Figure V-4. The first two figures are used to determine the bending energy in the Kirkwood model for a planar chain. The next figure shows the situation for $\phi \neq 0$. (j,P_x) is a displacement along x; P_x' is the projection of P_x on the $(j-1,j,j+1)$ plane. $\Delta\alpha$ is determined from C_x (see Eq. (V-5)).

$$a^{b}_{j-1,j} = \gamma_b \frac{2\cos\phi}{L}(1-\cos^2\phi)\ \sin^2\alpha\ \cos^2\alpha$$

$$a^{b}_{j-1,j+NC-1} = -\gamma_b \frac{(1\cos^2\phi)}{L}\ \sin\alpha\ \cos\alpha$$

$$a^{b}_{j-1,j+NC} = -\gamma_b \frac{2\cos\phi}{L}\ \sin\alpha\ \cos\alpha\ (\sin^2\alpha + \cos^2\alpha\ \cos\phi)$$

$$a^{b}_{j-1,j+NC+1} = \gamma_b\ \cos\alpha\ \sin\alpha\ \cos\phi$$

$$a^{b}_{j-1,j+2NC-1} = \gamma_b\ \sin\phi\ \cos\phi\ \sin\alpha$$

$$a^{b}_{j-1,j+2NC} = -\gamma_b \frac{\sin\phi}{L}\ \cos\phi\ \sin\alpha\ \cos^2\alpha$$

$$a^{b}_{j,j} = \gamma_b \left\{ 4x \frac{(1-\cos\phi)^2}{L^2}\ \sin^2\alpha\ \cos^4\alpha + \sin^2\alpha\ (1 + \cos^2\phi) \right\}$$

$$a^{b}_{j,j+1} = -\gamma_b \frac{2\sin^2\alpha}{L}\ \cos^2\alpha\ (1-\cos\phi)$$

$$a^{b}_{j,j+2} = -\gamma_b\ \sin^2\alpha\ \cos\phi$$

$$a^{b}_{j,j+NC-1} = -\gamma_b \left\{ 2\sin\alpha\ \cos\alpha - \frac{2(1-\cos\phi)}{L}\ \sin\alpha\ \cos^2\alpha\ \cos\phi \right\}$$

$$a^{b}_{j,j+NC} = \gamma_b \left\{ \sin\alpha\ \cos\alpha\ (1-\cos^2\phi) - \frac{4\cos^3\alpha}{L^2}\ (1-\cos\phi)\sin\alpha(\sin^2\alpha + \cos^2\alpha\ \cos\phi) \right\}$$

$$a^{b}_{j,j+NC+1} = \gamma_b \left\{ 2\sin\alpha\ \cos\alpha\ \cos\phi + \frac{2}{L}\ \cos^3\alpha\ (1-\cos\phi)\sin\alpha \right\}$$

$$a^{b}_{j,j+NC+2} = -\gamma_b\ \sin\alpha\ \cos\alpha\ \cos\phi$$

$$a^{b}_{j,j+2NC-1} = +\gamma_b \frac{2\sin\alpha}{L^2}\ \sin\phi\ \cos^2\alpha\ (1-\cos\phi)$$

$$a^{b}_{j,j+2NC} = -\gamma_b \left\{ \frac{2\cos^2\alpha}{L}\ (1-\cos\phi)\ \sin\alpha\ \sin\phi\ \cos^2\alpha + \sin\alpha\ \cos\phi\ \sin\phi \right\}$$

$$a^b_{j+1,j+NC-1} = -\gamma_b \sin\alpha \cos\alpha \cos\phi$$

$$a^b_{j+1,j+NC} = \gamma_b \frac{2}{L} \sin\alpha \cos\alpha (\sin^2\alpha + \cos^2\alpha \cos\phi)$$

$$a^b_{j+1,j+2NC-1} = -\gamma_b \sin\alpha \sin\phi$$

$$a^b_{j+1,j+2NC} = \gamma_b \frac{\cos^2\alpha}{L} \sin\alpha \sin\phi$$

$$a^b_{j+2,j+2NC} = \gamma_b \sin\alpha \sin\phi$$

$$a^b_{j+NC-1,j+NC-1} = \gamma_b(5\cos^2\alpha + \cos^2\alpha \cos\phi)$$

$$a^b_{j+NC-1,j+NC} = \gamma_b 2\cos^2\alpha \left(1 + \frac{\cos\phi}{L} (\sin^2\alpha + \cos^2\alpha \cos\phi)\right)$$

$$a^b_{j+NC-1,j+NC+1} = \gamma_b \cos^2\alpha \cos\phi$$

$$a^b_{j+NC-1,j+2NC-1} = \gamma_b \cos\alpha \cos\phi \sin\phi$$

$$a^b_{j+NC-1,j+2NC} = -\gamma_b \frac{\cos^3\alpha}{L} \cos\phi \sin\phi$$

$$a^b_{j+NC,j+NC} = \gamma_b \left\{\cos^2\alpha(1+\cos^2\phi) + \frac{4\cos^2\alpha}{L^2} (\sin^2\alpha + \cos^2\alpha \cos\phi)^2\right\}$$

$$a^b_{j+NC,j+NC+1} = -\gamma_b \left\{2\cos^2\alpha \cos\phi + \frac{2\cos^2\alpha}{L} (\sin^2\alpha + \cos^2\alpha \cos\phi)\right\}$$

$$a^b_{j+NC,j+NC+2} = \gamma_b \cos^2\alpha \cos\phi$$

$$a^b_{j+NC,j+2NC-1} = -\gamma_b \cos\alpha \sin\phi \frac{2}{L} (\sin^2\alpha + \cos^2\alpha \cos\phi)$$

$$a^b_{j+NC,j+2NC} = \gamma_b \left\{\frac{2\cos\alpha}{L^2} (\sin^2\alpha + \cos^2\alpha \cos\phi)\cos^2\alpha \sin\phi + \cos\alpha \cos\phi \sin\phi\right\}$$

$$a^{b}_{j+NC+1,j+2NC-1} = \gamma_b \cos\alpha \sin\phi$$

$$a^{b}_{j+NC+1,j+2NC} = -\gamma_b \left\{ \frac{\cos^3\alpha}{L} \sin\phi + 2 \cos\alpha \sin\phi \right\}$$

$$a^{b}_{j+NC+2,j+2N} = \gamma_b \cos\alpha \sin\phi$$

$$a^{b}_{j+2NC-1,j+2NC-1} = \gamma_b \sin^2\phi$$

$$a^{b}_{j+2NC-1,j+2NC} = -\gamma_b \frac{\sin^2\phi}{L} \cos^2\alpha$$

$$a^{b}_{j+2NC,j+2NC} = \gamma_b \left\{ \frac{(\cos^2\alpha \sin\phi)^2}{L^2} + \sin^2\phi \right\}$$

CONTRIBUTION OF THE TORSION POTENTIAL

For a planar chain, this energy is the sum:

$$V_t = \sum_{\{k,\ell,m,n\}} V_k^{\ell mn}$$

overall sets of 4 contiguous indices; $V_k^{\ell mn}$ is the deformation energy of the displacement of vertex k with respect to plane ℓ,m,n. When the chain is folded along (j-1,j), the terms $V_k^{\ell mn}$ for the indices

lower	upper
j-2	j-1, j, j+1
j-1	j-2, j, j+1
j	j-2,j-1,j+1
j+1	j-2,j-1,j

are meaningless, since the rigidity of the ribbon-like structure extends only over planar portions; hence we neglect these terms for $\phi \neq o$. We add these terms only for $\phi = 0$.

For all i = j, j-1, the out of plane displacements are parallel to the z axis of the corresponding reference system. At the vertices j-1, j, the motions transverse to the (j-1,j,j+1) plane have nonzero x and y components, when expressed in the previously defined Cartesian system. From Chapter IV and Figure IV-1 we have:

$$z^{r}_{j-1} = \cos\phi\, z^{\ell}_{j-1} + \sin\alpha \sin\phi\, x_{j-1} + \cos\alpha \sin\phi$$

The indices r, ℓ indicate the half plane (right or left) to which that displacement is orthogonal. A similar expression holds for z^{r}_{j}.

The components of the potential energy having coefficients dependent on ϕ are labeled in the following table.

Indices	
Lower	Upper
j-1	j, j+1, j+2
j	j-1, j+1, j+2
j	j+1, j+2, j+3
j+1	j-1, j, j+2
j+1	j, j+1, j+2
j+2	j-1, j, j+1
j+2	j, j+1, j+2
j+3	j, j+1, j+2

The modified matrix elements for torsion energy are then:

$$a^{t}_{j-1,j+2NC} = -\gamma_t/2 \sin\alpha \sin\phi$$

$$a^{t}_{j-1,j+2NC+1} = -\gamma_t \sin\alpha \sin\phi$$

$$a^t_{j-1,j+2NC+2} = \gamma_t \sin\alpha \sin\phi$$

$$a^t_{j,j} = 3\gamma_{t/2} \sin^2\alpha \sin^2\phi$$

$$a^t_{j,j+NC} = -3\gamma_{t/2} \sin\alpha \sin^2\phi \cos\alpha$$

$$a^t_{j,j+2NC} = 3\gamma_{t/2} \sin\alpha \sin\phi \cos\phi$$

$$a^t_{j,j+2N+1} = -\gamma_{t/2} \sin\alpha \sin\phi$$

$$a^t_{j,j+2NC+2} = -2\gamma_t \sin\alpha \sin\phi$$

$$a^t_{j,j+2NC+3} = \gamma_t \sin\alpha \sin\phi$$

$$a^t_{j+NC-1,j+2NC} = -\gamma_{t/2} \cos\alpha \sin\phi$$

$$a^t_{j+NC-1,j+2NC+1} = -\gamma_t \cos\alpha \sin\phi$$

$$a^t_{j+NC-1,j+2NC+2} = \gamma_t \cos\alpha \sin\phi$$

$$a^t_{j+NC,j+NC} = 3\gamma_{t/2} \cos^2\alpha \sin^2\phi$$

$$a^t_{j+NC,j+2NC} = -3\gamma_{t/2} \cos\alpha \sin\phi \cos\phi$$

$$a^t_{j+NC,j+2NC+1} = \gamma_{t/2} \cos\alpha \sin\phi$$

$$a^t_{j+NC,j+2NC+2} = 2\gamma_t \cos\alpha \sin\phi$$

$$a^t_{j+NC,j+2NC+3} = -\gamma_t \cos\alpha \sin\phi$$

$$a^t_{j+2NC-2,j+2NC-2} = 3\gamma_{t/2}$$

$$a^{t}_{j+2NC-2,j+2NC-1} = a^{t}_{j+2NC-2,j+2NC+1} = 0$$

$$a^{t}_{j+2NC-2,j+2NC} = -\gamma_t$$

$$a^{t}_{j+2NC-1,j+2NC-1} = 3\gamma_t/2$$

$$a^{t}_{j+2NC-1,j+2NC} = -\gamma_t(1 + 0.5\cos\phi)$$

$$a^{t}_{j+2NC-1,j+2NC+1} = -\gamma_t\cos\phi$$

$$a^{t}_{j+2NC-1,j+2NC+2} = \gamma_b\cos\phi$$

$$a^{t}_{j+2NC,j+2NC} = 1.5\,\gamma_t(1 + \cos^2\phi)$$

$$a^{t}_{j+2NC,j+2NC+1} = -0.5\,\gamma_t\cos\phi$$

$$a^{t}_{j+2NC,j+2NC+2} = -2\gamma_t\cos\phi$$

$$a^{t}_{j+2NC,j+2NC+3} = \gamma_t\cos\phi$$

There are 47 matrix elements modified by a fold; the proportion of perturbed to unperturbed elements is greater in this model because of the third dimension and the extended range of forces.

DISCUSSION OF RESULTS

Frequency distributions are calculated for chains of 20 and 30 carbon atoms. Three and five folds are introduced at various separations. We have used the Givens-Sturm method to solve the numerical problem (see Chapter II). The effects of folds are the separation of modes from the

continuum into the forbidden gap and redistribution of modes inside the allowed intervals (Figures V-5, V-6, V-7 and V-8). In Chapter IV it was argued that the local interaction between torsion and bending motions is not strong enough to yield out-of-band modes, but that interference of the stretch motion would however enable them to separate. Indeed numerical results indicate three out-of-band modes per fold. One separates from the torsion bending continuum (which is inferred by counting the modes in that interval). The two others are detached on both sides of the stretch band. The separation for the first is very strong as can be seen in Table IV.

TABLE IV

MODES PRODUCED BY FOLDS IN THE LOWER STRETCH-BEND FORBIDDEN GAP

No.	NC	Location of Folds	ϕ	Squared Frequencies*	Frequencies*
1	20	5,10,15	0.784	2.63,2.75,2.87	1.62,1.66,1.69
2	20	5,10,15	2.05	3 at 2.87	3 at 1.69
3	20	5,10,15	2.7	3 at 3	3 at 1.73
4	30	10,15,20	2.05		
5	30	12,15,18	2.05	2.65,2.75,2.8	1.63,1.66,1.67
6	30	5,10,15,20,25	2.05	2.75,2.8,2.8,2.85,2.85	1.16,1.67,1.67,1.69,1.69
7	30	7,11,15,19,23	2.05	2.75,2.8,2.8,2.85,2.9	1.66,1.67,1.67,1.69,1.7

*These numbers are unitless; the actual frequency at 1.73 is 670 cm^{-1}. Two other modes at 4.54(1.95) are to be mentioned in case 5.
Note: The cutoffs are at 1.45(1.2), 7.2(2.68).

The position of this out-of-band mode is given for different fold numbers ϕ angles, separation between folds and chain length. It is seen that as ϕ increases towards π, the out-of-band mode drifts upward; this is somewhat a surprise since the mixing of torsion with stretch-bend motions

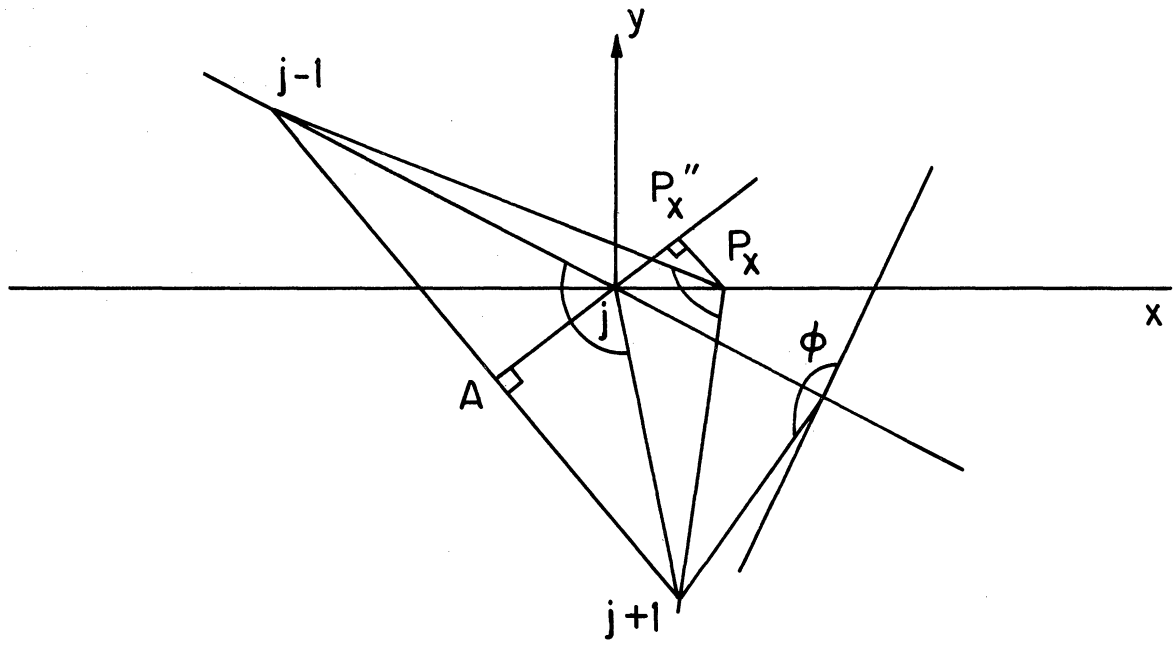

Figure V-5. In this figure P_x is projected along the (A,j) axis, where A is the center of the (j-1,j+1) interval. The change in the angle ($j-1,P_x,j+1$) due to the displacement P_x is calculated from the projection of (j,P_x) on (A,j).

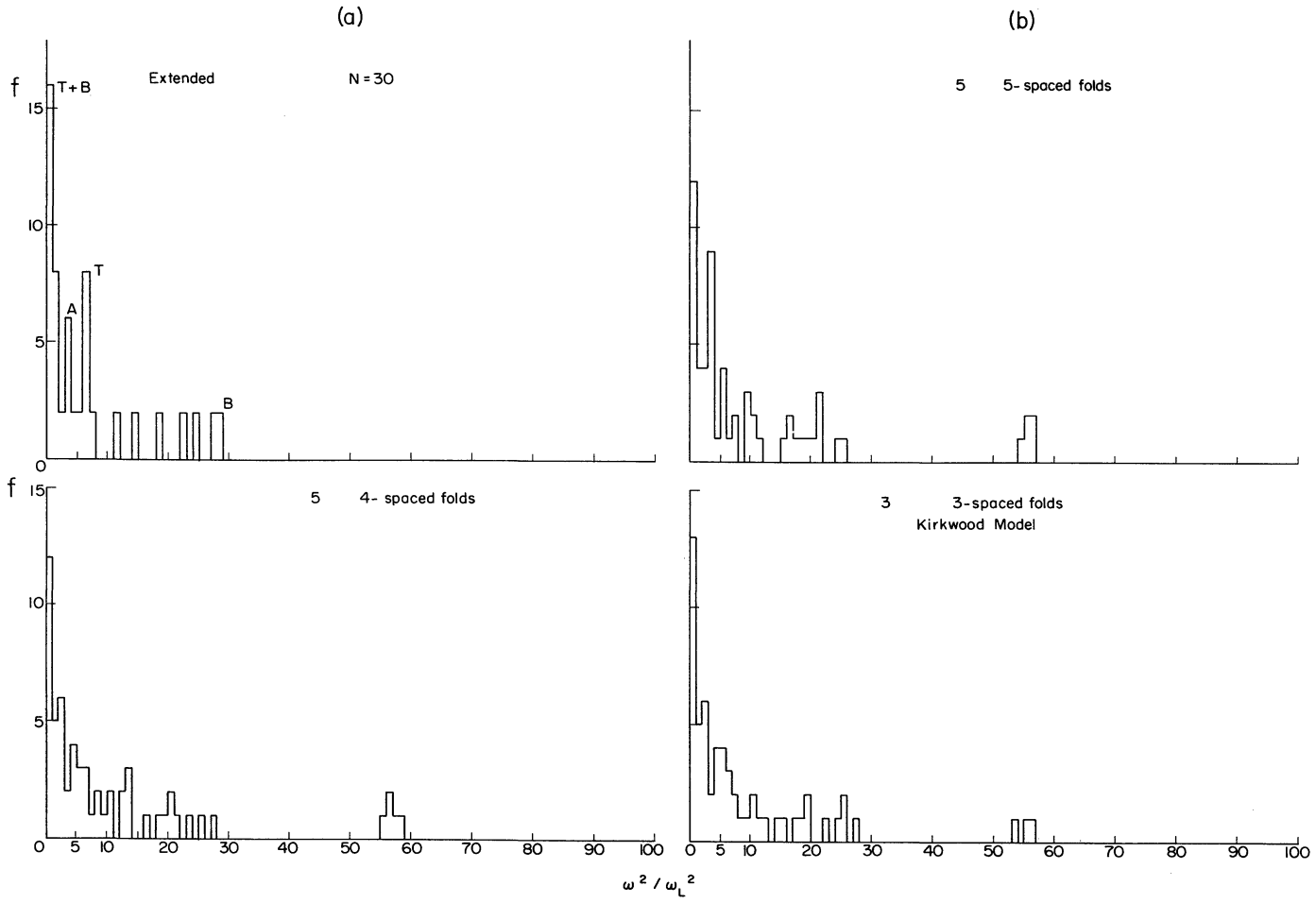

Figure V-6. Squared frequency distributions for the planar chain (N = 30), and various folded conformations. In (a) one identifies (T+B) with the zero energy singularity of torsion and bending motions. T and B are respectively the torsion and bending cut-off. Peak A is accidental. It does not show in the same distribution with a different squared frequency partition (Figure V-7a). Because of the ω^2 scale, the stretch band is further away. The out-of-band modes are easily identified. The folds are indicated in Table IV.

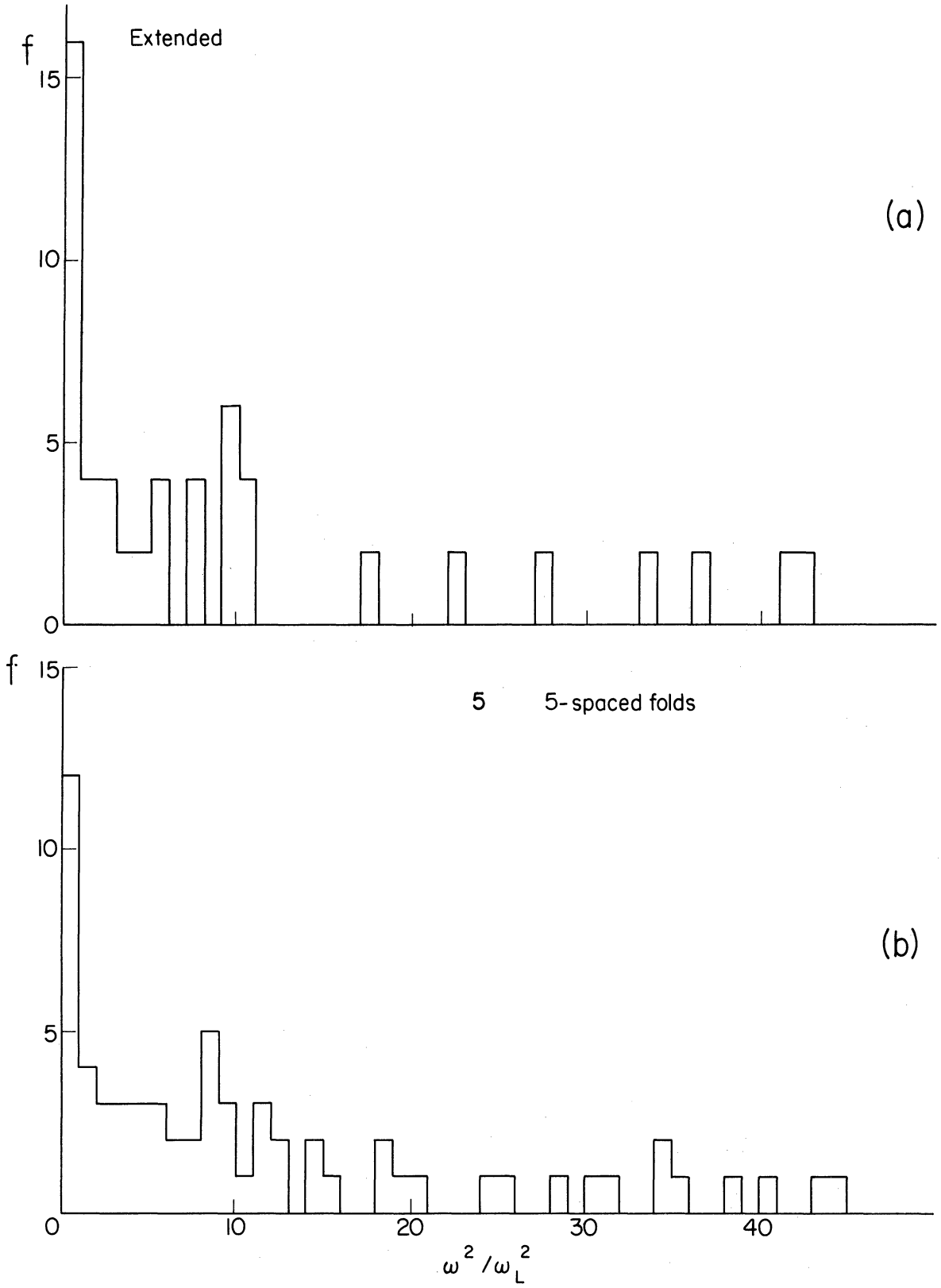

Figure V-7. Same frequency distribution as in Figure V-6a,b with a wider scale.

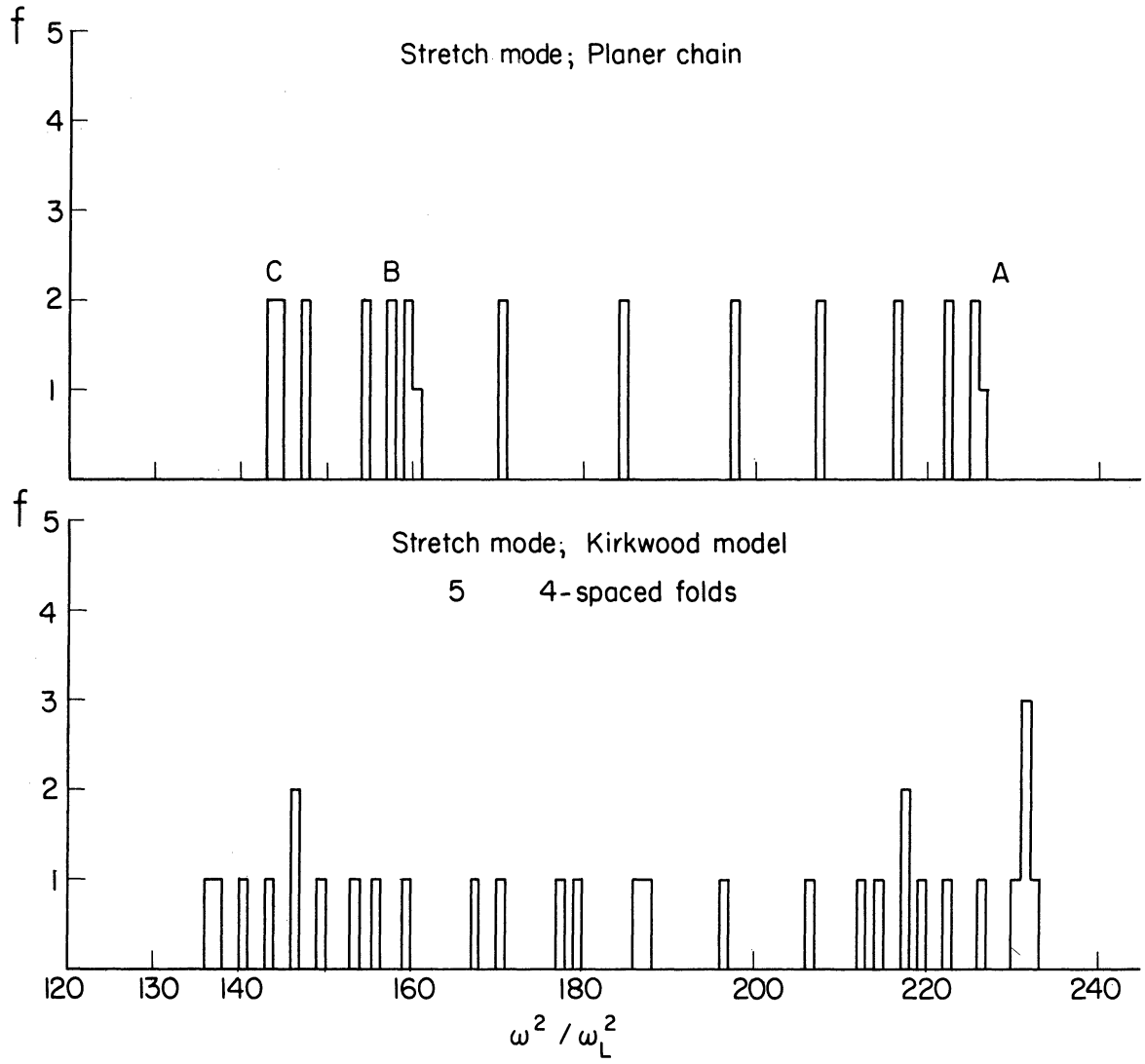

Figure V-8. Frequency distribution for the stretch mode in planar and folded conformation. The folds are indicated in Table IV. The accumulations A,B,C correspond to the horizontal tangents in Figure V-1.

is weak in this φ range.

As expected, a clustering of the folds splits these modes; a further study would allow identification of islands. It is interesting to note that fixed B.C. yield 2 modes at about the same location.

The redistribution in the torsion bending continuum indicates the same trend as in Chapter IV: the clustering of the folds "washes" out the torsion cut off. In addition, the three stretch mode accumulations follow the same pattern. These are however "negative" effects. An interesting question is whether folds contribute to an identifiable peak in any of the continuum. The frequency distributions suffer in the above examples of a "lack" of population, forbidding any further conclusion.

CHAPTER VI

THERMODYNAMICAL FUNCTIONS

We derive the thermodynamical functions from the hamiltonian (II-3)

$$H(c) = H_v(c) + H_p(c)$$

where v,p indicate respectively vibrational and potential energy and where c is a conformation. We consider these terms separately.

The partition function Z_v of the vibrational component is a quantity averaged over ensembles E_1 and E_2. E_1 is the ensemble of conformations specified by a given distribution of configuration angles. E_2 is the ensemble of sets $\{n_j(c)\}$ of occupation numbers $n_j(c)$ associated with the normal mode with energy $h\omega_j(c)$. There is one set for each label $j(j=1,\ldots 3N)$.

For N sufficiently large, the normal frequencies of a particular chain are the frequencies $\omega_j(c)$ averaged over E_1 (see Chapter II). The partition function is then obtained by the average over the ensemble of sets $\{n_j\}$

$$Z_v = \sum_{\{n_j\}} e^{-\sum_j (n+1/2)h\omega_j/k\Theta} = \prod_j \frac{e^{-h\omega_j/2k\Theta}}{1-e^{-h\omega_j/k\Theta}}$$

where Θ is the absolute temperature. Z_v depends on the characteristics of the configuration distribution as described in Chapter III. Further we have

$$F_V = -k\,\Theta \log Z_V$$

$$= k\,\Theta \sum_j \log\left(2 \operatorname{Sinh} \frac{h\omega_j}{2k\Theta}\right)$$

$$S_V = -\left(\frac{\partial F_V}{\partial \Theta}\right)_V \quad ; \quad C_{Vv} = -\,\Theta \left(\frac{\partial^2 F_V}{\partial \Theta^2}\right)_V$$

where V is the volume.

Figures VI-2, VI-3, VI-4 give the behavior of these functions for several configuration distributions. We first review important results given in the literature.

Thermodynamical effects of a single defect in a harmonic lattice are summarized in Figure 1 and 2 of Ref. 59. These effects are changes in free energy ΔF and in specific heat ΔC_V. The latter result is reproduced in Figure VI-1. It shows that the sign of ΔC_V depends on whether the isotope is heavier or lighter. A typical feature is the maximum (miminum) of ΔC_V in the vicinity of 1°K. It will be of interest to inquire whether this temperature is sensitive to the configuration distribution.

Effects of pairs of defects have also been determined. The defects considered in Ref. 59 are the isotope and the spring impurities. Each one has two possible outcomes, namely, light and heavy, weak and strong. There are 12 distinct pairings of such defects. Six of them yield an attractive force, the others repulsion between defects. We add a third species of defect, the fold of the chain. It also has two outcomes, a folding at a smaller or a larger angle ϕ_j than the regular configuration

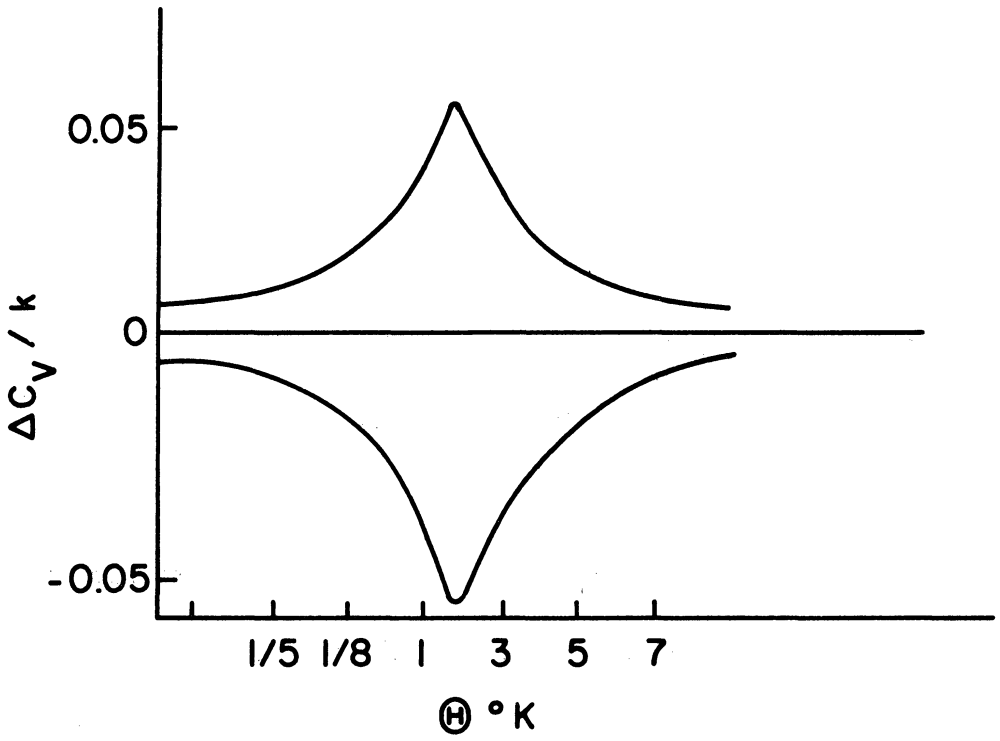

Figure VI-1. Change in specific heat due to a single defect. (From K. Yamahuzi and T. Tanaka, "Effects of Defects on Lattice Vibrations."[59]) The upper curve corresponds to the isotope defect $M' = 4/3\ \gamma$; the lower curve to $M' = 2/3\ M$ or $\gamma' = 3/2\ \gamma$.

angle $\tilde{\phi}$ (see Chapter III). Combining the three types of defects, there are 36 additional distinct pairings. We consider here 2 of them

$$\begin{matrix} \phi_1, \ \phi_2 > \tilde{\phi} \\ \phi_1, \ \phi_2 < \tilde{\phi} \end{matrix} \qquad 0 < \phi_1, \phi_2, \tilde{\phi} < \pi/2$$

where ϕ_1, ϕ_2 are the defect angles. Other cases are of interest, especially the interference of force constant and angular defects at a same site. We reproduce Table 3 of Ref. 59, with these 2 added cases.

TABLE V

SIGN OF THE FREE ENERGY CHANGE DUE TO VARIOUS PAIRS OF DEFECTS

Sign of ΔF_v*	Defect 1	Defect 2
-	$M_1' < M$	$M_2' < M$
-	$\gamma_1' > \gamma$	$\gamma_2' > \gamma$
-	$\phi_1' < \tilde{\phi}$	$\phi_2' < \tilde{\phi}$
+	$M_1' > M$	$M_2' > M$
+	$\gamma_1' > \gamma$	$\gamma_2' < \gamma$
+	$\phi_1' > \tilde{\phi}$	$\phi_2' > \tilde{\phi}$
+	$M_1' < M$	$M_2' > M$
+	$\gamma_1' > \gamma$	$\gamma_2' < \gamma$
-	$M_1' < M$	$\gamma_2' < \gamma$
+	$M_1' < M$	$\gamma_2' > \gamma$

*The interpretation of a negative ΔF_v is attraction of defects; a positive sign corresponds to repulsion. The above free energy is however only a component of our system. Hence we must postpone this interpretation until we calculate the potential energy contribution.

Clustering or repulsion of defects is also derived from comparison of vibrational self-energies[53] (this is the normalization factor of the frequency distribution). For the light isotope defect, a positive difference between defect and reference self-energies implies clustering.

The sign of ΔF_v is related to the appearance of out-of-band modes. For instance two light isotopes, two stronger force constants or two smaller angular folds, yield negative ΔF_v and out-of-band modes. The case of defects of different types is less clear since the appearance of out-of-band modes depends on their relative importance, whereas the sign of ΔF_v does not (see Table V).

We consider distribution of defects in simple chains. Figures VI-2a,b give the entropy and specific heat functions for different concentrations and orderings of T,G configurations. We see that for temperatures lower than 100°K .

- lower concentrations of G's randomly distributed (Bernoulli) have higher entropies.
- at a given concentration, the clustered distributions ($\sigma_B < 0$) have higher entropies than the alternating distributions ($\sigma_B > 0$).

At temperatures above 100°K there is a complete reversal of the "preference." The relative entropy differences are however of smaller order than in the previous temperature range. It is noteworthy that the reversal in entropy differences takes place in a small temperature interval (about 15°), as if the entropy curves had a common intersection.

The heat capacities have a similar behavior: a lower concentration in G configurations and a more clustered order at a given concentration yield higher heat capacities, from absolute zero onwards. Here also a reversal occurs, at however a lower temperature than the entropy.

Information on the structure of macromolecules has been derived from the analysis of the slope of thermodynamical functions. This analysis amounts to a determination of the next higher derivative of the partition function. The point is however that there are temperature intervals in which the specific heat is found to behave typically as a power of Θ. These intervals and the corresponding exponents are determined from observation or calculated from models as a function of several parameters. Using the Stockmayer-Hecht model of polyethylene, Genensky and Newell[21] have partitioned the temperature interval $(0,\Theta_m = \hbar\omega_L/k)$ in five such intervals. The specific heat component for the phonon propagation along the c axis varies as the cubic law up to $\sqrt{\alpha}\Theta_m$, where α is the normalized force constant for nearest neighbor interaction ($\sqrt{\alpha} \cong 0.2$). Thereafter it varies linearly. For the propagation along the other axes, the specific heat components vary from the cubic to the square root law. The cubic law holds only up to $(\gamma/\sqrt{4\ \kappa})\ \Theta_m$, where γ is the diagonal force constant, κ the bending force constant ($\cong 0.003\ \Theta_m$). For the remaining part of the description we refer to Ref. 21.

We analyze the thermodynamical functions of simple chains in a similar manner, relating the characteristic temperature intervals to the ordering of configurations instead of the force constants. We find 3 such intervals

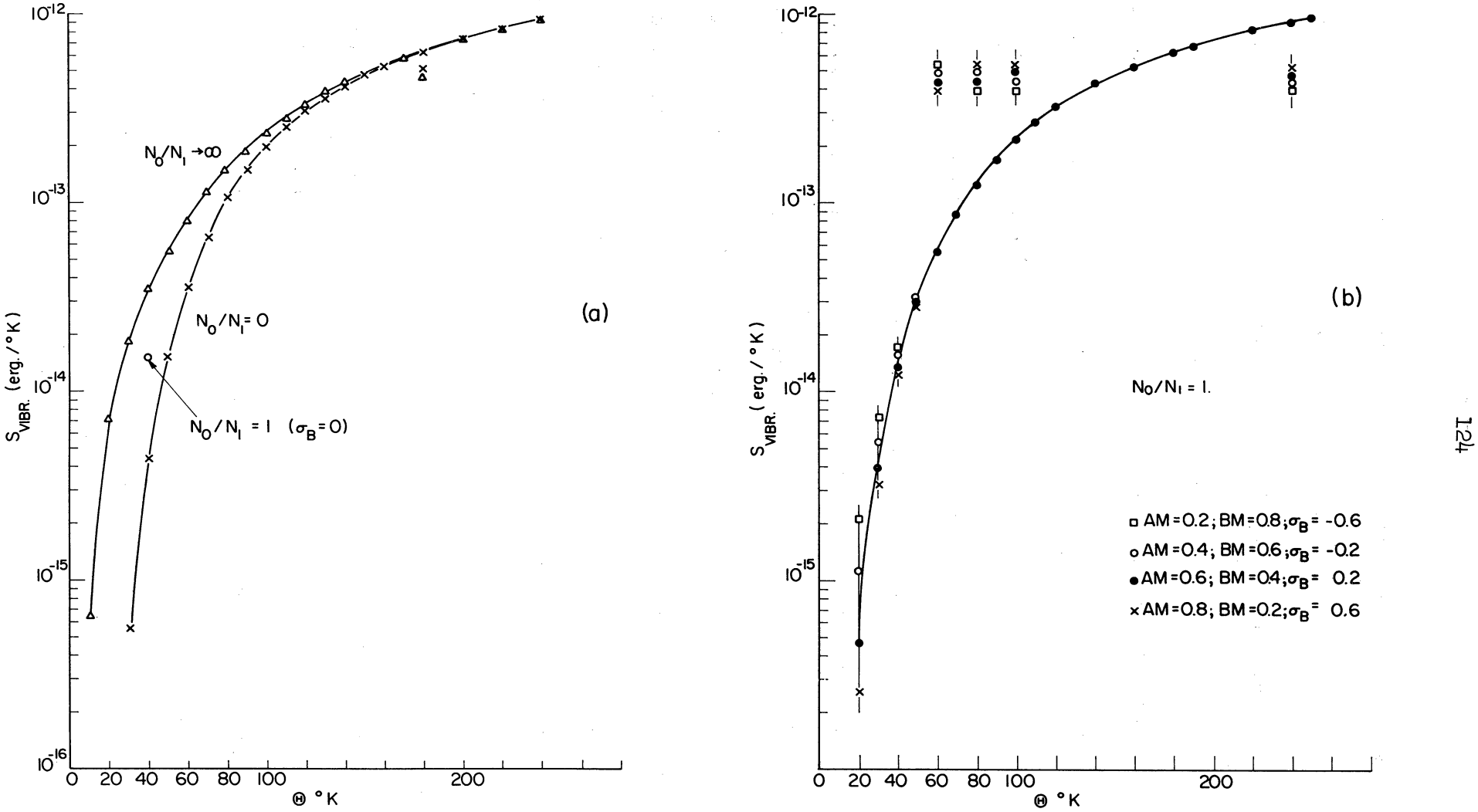
10^{-12}
10^{-13}
10^{-14}
10^{-15}
10^{-16}
$S_{VIBR.}$ (erg./°K)
$N_0/N_1 \to \infty$
$N_0/N_1 = 0$
$N_0/N_1 = 1$ ($\sigma_B = 0$)
(a)
0 20 40 60 80 100 200
Θ °K
10^{-12}
10^{-13}
10^{-14}
10^{-15}
$S_{VIBR.}$ (erg./°K)
(b)
$N_0/N_1 = 1.$
□ AM=0.2; BM=0.8; σ_B = -0.6
○ AM=0.4; BM=0.6; σ_B = -0.2
● AM=0.6; BM=0.4; σ_B = 0.2
× AM=0.8; BM=0.2; σ_B = 0.6
0 20 40 60 80 100 200
Θ °K

Figure VI-2

Figure VI-2. Entropy as a function of temperature for a simple chain of 3000 atoms; force constant $\gamma = 0.25$ millidynes/A°. N_o, N_1 are the number of T, G configurations, respectively.

(a) Effect of concentration of G; the pure G curve has lower entropy up to 180°K; thereafter the two curves are nearly joint with however a higher entropy for the G chain. (This is indicated by the succession of the two separate points on the line $\Theta = 180°K$.)

(b) Effect of order at a concentration $N_o/N_1 = 1$. Four types of order are considered; the coefficients AM, BM are the conditional probabilities that G follow T and that G follow G, respectively. σ_B is the short range order (Bethe). A negative σ_B indicates a concentration of a like pair; a positive σ_B, an alternation. $\sigma_B = 0$ is the Bernoulli process. (See Chapter II for the special case $N_o/N_1 = 1$.) Only one of the curves is traced. The points of the other functions are given in the interval (0,60). Thereafter, only the order in which they appear is indicated. One notices the reversal occurring in the interval (60°, 80°). The corresponding frequency distributions are given in Figure II-1.

(Figures VI-3a,b). The pure T chain has a heat capacity that follows the cubic law in the (0, 80°) interval. The behavior is linear in (80°, 180°) interval and of square root type beyond 180°. For the pure G chain however this function increases faster than the cubic law at lower temperatures. It does follow the square root law beyond 180°. Hence the transition interval between low and high temperature behavior is shorter. This transition is less smooth than in the pure T case.

As for the effect of order at equal concentrations of T and G configurations, it is seen that the transition from the cubic law to the square root law is smoother for the alternating ($\sigma > 0$) than for the clustered ($\sigma < 0$) order.

In general, ordering yields a characteristic temperature dependence of the thermodynamical functions similar in importance to the effects of dimension of the lattice and force range. At this stage it is difficult to say to which effect these functions are more sensitive. We can however assign a temperature interval in which the effects of order are most noticeable. From Figures VI-1, VI-2 and VI-3 this is the (0,10°K) interval.

We now consider more specifically polyethylene. Figure VI-4 shows the heat capacity for a chain of 30 CH^2 grouped units. The frequency distribution is calculated from the Kirkwood-Pitzer model (Figure V-6). In one case the chain is extended, in the other it has three folds specified by the bond axes of units (11,12), (14,15), and (17,18). The heat capacity

of the extended chain has a characteristic behavior, given by the succession of cubic, square, and linear laws in the respective intervals (0, 20°), (20°, 120°), and (120°, 200°). When folds are introduced the coefficients of the power laws are modified and there seems to be a departure from linearity in the (120°, 200°) interval. The question is whether the modes in the forbidden gap or the attenuation of the cut off peaks are responsible for this change in pattern. According to Ref. 60, the linear law is attributed to the flatness of the bending continuum. In this respect we may interpret Figure VI-4 as a result from the redistribution of the cut off in the bending continuum. However, in view of the argument in Ref. 54 (see Chapter III), we give a greater importance to the modes in the stretch-bend gap.

We compare this result with the data gathered by Wunderlich[60] for 100% crystalline polyethylene chains. These are calculated from three dimensional lattice modes and fit the observed heat capacities at all temperatures below 250° except for the (0, 10°) and (50°, 80°) intervals. There is a major difference and some mimilitude with the results of the Kirkwood-Pitzer model. The heat capacities follow the same power laws in the same temperature intervals. However the coefficients of the power laws are different.

A 100% crystalline sample in the folded chain structure may have 3% of folds. These could explain[60] the bad fit in the above mentioned temperature intervals. We find however that folds modify the heat capacity more uniformly in the entire temperature range (Figure VI-4).

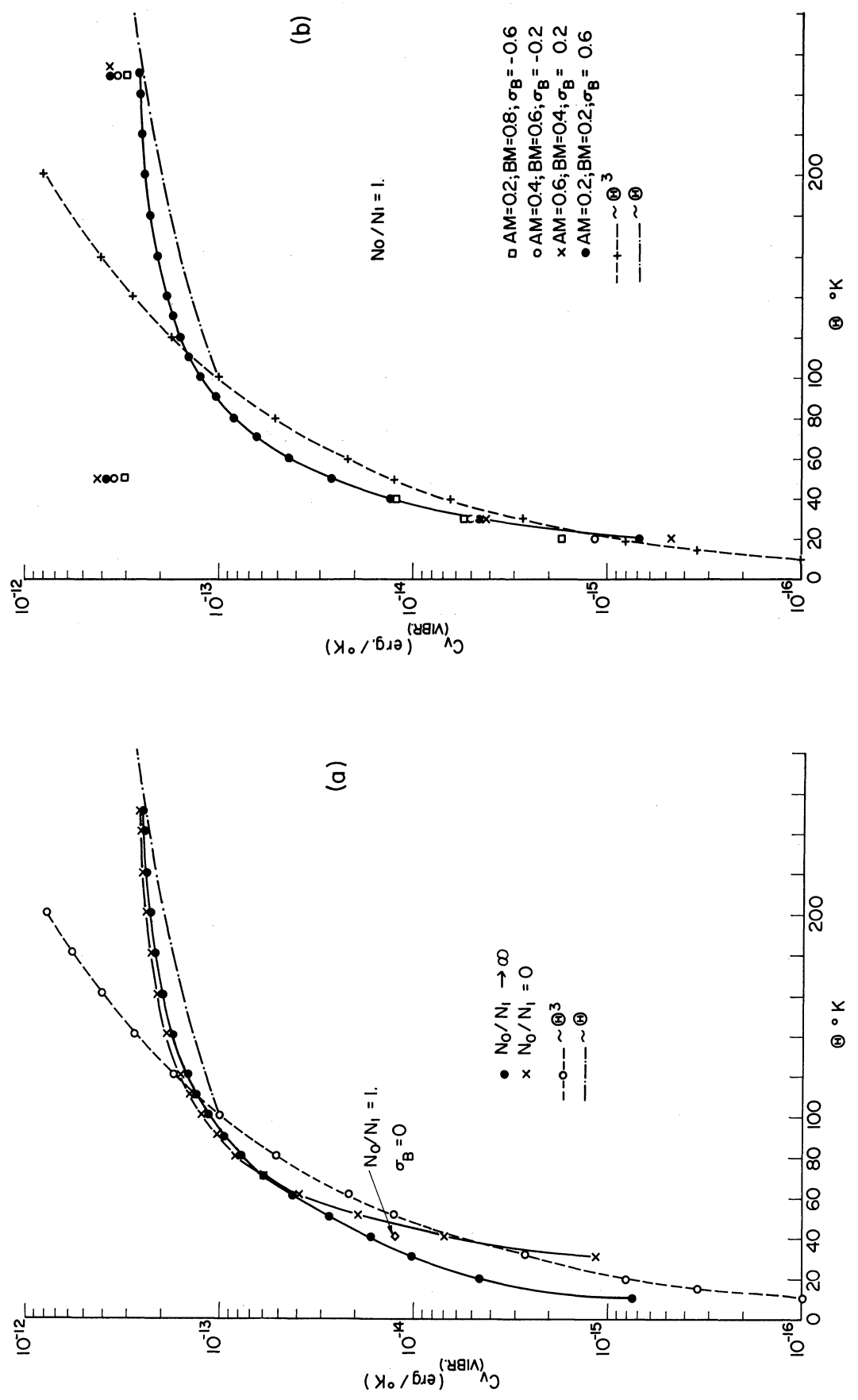
(a)
(b)
$C_{v_{(VIBR.)}}$ (erg / °K)
Θ °K
$N_o/N_1 = 1.$
$\sigma_B = 0$
$N_o/N_1 \to \infty$
$N_o/N_1 = 0$
$\sim \Theta^3$
$\sim \Theta$
AM=0.2; BM=0.8; σ_B = -0.6
AM=0.4; BM=0.6; σ_B = -0.2
AM=0.6; BM=0.4; σ_B = 0.2
AM=0.2; BM=0.2; σ_B = 0.6

Figure VI-3

Figure VI-3. Specific heat at constant volume for the same chains as in Figures VI-2a and b.

(a) Effect of concentration of G configurations. The pure T chain has a greater heat capacity up to 70°K. Thereafter it is lower than the pure G chain. The dotted curves are shown for reference to the cubic and linear laws.

(b) Only the curve for $\sigma_B = 0.6$ is drawn. The values for the other orders are inserted up to $\Theta = 50°K$. Thereafter only the succession in which they appear is indicated. The more clustered conformation has a higher capacity at lower temperature than the alternating order. The frequency distribution corresponding to these functions is given in Figure II-1.

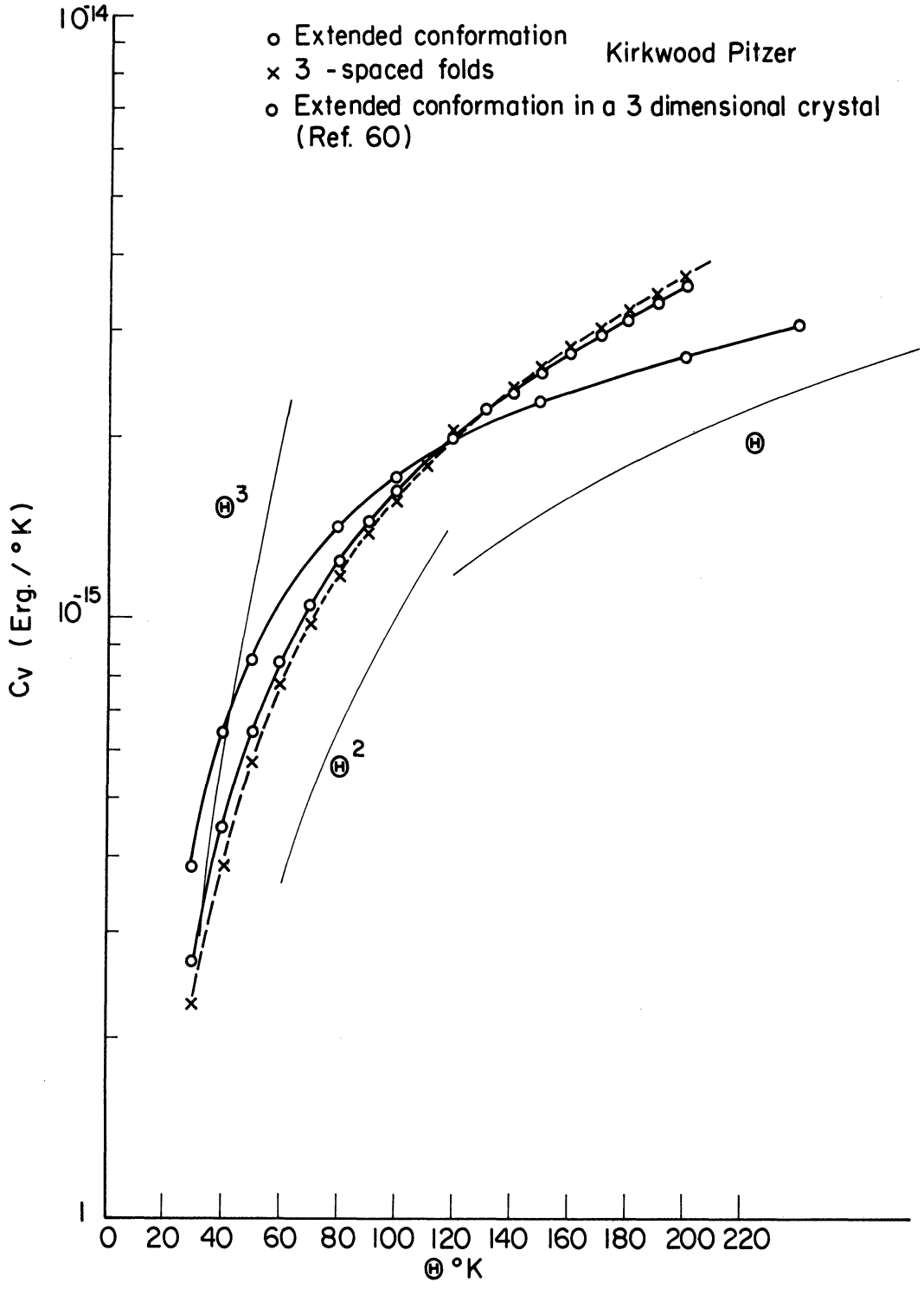

Figure VI-4. Specific heat at constant volume of a CH_2 zigzag chain of 30 units (Kirkwood-Pitzer model). The force constants are in millidynes/A°: 4.1; 0.2676; 0.035, for stretching, bending, and torsion, respectively. The valence angle is 67.5°. The frequency distribution corresponding to the 2 cases is given in Figure V-7. The three 3-spaced folds is the conformation—TTTGTTGTTGTTT. The dashed curve is the "best fit" function of Ref. 60.

We note in Ref. 60 that for 100% and 50% crystallinity, the observed heat capacities are identical below the glass transition, whereas the Kirkwood-Pitzer model of the isolated chain yields small but noticeable differences for a 10% crystallinity difference.

THERMODYNAMICAL FUNCTIONS DERIVED FROM THE POTENTIAL ENERGY

The next considerations apply to the temperature range[61] of "rubbery behavior," where substitution of T and G configurations are allowed. In an ideal rubber T and G have the same energy. In polyethylene there is a difference of 540 cal/mole between the two configurations. Such a value is experimentally determined[61] from the stress-temperature curve for a sample maintained at constant extension. The partition function for the one-dimensional model with the above energy assignments is found in several references.[61] It is derived from a random (Bernoulli) process that corresponds formally to the one-dimensional Ising model with magnetic field and no interaction between neighboring spins. It does not account for volume exclusion. We shall continue to neglect this effect, but we apply the results of the general one-dimensional Ising model by introducing a correlation energy a between neighboring configurations. Recently, Montroll[62] has considered such a correlation energy in a system of substitution of "complexes," rather than configurations.

We recall that the configuration is given by the succession of 4 consecutive carbon atoms. The "in plane" configuration is labeled T as before and has energy $\sim -J$. The other configurations are labeled G as before

and have energy ~ J (by others we mean the two gauche, unless otherwise specified). The index σ of a configuration indicates in which state it is: $\sigma = 1$ corresponds to T, $\sigma = -1$ to G.

For the random chain, the probability of occurrence of T is $e^{-J/2} \cosh J$; the occurrence of G has the complementary probability (compare with (II-18)). The partition function is then

$$Z_p = \sum_{\{\sigma\}} e^{\sigma J} = 2^N \cosh^N J$$

where $\{\sigma\}$ is the set of all conformations and where N is the number of units of 4 consecutive carbon atoms (which is two less than the number of carbon atoms). The free energy is:

$$F_p = - k \Theta \log (2^N \cosh^N J) \qquad \text{(VI-1)}$$

assuming $J = \frac{\epsilon}{k\Theta}$

we have: $S_p = \left.\frac{\partial F}{\partial \Theta}\right)_V = 2 N k \left\{ \log (\cosh J) - J \tanh J \right\}$

$$C_{Vp} = \left.\frac{\partial S}{\partial \Theta}\right)_V = 2 N k J^2 / \cosh^2 J$$

The similar Ising model would have a magnetic field H = J and no nearest neighbor interaction. The comparison is purely formal: in fact T and G are equivalence relations between neighbor atoms and the energy J does correspond to a nearest neighbor interaction. If some confusion arises, it is due to the way of assigning J to elements of a sequence. For example

in the sequence of spin states:

U	D	U	D	D	U	D	U	U
	d	d	d	s	d	d	d	s
	J	J	J	-J	J	J	J	-J

where U, D are the up, down spin states respectively; d, s indicate pairs of disimilar, similar states respectively. The energy is assigned to <u>pair</u> of spins; whereas in the sequence of configurations

G	T	G	T	T	G	T	G	G
J	-J	J	-J	-J	J	-J	J	J

the energy is assigned to each <u>element</u>.

We introduce now the interaction U between nearest neighbors. The partition function is calculated from the "transfer" matrix

$$\tau = \begin{pmatrix} e^{u-J} & e^{-u} \\ e^{-u} & e^{u+J} \end{pmatrix} \qquad \text{(VI-2)}$$

For comparison, the "transfer" matrix in the Ising model with magnetic field H and nearest neighbor interaction J is

$$\tau_I = \begin{pmatrix} e^{J-\mu H} & e^{-J} \\ e^{-J} & e^{J+\mu H} \end{pmatrix} \qquad \text{(VI-3)}$$

These "transfer" matrices are not the transfer matrices of Chapter II, their matrix elements are thermodynamical weights rather conditional probabilities. However, they define a Markovian process.

The eigenvalues of τ are:

$$\lambda_{1,2} = e^{u}\left\{\cosh J \pm \operatorname{Sinh} J\left(1 + \frac{e^{-4u}}{\operatorname{Sinh}^2 J}\right)^{1/2}\right\}$$

Then we write Z as: $\lim_{N\to\infty} Z = \lambda_1^N$, $|\lambda_1| > |\lambda_2|$

We now derive the free energy as:

$$F = -2\,k\,N\,\Theta\left\{U + \log\left(\cosh J + \operatorname{Sinh} J\left(1 + \frac{e^{-4u}}{\operatorname{Sinh}^2 J}\right)^{1/2}\right)\right\}$$

If we assume U independent of temperature then the entropy is

$$S = -F/\Theta + 2\,Nk\,\frac{J}{\cosh J + \operatorname{Sinh} J\left(1 + \frac{e^{-4u}}{\operatorname{Sinh}^2 J}\right)^{1/2}}\left\{\operatorname{Sinh} J\right.$$

$$\left. + \cosh J\left(1 + \frac{e^{-4u}}{\operatorname{Sinh}^2 J}\right)^{1/2} - \operatorname{Sinh} J\left(1 + \frac{e^{-4u}}{\operatorname{Sinh}^2 J}\right)^{-1/2}\frac{e^{-4u}}{\operatorname{Tanh} J\,\operatorname{Sinh}^2 J}\right\}$$

If U depends on Θ the last term in the parenthesis is:

$$\operatorname{Sinh} J\left(1 + \frac{e^{-4u}}{\operatorname{Sinh}^2 J}\right)^{-1/2}\left(\frac{1}{\operatorname{Tanh} J\,\operatorname{Sinh}^2 J} - \frac{4\,dU/d\Theta}{\operatorname{Sinh}^2 J}\right)e^{-4u}$$

and the term $2\,Nk\,\Theta\,(dU/d\Theta)$ is to be added to S. In order to compare these functions with the thermodynamical functions of the vibrational energy, we need to determine the overall characteristics of the chain as a function of U and Θ. These are the concentrations of T and G elements and the conditional probabilities or transfer matrix elements described in Chapter II. As in Ref. 62 we have:

$$\frac{\partial \log Z}{\partial J} = -\frac{1}{2}\sum_{j=1}^{\infty} \langle \sigma_j + \sigma_{j+1} \rangle$$

this gives the concentration in T configurations; in our notation:

$$\frac{N_o}{N_1} = \frac{1 + (1 + e^{-4u}/\mathrm{Sinh}^2 J)^{1/2}}{1 - (1 + e^{-4u}/\mathrm{Sinh}^2 J)^{1/2}} \qquad \text{(VI-4)}$$

The conditional probability that a configuration at vertex yields a configuration at vertex ℓ is related to the pair correlation function: $< \sigma_\ell \sigma_r >$, i.e., the average configuration of ℓ for a T configuration at k ($k = \ell + r$). From Ref. 14 we have:

$$< \sigma_\ell \sigma_{\ell+r} > = Z^{-1} \sum_{stu} \tau_{st}^{\ell-1} \sigma_t \tau_{tu}^{r} \sigma_u \tau_{us}^{N-\ell-r+1}$$

where the indices s,t,u take the values 1,2. τ_{st} is the st matrix element of τ and σ_t is 1 for t = 1, -1 for t=2. τ_{st}^r is the s,t matrix element of the r'th power of τ.

$$< \sigma_\ell \sigma_{\ell+r} > = Z^{-1} \sum_{tu} \sigma_t \tau_{tu}^{r} \sigma_u \tau_{ut}^{N-r}$$

$$= Z^{-1} \sum_{tu} \sigma_t \Big(\sum_j \lambda_j^r \varphi_j(t) \varphi_j(u) \Big) \times$$

$$\sigma_u \Big(\sum_k \lambda_k^{N-r} \varphi_k(t) \varphi_k(u) \Big)$$

We have decomposed τ_{tu}^r into a function of the eigenvectors of τ. $\varphi_1(1)$, $\varphi_1(-1)$ are the 2 components of the eigenvector associated with λ_1. We can write this expression as

$$< \sigma_\ell \sigma_{\ell+r} > = Z^{-1} \sum_{jk} \lambda_j^r \lambda_k^{N-r} (\varphi_j, \sigma \varphi_k)^2$$

where $(\varphi_j,\sigma\,\varphi_k) = 1 \times \varphi_j(1)\varphi_k(1) - 1 \times \varphi_j(-1)\varphi_k(-1)$

$$< \sigma_\ell\ \sigma_{\ell+r} > = Z^{-1}\left\{ \lambda_1^N\,(\varphi_1,\sigma\,\varphi_1)^2 + \left(\frac{\lambda_1}{\lambda_2}\right)^r \lambda_2^N\,(\varphi_1,\sigma\,\varphi_2)^2 \right.$$

$$\left. + \left(\frac{\lambda_2}{\lambda_1}\right)^2 \lambda_1^N\,(\varphi_2,\sigma\,\varphi_1)^2 + \lambda_2^N\,(\varphi_2,\sigma\,\varphi_2)^2 \right\} \qquad \text{(VI-5)}.$$

If $\lambda_1 > \lambda_2$, at the limit $N \to \infty$ we have:

$$< \sigma_\ell\ \sigma_{\ell+r} > = (\varphi_1,\sigma\,\varphi_1)^2 + \left(\frac{\lambda_2}{\lambda_1}\right)^r (\varphi_2,\sigma\,\varphi_1)^2 \qquad \text{(VI-5a)}$$

where $Z = \lambda_1^N + \lambda_2^N$

We consider the expression (VI-5a) for different values of J and U.

$$(\varphi_1,\sigma\,\varphi_1)^2 = \frac{\mathrm{Sinh}^2 J}{\mathrm{Sinh}^2 J + e^{-4u}} \qquad \text{(VI-6)}$$

$$(\varphi_1,\sigma\,\varphi_2)^2 = 3\varphi_1^2(1)\,\varphi_2^2(1) + \varphi_1^2(-1)\,\varphi_2^2(-1)$$

$$= \left\{ -3(\cosh J + (e^{-4u} + \mathrm{Sinh}^2 J)^{1/2} - e^{J})(\cosh J - (e^{-4u} + \right.$$

$$\mathrm{Sinh}^2 J)^{1/2} - e^{J}) - (\cosh^2 J + e^{-4u} + \mathrm{Sinh}^2\,J)^{1/2} - e^{-J})$$

$$\left. \times\ (\cosh J - (e^{-4u} + \mathrm{Sinh}^2 J)^{1/2} - e^{-J}) \right\} / 4e^{u}(e^{-4u} + \mathrm{Sinh}^2 J) \qquad \text{(VI-7)}$$

$$\left(\frac{\lambda_2}{\lambda_1}\right)^r = \left(\frac{1 - \mathrm{Tanh}\ J(1 + e^{-4u}(\mathrm{Sinh}\ J)^{-2})^{1/2}}{1 + \mathrm{Tanh}\ J(1 + e^{-4u}(\mathrm{Sinh}\ J)^{-2})^{1/2}} \right)^r \qquad \text{(VI-8)}$$

In Table VI we indicate the variation of these three components.

TABLE VI

COMPONENTS OF THE PAIR CORRELATION AS A FUNCTION OF U AND J

J	U	Component (VI-6)	(VI-7)	(VI-8)
0	0	0	f	0
0	f*	0	f	f
f	0	f	f	0
f	f	f	f	f
∞	0	1	0	0
∞	f	1	0	f

*f means finite

The limit $U \to \infty$ must be considered with care since (VI-6) does not converge uniformly in U as $J \to 0$. In fact $(\varphi_1, \sigma\, \varphi_1)$ tends to 1 as $U \to \infty$, for $J = 0$. Also in that case, λ_2 tends towards λ_1 and one of the terms neglected in (VI-5) tends towards a finite number. But (VI-7) tends to 0 as $U \to \infty$, independently of J. Leaving three special cases aside, we consider the pair correlation as given by (VI-5a).

For $J = 0$, the pair correlation varies from zero to one as U increases. When $J = 0$, there are two contributions to the pair correlation. One is independent of r (VI-6); the other depends on r (VI-8). They could be respectively labeled as "long range" and "short range" orders. This "long range" order is however not the one defined in Chapter II. It only affects the average number of G,T configurations. The process can still be random (Bernoulli) or Markovian if "long range" order does not vanish. As λ_2 tends towards λ_1 we have a long range order in the sense of Chapter II.

If we determine the pair correlation (VI-5a) from the transfer matrix of Chapter II (instead of (VI-2)) we obtain a relation between the respective matrix elements. Bethe's short range order (II-15) can then also be related to $< \sigma_\ell \sigma_{\ell+1} >$.

In this chapter we attempt to derive ordering of configurations from the thermodynamical functions. Such derivations are found in the literature from which we consider two examples.

A model[62] of the DNA molecule is a ladder where the rungs are complexes of type 1 or 2. Each complex is in either broken or intact state. From the experimental data of thermal uncoiling of pure and mixed type molecules, Montroll[62] derived the temperature dependence of J_i

$$J_i = \alpha_i (T - T_{ci}) \qquad \text{(VI-9)}$$

(where i is the index of the type and T_{ci} the temperature at which half of the complexes are broken) and the values of α_i. He showed further that the state of a complex could not be independent of the neighboring states. However the short range order as defined in Chapter II was not calculated.

Another author[64] established the effect of ordering in stereosequences, from the calculation of the freezing temperature. The result was that for a random tacticity (Bernoulli)

$$T_f < \left[\frac{1}{T_1} - R \frac{\ell n \alpha}{\Delta H_u} \right]^{-1}$$

where H_u is the heat of fusion of a mole and T_1 the melting point for a concentration $\alpha = 1$ of isotactic groups. In the case of a simple Markov chain however:

$$T_f < \left[\frac{1}{T_1} - R \frac{\ell n\, \alpha i}{\Delta H_u} \right]^{-1}$$

where α is the conditional probability that an isotactic group be followed by another isotactic group. From these examples it is seen that ordering can be inferred, but that the results are yet only qualitative.

We now return to the amorphous structure of chains where an energy $\sim \Delta J$ is assigned to each configuration and where an energy $\sim U$ is assigned to neighboring pairs of configurations. The dependence of J on temperature is given by (VI-1). We could infer the U temperature dependence in a manner similar to the J dependence in (VI-9). We assume however U constant, which leaves ordering of configurations as a single unknown parameter. Ordering can be inferred from maximum entropy. The fact the entropy rather than energy differences is responsible for conformation of simple chains is discussed in Ref. 51 (where a "cooperative phenomena" similar to the DNA uncoiling is also described). In Figures VI-5a,b the potential entropy functions S_p are given for several U, ΔJ values. Typical patterns for $U < 0$, $U = 0$, $U > 0$ are recognized. The curves tend toward an asymptotic value as temperature increases. A finite correlation U yields however a greater asymptotic value, which seems independent of the sign and absolute value of U, as long as it is finite. The difference between positive and negative sign is seen in the transi-

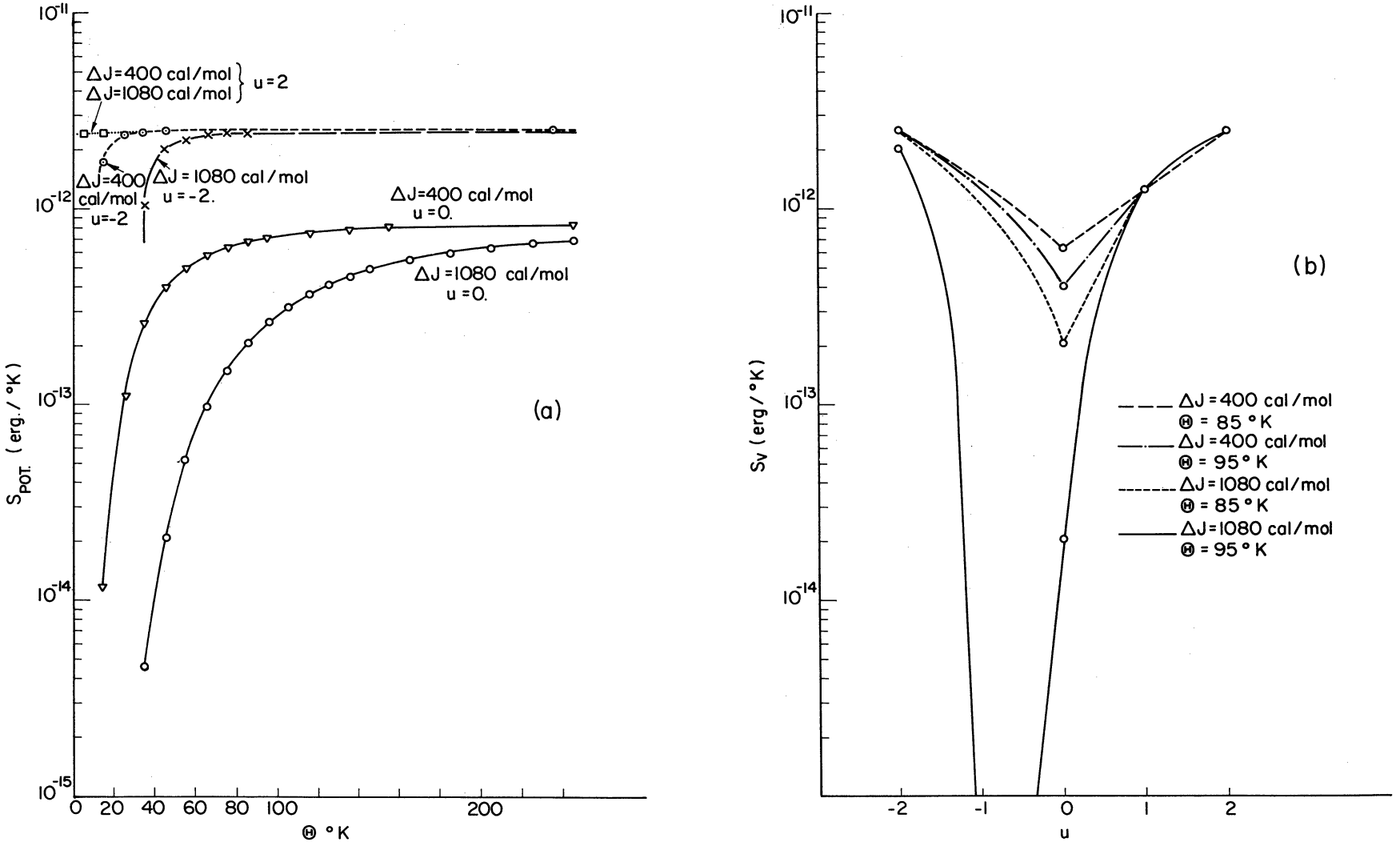
ΔJ=400 cal/mol
ΔJ=1080 cal/mol
u=2
ΔJ=400 cal/mol u=-2
ΔJ = 1080 cal/mol u = -2.
ΔJ=400 cal/mol u=0.
ΔJ=1080 cal/mol u=0.
(a)
S_POT. (erg./°K)
Θ °K
(b)
Sv (erg/°K)
u
ΔJ=400 cal/mol Θ = 85 °K
ΔJ=400 cal/mol Θ = 95 °K
ΔJ=1080 cal/mol Θ = 85 °K
ΔJ=1080 cal/mol Θ = 95 °K

Figure VI-5

Figure VI-5. Entropy derived from potential energy as a function of temperature Θ, correlation U, and potential $\Delta J = 2$ E. For polyethylene $\Delta J = 590$ calories/mol.

(a) Entropy as a function of temperature for several U, ΔJ.

(b) Entropy as a function of correlation U for several temperatures, ΔJ. One notices that correlation introduces a sharper transition to the asymptotic values and enhances entropy for a given ΔJ, Θ.

tion to the asymptote. For $U > 0$ this transition is sharper than for $U < 0$.

To infer ordering, we add the vibrational and potential entropies. We see that S_v depends noticeably on the short range order σ_B for temperatures below 60°K, whereas S_p is independent of U beyond 15°K. Hence there is an interval (15°, 60°) where the maximum total entropy is dictated by the harmonic activity of the chain. In this case, we find that clustered conformations (i.e., where T configurations tend to concentrate) are favored, as interpreted from the vibrational component of the hamiltonian.

The parameters U, ΔJ, Θ, σ_B, N_o/N_1 are not all independent. If U, ΔJ, Θ are given, N_o/N_1 follows from (VI-4) (Figure VI-6) and σ_B is derived from (VI-5). From a measurement of entropy, one could determine whether there is such a finite correlation U and whether it is temperature dependent. The heat capacity function is given in Figure VI-7. It is interesting to compare this result with the heat capacities of the one-dimensional Ising model for various values[63] of J and μ H (see Figure 29 in Ref. 63). There J depends on temperature, whereas in our case U does not.

We notice that the heat capacity of potential energy is more sensitive to U and ΔJ than the heat capacity of vibrational energy is sensitive to σ_B.

A phase transition could be formalized in the following terms. The gauche configuration represents a continuum of configuration angles $\phi \neq 0$. To each ϕ is assigned the energy ΔJ (ϕ). At low temperature, only the values ϕ = 0, 120°, 290° are probable. As the temperature increases, other

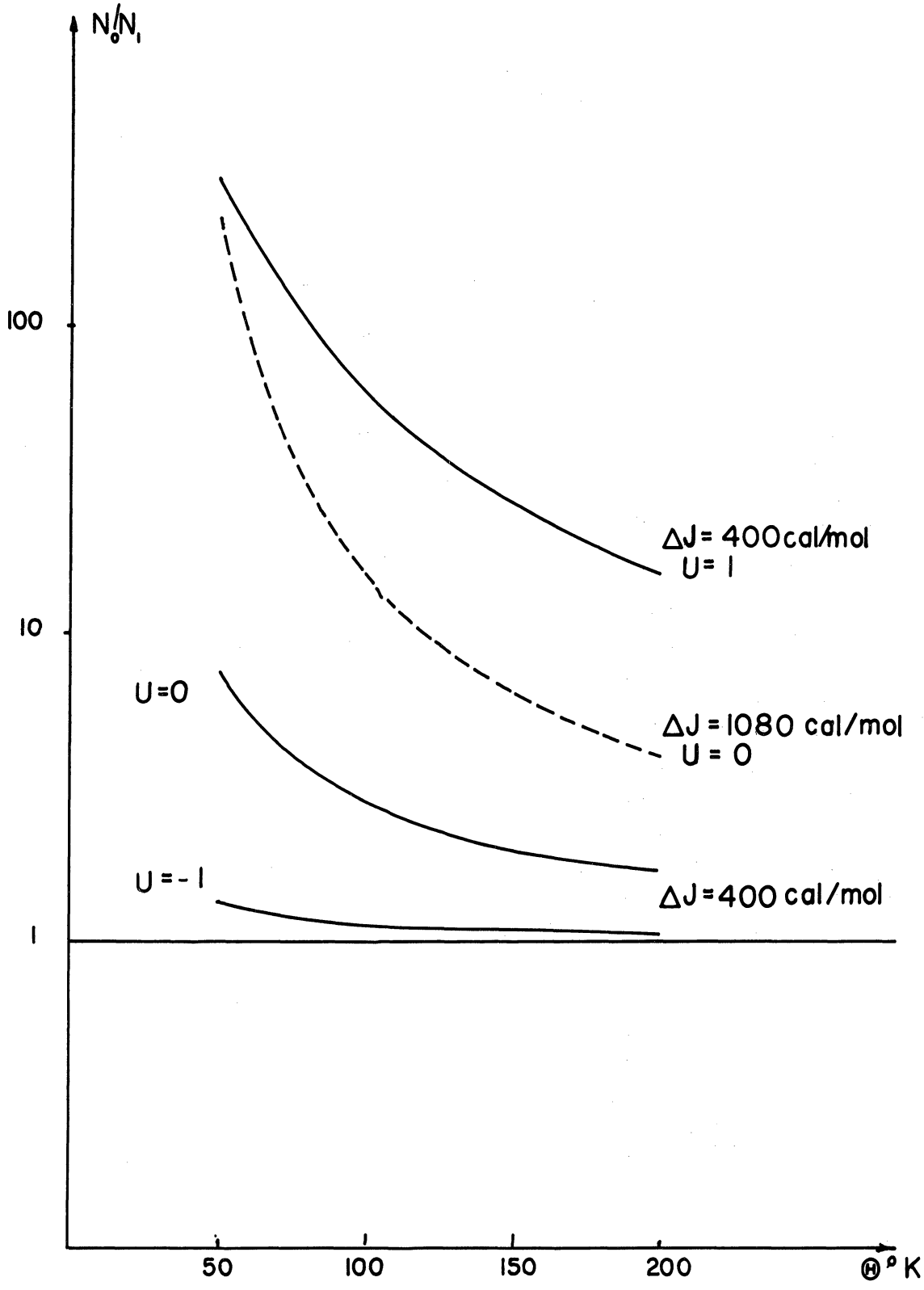

Figure VI-6. Fraction of T to G configurations as a function of temperature. For U = 0, the number of G's tends to the number of T's as the temperature increases. A negative correlation forces all curves down to the asymptote $N_0/N_1 = 1$.

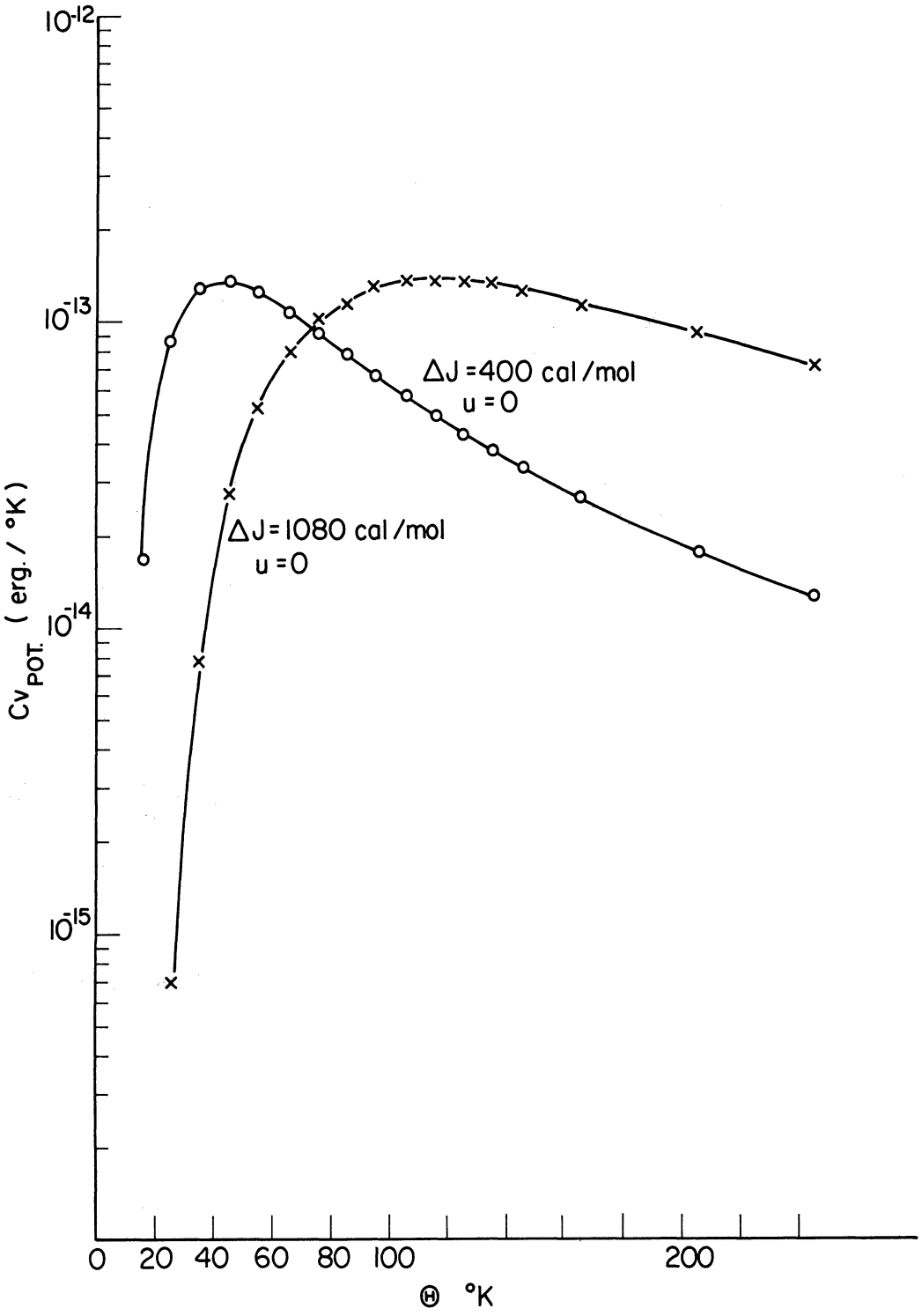

Figure VI-7. Specific heat derived from potential energy as a function of temperature for two values of ΔJ. The effect of correlation can be seen from Figure VI-5, since C_V is the derivative of S with respect to temperature; correlation enhances the heat capacity peak and shifts it to lower temperature. See also Figure 29, Ref. 63.

values become probable. The range $(0,2\pi)$ could be partitioned in q intervals. The index σ consequently has a range of q values and the transfer matrix is of order q. A degeneracy of the greatest eigenvalue could be associated with temperatures below the glass transition, at the limit $q \to \infty$.

CHAPTER VII

CONCLUSION

In a system of coupled atoms such as a chain, the harmonic forces on a particular atom are generated by its displacements with respect to neighbor atoms. The number of such neighbors depends on the range of interaction. The orientation of forces can be given by the line connecting each interacting pair. A fold in the extended chain reorients the forces on those atoms which are in the vicinity of the fold. The resultant of these forces is accordingly modified in magnitude and in orientation.

When there is only one degree of freedom per oscillating atom or group of atoms, a fold tends to uncouple motions on each side of the fold. When there are two or more degrees of freedom, the fold also couples motions among different motion species.

Discernible effects of folds are the splitting and the shifting of normal modes and modification of polarization vectors. These effects were first observed in Raman scattering. For paraffins, the different intensities of the (325, 432) and (789, 835) cm^{-1} Raman lines were attributed to trans and gauche configurations. The number of isomers in a sample is counted on this basis.

In this work, we are concerned not only with the number of isomers, but also with their distributions along the chain. The analysis of the normal frequency distribution in terms of configuration distribution is possible to a good extent when either trans or gauche configurations pro-

duce out-of-band modes. This is the case of the one degree of freedom or simple chain problem for conformations in which the G configurations are in greater number than the T's. The analysis is then based on the ordering of out-of-band modes in terms of "islands" of T configurations bordered by an equal number of G's. The out-of-band mode associated with T islands is easily determined by the Green's function method. The contribution of other islands such as TT, TGT can be calculated in the same way, where however the numerical difficulty increases with number of non-zero elements of the defect matrix. An important parameter of the analysis is the number of squared frequency intervals N partitioning the forbidden gap. The width of the gap is itself a function of the gauche configuration angle $\tilde{\psi}$ and is $(4\gamma/M)\ (1 - \cos \tilde{\psi})$. We found that N must be at least equal to 20 for meaningful interpretation of the frequency distribution in the gap. If $4\gamma/M = \omega_L^2$ is taken as a basic interval, the requirement is that the number of modes be counted in each $\omega_L^2\ (1 - \cos \tilde{\psi})/N$ subinterval. Hence the difficulty for a meaningful measurement increases as $\tilde{\psi}$ departs from $\pi/2$.

A limitation of the island technique is its inability to yield anything but the diagonal elements of the transfer matrix defining a Markov process. Whether there is statistical aftereffect can however be inferred from the rates of occurrence of the T and the TT islands.

For the case of a greater number of T than G configurations we found an empirical relation allowing the determination of the rate of occurrence of G in a random (Bernoulli) distribution.

In the case of two degrees of freedom the appearance of out-of-band modes is not necessarily related to T configurations. Whether T or G, or both T and G, or neither T and G produce out-of-band modes is decided by the force constants ratio, the value $\tilde{\psi}$ of the gauche configuration angle, and the type of motions. We saw in Chapter IV that no out-of-band mode separates from the bending-torsion continuum for any γ_b/γ_t ratio if $\tilde{\psi} = 120°$ (this value however ultimately depends on the valence angle α as seen in Eq. (IV-6)). For other values of $\tilde{\psi}$ there are intervals of the force constant ratio characterized by appearance or non-appearance of out-of-band modes due to G configurations. The situation is different if one considers the torsion-stretch interaction. Here a fold produces two out-of-band modes for any value of $\tilde{\psi}$ and a third for some $\tilde{\psi}$ values.

In the Kirkwood-Pitzer model each G configuration produces exactly one mode in the lower half of the stretch-bend gap, for low concentration of folds.

In general for a given configuration distribution, i.e., a given conformation, the frequency distribution reflects the force constant ratios. Conversely for given force constant ratio, the frequency distribution reflects the ordering of configurations along the chain. A similar relation was found between force constant ratios and dimension of the lattice for crystalline polyethylene in the Stockmayer-Hecht model. There the coalescence of two slope singularities (three-dimensional effect) into a logarithmic singularity (two-dimensional effect) is due to the small

ratio of diagonal to aligned force constants. Here the ratio γ_t/γ_b determines whether the frequency distribution is of the forbidden or "allowed" gap type.

It is convenient to assign a frequency interval in which effects of conformation are most typical in the Kirkwood-Pitzer model. We find that for low G concentrations, the characteristics of the conformation are best reflected in the mode distribution of the stretch-bend gap. As the concentration of folds increases, this gap is still a good interval. However other intervals are then just as good.

We show now in which manner the frequency distribution of polyethylene chains reflects the fringed micelle and the folded chain structures. A fold in an extended conformation yields a single mode in the stretch-bend gap and this mode occurs at 670 cm^{-1} (Table IV). It is conjectured that for small concentrations of folds ($p \leq 0.33$) there still is a one-to-one correspondence between the number of G configurations and the number of modes in the forbidden gap. Such a correspondence was found in the problem of simple chains between T configurations and pairs of out-of-band modes. Beyond a certain concentration of T's the number of these localized modes per T decreases however and follows a simple power law whose exponent is determined empirically. The same pattern is expected in the Kirkwood-Pitzer model, where G is substituted for T. As a consequence the area of frequency distribution in the stretch-bend gap measures the number of folds. It also yields information on their distribution along the chain. Table IV indicates namely that there is an interac-

tion effect between G defects, which produces a splitting of their respective frequency contributions. In this way the localized mode distribution reflects the conformation of the chain. Identification of the peaks in the forbidden gap is feasible by numerical calculations or by the Green's function method as in the problem of simple chains.

Hence in a folded chain structure we would observe three dominant peaks if the GGG island maps correctly the folding of the chain or two dominant peaks if the GTGTG island is a better model. The contribution of amorphous regions would appear as a background. In the case of fringed miscelles, the above mentioned peaks would not emerge from the background. The structure around 670 cm^{-1} could also indicate the relative amounts of regularly spaced folds and fringed miscelles, if both coexist.

We have not found any indication of a 670 cm^{-1} mode in observed frequencies. The nearest datum is the very weak infrared mode at 600 cm^{-1}. Raman modes above 700 cm^{-1} pertain to CH^2 rocking motions.

Another geometrical characteristic reflected by the frequency distribution is the range of values taken by the configuration angle. We have seen in Chapter III how the transverse modes are sensitive to this range, especially in the neighborhood of $\psi = \pi/2$ which corresponds to total uncoupling. The question is first whether such a value ever occurs at lower temperatures, where there are only three stable configurations $\phi = 0$, 120°, and 240°. These correspond to a minima of potential energy. Outside of these values the configuration is unstable. In amorphous regions there may however be deviations from these values. Consider namely

the last vertex of a growing chain. A bond can be added in three stable ways provided that there is no self-intersection. If however one of the outcomes violates the volume exclusion, the configuration angle may either take another stable and allowed value or an unstable and allowed value. In the first case the potential energy is lower, in the second the atoms are packed in a smaller volume. The two tendencies would be reflected in the lower part of the acoustical frequency distribution, if the interaction effect brought about by the fold does not perturb this result too strongly. We saw that the coupling with the bending mode is weak at $\psi = \pi/2$, that however the coupling with the stretch motion is very strong. We could not test the overall effect on the Kirkwood-Pitzer model because of time and storage problems in the numerical calculation.

The thermodynamical functions derived from the Kirkwood-Pitzer model show the effects of folds introduced in a planar structure. The deviations are small compared to the correction introduced by the three-dimensional environment effect. We note however that the heat capacity curves reported by Wunderlich[60] for 100% and 50% crystallinity do not differ below the glass transition temperature. The differences are probably too small to be observed. If however our result of Figure VI-4 for the isolated chain holds for chains with intermolecular forces, we conclude that the frequency distribution is sensitive to conformations through local (or direct, as in Chapter I) rather than environment effects.

The ordering of configurations along the chain raises the question of correlation energy U between neighbor configurations. Each four con-

secutive carbon atom sequence is either in T or in G configuration. An energy $J(\sigma)$ is assigned to each type σ = T, G. Accordingly in the Pitzer equation for our of plane motion, the range of forces is of order three.

The introduction of a correlation U between successive configurations amounts to considering sequences of five consecutive carbon atoms with the four possible outcomes:

GG, GT, TT, TG

and the assignment

$$2J(G) + U(GG),\ J(G) + J(T) + U(GT),\ 2J(T) + U(TT),\ J(T) + J(G) + U(TG)$$

The corresponding equation for the out of plane motion would then have a force range of four. Figure V-2 shows that the extension of the force range transfers the "inside" normal modes $o < \omega < \omega_L$ to the singular points o and ω_L. Hence a discernible effect of the correlation U would be a more dominant torsion cut-off peak.

The measurement of J has been performed from several experiments such as Raman scattering,[65] thermodynamical functions,[18] and stress-temperature functions.[66] In the interpretation of the data it is assumed that there is no correlation U. However the same data could be interpreted with a model where J and U are both different from zero.

We have seen how the frequency distribution reflects structural and dynamical properties of the chains considered and how it is related to

observables such as thermodynamical functions. The frequency distribution is however not the only information yielded by the dynamical matrix. The eigenvectors are a natural complement to the normal frequencies. They are components of several observables such as the incoherent inelastic neutron scattering cross section.[12] A calculation of this quantity requires the determination of scalar products of these eigenvectors. An intermediate step is the calculation of the pair correlation function. There are methods[67,68] to perform this calculation, which could be applied to simple chains.

BIBLIOGRAPHY

1. Peterlin, A., "Crystalline Character in Polymers," J. Polymer Sci. C9, 61 (1965).

2. Krimm, S., and Tobolsky, A., "Determination of Crystallinity in Polyethylene," J. Polymer Sci. 7, 57 (1952).

3. Sauer, J. A., and Woodward, A. E., "Transition in Polymers," Rev. Mod. Phys. 32, 89 (1960).

4. Kakudo, M., and Ullman, R., "Polyethylene Crystallinity," J. Polymer Sci. 45, 91 (1960).

5. Keller, A., and O'Connor, A., "Study of Single Crystals and Their Associations in Polymers," Discussions Faraday Soc. 25, 114 (1958).

6. Tobolsky, A., "Some View Points on Polymer Physics," J. Polymer Sci. C9, 157 (1965).

7. Danner, H, R., et al., "Polyethylene by Neutron Inelastic Scattering," J. Chem. Phys. 40, 1417 (1964).

8. Tobolsky, A., "Physics of Semi-Crystalline Polymers," J. Chem. Phys. 37, 1139 (1962).

9. Peterlin, A., and Fisher, E. W., "Thermodynamisher Stabilität Makromolekularer Kristalle," Z. Physik 159, 272 (1963).

10. Temperley, H.N.V., "Available Methods of Estimating the Most Probable Configuration of Simple Models of a Macromolecule," Discussions Faraday Soc. 25, 92 (1958).

11. Bresler, S. E., "Macromolecules—General Discussion," Discussions Faraday Soc. 25, 205 (1958).

12. Summerfield, G. C., "Determination of the Phonon Spectrum of Polyethylene by Neutron Scattering," J. Chem. Phys. 43, 1079 (1965).

13. Krimm, S., "Recent Developments in Vibrational Spectroscopy of High Polymers," J. Polymer Sci. C7, 3 (1964).

14. Kac, M., Lecture Notes, Physics Summer Institute, Brandeis, 1966.

BIBLIOGRAPHY (Continued)

15. Kirkwood, J. G., "The Skeletal Modes of Vibration of Long Chain Molecules," J. Chem. Phys. 7, 506 (1939).

16. Montroll, E. W., Lattice Statistics: Applied Combinatorial Mathematics, E. F. Beckenbach, Ed., John Wiley and Sons, New York, 1964, p. 97.

17. Stockmayer, W. H. and Hecht, C. E., "Heat Capacity of Chain Polymeric Crystals," J. Chem. Phys. 21, 1954 (1953).

18. Pitzer, K. S., "The Vibration Frequencies and Thermodynamic Functions of Long Chain Hydrocarbons," J. Chem. Phys. 8, 711 (1940).

19. Miyazawa, T., and Kitagawa, T., "Crystal Vibrations, Specific Heat and Elastic Moduli of the Polyethylene Crystal," Polymer Letters 2, 395 (1964).

20. Weinreich, G., Solids: Elementary Theory for Advanced Students, John Wiley and Sons, New York, 1965, p. 75.

21. Genensky, S. M., and Newell, G. F., "Spectrum and Heat Capacity of a Chain Polymer," J. Chem. Phys. 26, 486 (1957).

22. Tasumi, M., and Simanouchi, T., "Crystal Vibrations and Intermolecular Forces of Polymethylene Crystals," J. Chem. Phys. 43, 1295 (1965).

23. Myers, W., Summerfield, G. C., and King, J. S., "Neutron Scattering in Stretch Oriented Polyethylene," J. Chem. Phys. 44, 184 (1966).

24. Donovan, J. L., "Measurement of the Phonon Frequency Distribution for Polyethylene by Neutron Scattering, Thesis, The University of Michigan (unpublished).

25. Dyson, F. J., "Statistical Theory of the Energy Levels of Complex Systems, I," J. Math. Phys. 3, 190 (1962).

26. Wigner, E. P., "Statistical Properties of Real Symmetric Matrices with Many Dimensions," Can. Math. Congr. Proc., University of Toronto Press, p. 174. Reproduced in Statistical Theories of Spectra: Fluctuations, C. Porter, Ed., Academic Press, 1965, p. 188.

27. Hosemann, R., and Bagchi, S. N., Direct Analysis of Diffraction by Matter, North Holland Publishing Company, Amsterdam, 1962.

BIBLIOGRAPHY (Continued)

28. Dyson, F. J., "The Dynamics of Disordered Linear Chains," Phys. Rev. 92, 1331 (1953).

29. Dean, P., "The Spectral Distribution of a Jacobian Matrix," Proc. Cambridge Phil. Soc. 52, 752 (1956).

30. Brout, R., and Visscher, W. M., "Suggested Experiment on Approximate Localized Modes in Crystals," Phys. Rev. Letters 9, 59 (1962).

31. Schmidt, H., "Disordered One-Dimensional Crystals," Phys. Rev. 105, 425 (1957).

32. Rosenstock, H. B., and McGill, R. E., "Vibrational Modes of Disordered Linear Chains," J. Math. Phys. 3, 200 (1962).

33. Payton, D. N., and Visscher, W. M., "Dynamics of Disordered Lattices in One, Two, and Three Dimensions," Los Alamos Scientific Laboratory Report LA-3471-MS.

34. Dean, P., and Bacon, M. D., "Vibrations of Two-Dimensional Disordered Lattices," Proc. Roy. Soc. (London) 283A, 64 (1965).

35. Givens, J. W., "A Method of Computing Eigenvalues and Eigenvectors Suggested by Classical Results on Symmetric Matrices," Natl. Bur. Std. Appl. Math. 29, 117 (1953).

36. Langer, J. S., "Frequency Spectrum of a Disordered One-Dimensional Lattice," J. Math. Phys. 2, 584 (1961).

37. Poon, A. C., and Bienenstock, A., "Vibrational Spectrum of a One-Dimensional Chain with Randomly Distributed Impurity Springs," Phys. Rev. 141, 710 (1966).

38. Krein, M. G., "The Ideas of P. L. Cebysev and A. A. Markov in the Theory of Limiting Values of Integrals and Their Further Development," Am. Math. Soc. Transl. (2) 12, 1-121 (1959).

39. Krein, M. G., and Rehtman, P. G., "Development in a New Direction of the Cebysev-Markov Theory of Limiting Values of Integrals," Am. Math. Soc. Transl. (2) 12, 123-135 (1959).

40. Shohat, J. A., and Tamarkin, J. D., "The Problem of Moments," Am. Math. Soc. Math. Surveys 1 (1943).

BIBLIOGRAPHY (Continued)

41. Bethe, H. A., "Statistical Theory of Superlattices," Proc. Roy. Soc. (London) A150, 552 (1935).

42. Coleman, B. E., and Fox, T. G., "General Theory of Stationary Random Sequences with Application to the Tacticity of Polymers," J. Polymer Sci. A1, 3183 (1963).

43. Varga, R. S., Matrix Iterative Analysis, Prentice Hall, 1962, p. 35.

44. Bovey, F. A., and Tiers, G.V.D., "Polymer Nuclear Spin Resonance Spectroscopy," J. Polymer Sci. 44, 173 (1960).

45. Price, F. P., "Copolymerization and Stereoregular Polymers," J. Chem. Phys. 36, 210 (1962).

46. Coleman, B. D., and Fox, T. G., "Multistate Mechanism for Homogeneous Ionic Polymerization," J. Chem. Phys. 38, 1065 (1963).

47. Fisher, M. E., and Sykes, M. F., "Excluded Volume Problem and Ising Model of Ferromagnetism," Phys. Rev. 114, 45 (1959).

48. Berge, C., Theorie des graphes et ses applications, Dunod, Paris, 1963.

49. Dean, P., "Vibrational Spectra of Diatomic Chains," Proc. Roy. Soc. (London) A254, 507 (1960).

50. Brillouin, L., and Parodi, M., Propagation des ondes dans les milieux périodiques, Masson, Dunod, Paris, 1958.

51. Longuet-Higgins, H. C., "The Entropy of a Flexible Macromolecule," Discussions Faraday Soc. 25, 86 (1958).

52. Jannink, G., and Summerfield, G. C., "Effect of Chain Conformations on the Frequency Distribution of an Idealized Chain." To appear in J. Appl. Phys. (October 1966).

53. Maradudin, A., Montroll, E. W., and Weiss, G. H., Theory of Lattice Dynamics in the Harmonic Approximation, Academic Press, 1963.

54. Montroll, E. W., and Potts, R. B., "Effects of Defects on Lattice Vibrations," Phys. Rev. 100, 525 (1955).

BIBLIOGRAPHY (Concluded)

55. Mahanty, J., Maradudin, A. A., and Weiss, G. H., "Vibrational Thermodynamic Properties of Lattices with Defects 1," Progr. Theoret. Phys. (Kyoto) 20, 369 (1958).

56. Jeffreys, H., and Jeffreys, B. S., Methods of Mathematical Physics, Cambridge Press, 1950.

57. Parodi, M., Application de l'algèbre moderne à quelques problèmes de physique classique, Gauthier-Villars, 1961.

58. Björk, R. L., "Impurity Induced Localized Modes of Lattice Vibration in a Diatomic Chain," Phys. Rev. 105, 456 (1957).

59. Yamahuzi, K., and Tanaka, T., "Effects of Defects on Lattice Vibrations," Progr. Theoret. Phys. (Kyoto) 20, 343 (1958).

60. Wunderlich, B., "Motion in Polyethylene, I, II," J. Chem. Phys. 37, 1204 (1962).

61. Tobolsky, A., Properties and Structure of Polymers, John Wiley and Sons, 1960.

62. Montroll, E. W., "On the Theory of Coiling and Uncoiling of DNA Molecules," Symposium on Inelastic Scattering of Neutrons by Condensed Systems, p. 57, BNL 940 (C-45).

63. Newell, G. F., and Montroll, E. W., "Theory of the Ising Model of Ferromagnetism," Rev. Mod. Phys. 25, 353 (1953).

64. Coleman, B. D., "Polymers with Random Stereosequences," J. Polymer Sci. 31, 155 (1958).

65. Sheppard, H., and Szasz, G. J., "Rotational Isomerism, III," J. Chem. Phys. 17, 86 (1949).

66. Flory, P. J., Hoeve, C.A.J., and Ciferri, A., "Bond Angle Restriction and Polymer Elasticity," J. Polymer Sci. 39, 337 (1959).

67. Ford, G. W., Kac, M., and Mazur, P., "Statistical Mechanics of Coupled Oscillators," J. Math. Phys. 6, 509 (1965).

68. Wintner, A., Spektraltheorie der Unendlichen Matrizen, Leipzig, 1929.